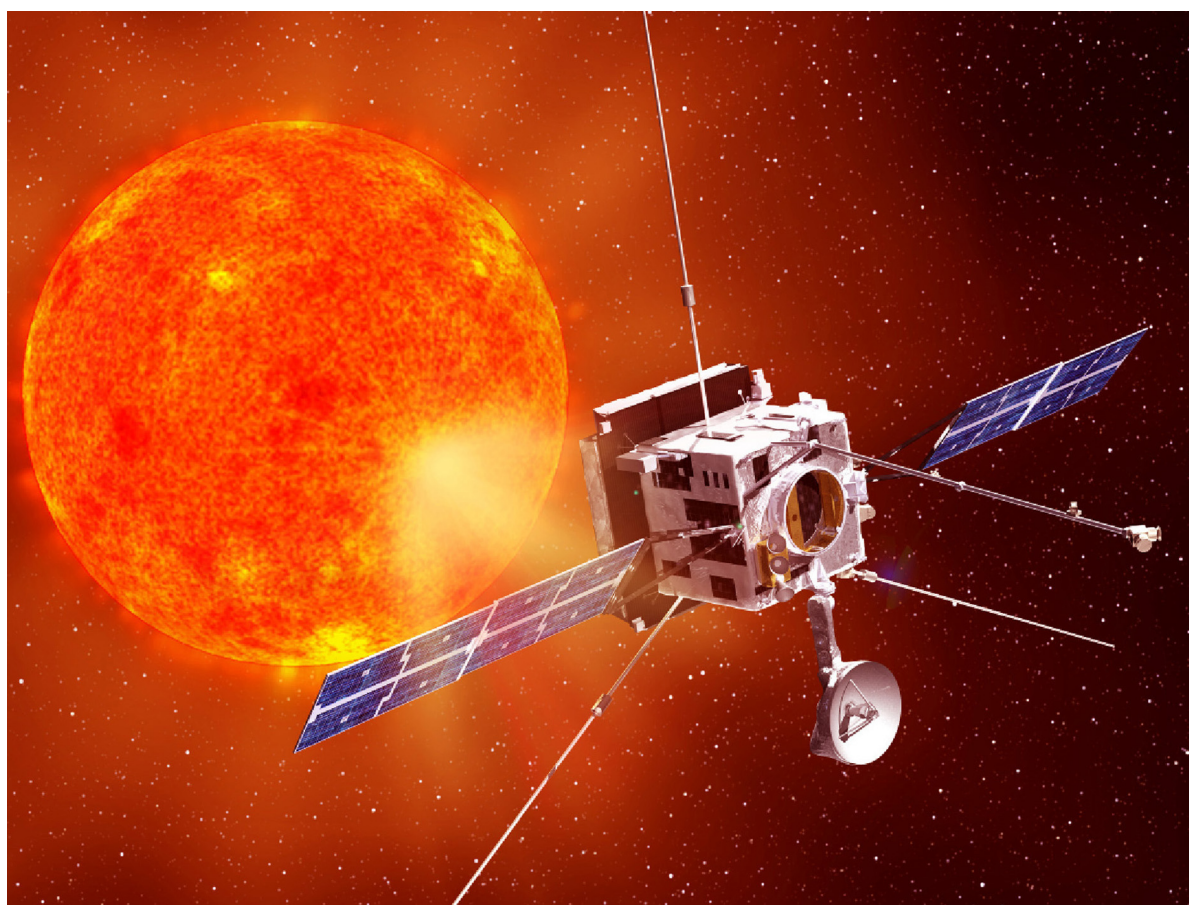


Solar Orbiter

Exploring the Sun-heliosphere connection



Definition Study Report

Contents

1	Executive Summary	1
2	Science Objectives	5
2.1	How and where do the solar wind plasma and magnetic field originate in the corona?	7
2.1.1	What are the source regions of the solar wind and the heliospheric magnetic field?	8
2.1.2	What mechanisms heat and accelerate the solar wind?.....	12
2.1.3	What are the sources of turbulence in the solar wind and how does it evolve?.....	14
2.2	How do solar transients drive heliospheric variability?	15
2.2.1	How do CMEs evolve through the corona and inner heliosphere?	16
2.2.2	How do CMEs contribute to the solar magnetic flux and helicity balance?	18
2.2.3	How and where do shocks form in the corona and inner heliosphere?	19
2.3	How do solar eruptions produce energetic particle radiation that fills the heliosphere?	21
2.3.1	How and where are energetic particles accelerated at the Sun?.....	21
2.3.2	How are energetic particles released from their sources and distributed in space and time? ..	25
2.3.3	What are the seed populations for energetic particles?	27
2.4	How does the solar dynamo work and drive the connections between the Sun and heliosphere? ..	28
2.4.1	How is magnetic flux transported to and reprocessed at high solar latitudes?	29
2.4.2	What are the properties of the magnetic field at high solar latitudes?	30
2.4.3	Are there separate dynamo processes acting in the Sun?	32
3	Scientific Requirements	35
3.1	Observations, Measurements, and Orbital Characteristics	35
3.1.1	Measurement Requirements and Instrument Capabilities.....	35
3.1.2	Orbit Requirements	50
4	Payload	51
4.1	In-Situ Instruments	52
4.1.1	Solar Wind Analyzer (SWA)	52
4.1.2	Energetic Particle Detector (EPD)	55
4.1.3	Magnetometer (MAG).....	57
4.1.4	Radio and Plasma Waves (RPW)	57
4.2	Remote-Sensing Instruments.....	59
4.2.1	Polarimetric and Helioseismic Imager (PHI).....	59
4.2.2	Extreme Ultraviolet Imager (EUI)	60
4.2.3	Spectral Imaging of the Coronal Environment (SPICE).....	61
4.2.4	Spectrometer/Telescope for Imaging X-rays (STIX)	62
4.2.5	Multi Element Telescope for Imaging and Spectroscopy (METIS).....	63
4.2.6	Solar Orbiter Heliospheric Imager (SoloHI).....	65
5	Mission Design	67
5.1	Mission and Spacecraft Requirements	67
5.1.1	Mission Requirements.....	67
5.1.2	Spacecraft Requirements.....	67
5.1.3	Launch and Launch Vehicle Selection	67
5.2	Baseline Orbit Design.....	68
5.2.1	Mission Profiles.....	68
5.3	Spacecraft Design Overview	73
5.3.1	Mission Architecture Overview	73
5.3.2	Mission Elements	73
5.3.3	Launch Segment.....	73

5.3.4	Space Segment	73
5.3.5	Ground Segment.....	73
5.3.6	Functional Architecture.....	74
5.4	Solar Orbiter Configuration.....	75
5.4.1	Introduction & Configuration Drivers.....	75
5.4.2	Spacecraft Configuration.....	77
5.4.3	Configuration Features to Support Industrialization.....	79
5.4.4	Spacecraft Configuration versus Mission Timeline	81
5.4.5	Payload Accommodation.....	81
5.5	System Budgets	84
5.5.1	Mass Budget.....	84
5.5.2	Power Budget.....	84
5.5.3	Link Budget.....	85
5.5.4	Data Storage Budget.....	85
5.5.5	Pointing Budget.....	86
5.6	Technical Challenges.....	86
5.7	Mission Environment	87
6	Supporting Observations and Models	89
6.1	Space-Based Observations Supporting Solar Orbiter Science	89
6.1.1	Solar Probe Plus	89
6.1.2	Solar-C.....	89
6.2	Ground-Based Observations Supporting Solar Orbiter Science.....	90
6.3	Theory, Modelling, and Scientific Closure.....	90
7	Ground Segment and Operations.....	93
7.1	Ground Segment Facilities and Services.....	93
7.1.1	Ground Stations and Communications Network.....	93
7.1.2	Mission Operations Centre.....	93
7.2	Science Operations	94
7.2.1	Science Operations Centre	94
7.2.2	Science Operations Planning.....	94
7.2.3	Sample Science Orbits	95
7.2.4	Inter-Instrument Communication and Burst Mode	95
7.3	Mission Operations Concept	96
7.3.1	Principles.....	96
7.3.2	Spacecraft Operations Approach.....	96
7.3.3	Payload Operations Approach.....	97
7.3.4	Data Delivery	97
7.3.5	Mission Planning.....	97
7.3.6	Science Management Plan	98
8	Management.....	101
8.1	Project Background Within the Cosmic Vision Programme	101
8.2	Procurement Approach, Industrial Organization and Project Phasing	101
8.3	ESA-NASA Collaboration.....	102
8.4	Summary Master Schedule.....	103
8.5	Management Requirements	103
A	Appendix.....	105
A.1	References	105
A.2	Acronyms.....	107

Mission Description

Solar Orbiter Mission Summary	
Top-level Science Questions	<ul style="list-style-type: none"> • How and where do the solar wind plasma and magnetic field originate in the corona? • How do solar transients drive heliospheric variability? • How do solar eruptions produce energetic particle radiation that fills the heliosphere? • How does the solar dynamo work and drive connections between the Sun and the heliosphere?
Science Payload	<ul style="list-style-type: none"> • Heliospheric In-Situ Instruments: <ul style="list-style-type: none"> • Solar Wind Analyser (SWA) • Energetic Particle Detector (EPD) • Magnetometer (MAG) • Radio and Plasma Wave analyser (RPW) • Solar Remote-Sensing Instruments: <ul style="list-style-type: none"> • Polarimetric and Helioseismic Imager (PHI) • EUV full-Sun and high-resolution Imager (EUI) • EUV spectral Imager (SPICE) • X-ray spectrometer/telescope (STIX) • Coronagraph (METIS) • Heliospheric Imager (SoloHI)
Mission Profile	<ul style="list-style-type: none"> • Launch on NASA-provided Evolved Expendable Launch Vehicle (Ariane 5 as back-up) • Interplanetary cruise with chemical propulsion and gravity assists at Earth and Venus • Venus resonance orbits with multiple gravity assists to increase inclination
Spacecraft	3-axis stabilized platform, heat shield, two adjustable, 2-sided solar arrays, dimensions: 2.5 x 3.0 x 2.5 m ³ (launch configuration)
Orientation	Sun-pointing
Telemetry Band	Dual X-band
Data Downlink	150 kbps (at 1 AU S/C-Earth distance)
Launch Date	Jan-2017 (Mar-2017 and Sep-2018 back-ups)
Nominal Mission Duration	7 years (incl. cruise phase)
Extended Mission Duration	3 years
Post-Ops & Archiving	2 years
Ground Station	Malargüe (Argentina), 35-m antenna, 4 to 8 hours/day (effective)
Programmatic	<ul style="list-style-type: none"> • ESA is responsible for the Solar Orbiter spacecraft, transfer to nominal science orbit, mission operations • NASA is responsible for launch vehicle provision and launch operations • Science payload provided by ESA member states and NASA

Foreword

Over the last 12 years since the first Solar Orbiter mission studies were conducted, results from new missions have become available that show that the scientific relevance and timeliness of the mission have only increased. The extent of the recent solar minimum, much deeper than any in the space age, was not predicted and serves to illustrate both the complexity of solar activity and the challenges remaining in our quest to understand the Sun.

The Solar Orbiter mission was first discussed at the meeting “Crossroads for European Solar and Heliospheric Physics” held in March 1998, where the heliophysics community recommended to “launch an ESA Solar Orbiter as ESA’s [next flexible] mission, with possible international participation, [for launch] around 2007.” The kick-off meeting for a pre-assessment study of the “ESA Solar Orbiter” concept was held at ESTEC on 25 March 1999. Solar Orbiter was subsequently proposed in 2000 by E. Marsch et al., and was selected by the Science Programme Committee (SPC) in October 2000 as a Flexi-mission for launch after BepiColombo (in the 2008-2013 time frame). A number of internal and industrial studies were then carried out, including parallel system-level Assessment Studies performed in industry between April and December 2004. At its 107th meeting in June 2004, the SPC confirmed Solar Orbiter’s place in the Horizon 2000+ programme, with the goal of a launch in October 2013 and no later than May 2015.

Work continued on the mission and payload definition throughout 2005 and 2006, and at its meeting in February 2007, SPC instructed the Executive to find ways to implement Solar Orbiter within a financial envelope of 300 M€ (at 2006 EC). In response to this request, a Joint Science and Technology Definition Team comprising scientists and engineers appointed by ESA and NASA, studied the benefits to be gained by combining ESA’s Solar Orbiter mission and NASA’s Solar Sentinels into a joint programme.

This led to the release of an ESA Announcement of Opportunity (AO) for the Solar Orbiter payload on 18 September 2007 and a NASA Small Explorer Focused Opportunity for Solar Orbiter AO that was issued on 22 October 2007. In total, 14 proposals were received by ESA in response to the Payload AO. The final report of the Payload Review Committee (PRC), giving a recommended payload for selection, was issued on 24 May 2008. Meanwhile, at its meeting in November 2007, SPC gave approval to start an 18-month industrial Phase B1 study lead by Astrium UK, which started in March 2008.

A major change in the progress of Solar Orbiter occurred in November 2008, when SPC decided to integrate it into the first planning cycle of Cosmic Vision 2015-25 as an M-mission candidate for the first launch opportunity in 2017. In addition, in view of NASA’s high prioritization of Solar Probe Plus (SPP) and its strong science synergies with Solar Orbiter, ESA called for an independent review of the PRC’s recommended payload, now in the context of a joint Solar Orbiter-SPP scientific programme. The joint ESA-NASA review panel confirmed the validity of the recommended payload in its report of March 2009. As a result, the instrument selections, as recommended by the PRC in 2008, were formally announced on 20 March 2009. In parallel, NASA announced the results of the FOSO selection, and selected 2 instruments and portions of 2 instruments to be included in the Solar Orbiter payload. In March 2011, NASA informed ESA that, as a consequence of budgetary pressures, it had become necessary to reduce its contribution to the payload to 1 full instrument and 1 sensor. Specifically, the Spectral Imaging of the Coronal Environment and Suprathermal Ion Spectrograph investigations would not be funded. Given the scientific importance of these investigations, their measurement capabilities will be recovered through the inclusion of European-lead instruments with contributions from member states and ESA.

At its 128th meeting on 17-18 February 2010, ESA’s Science Programme Committee recommended that Solar Orbiter be one of the three M-class candidates to proceed into definition phase and made a further programmatic change by endorsing a “fast track” approach outlined in ESA/SPC(2010)3, rev. 1. This approach was based on the scientific acceptability of increasing the minimum perihelion to 0.28 AU and making maximum re-use of BepiColombo technologies. Furthermore, it called for the start of the spacecraft implementation programme (Phase B2) in early 2011, with a view, if selected, to mission approval and adoption by the SPC in October 2011, leading to a launch in 2017. In line with this approach, the industrial Phase B2 activities were kicked-off in February 2011, and the System Requirements Review was completed in mid-2011. This report presents an overview of the Solar Orbiter mission in its present state of advanced definition, based largely on the recent industrial activities, and demonstrates the scientific importance of the mission as the next logical step in solar and heliospheric physics.

Authorship and Acknowledgements

The material for this report, an update to the Assessment Study Report ESA/SRE(2009)5, was provided by the members of the Solar Orbiter Science Working Team, together with the ESA Solar Orbiter Project Team, the ESA Study Scientists, the industrial study team led by Astrium UK, and members of the science community. The final document was compiled and edited by the ESA Study Scientists.

Key contributions to the science and payload sections were provided by:

Ester Antonucci (Obs. Torino)	Glenn Mason (JHU/APL, Laurel)
Arnold Benz (FHNW, Windisch)	Valentin Martinez Pillet (IAC, La Laguna)
Craig DeForest (SwRI, Boulder)	Chris Owen (UCL/MSSL)
Richard Harrison (RAL, Didcot)	Pierre Rochus (CSL, Liège)
Don Hassler (SwRI, Boulder)	Javier Rodriguez-Pacheco (U. Alcalá)
Timothy Horbury (ICSTM, London)	Sami Solanki (MPS, Lindau)
Russ Howard (NRL, Washington, DC)	Marco Velli (JPL/U. Firenze)
William Lewis (SwRI, San Antonio)	Angelos Vourlidas (NRL, Washington, DC)
Milan Maksimovic (Obs. Meudon)	Robert Wimmer-Schweingruber (U. Kiel)
Eckart Marsch (MPS, Lindau)	

Technical content was provided by:

Philippe Kletzkine (Project Manager, ESA)
 Giorgio Bagnasco (Payload System Manager, ESA)
 Christopher Jewell (System Engineer, ESA)
 Paolo Ferri (Mission Operations, ESA)
 José-Luis Pellón-Bailón (Mission Operations, ESA)
 José Manuel Sánchez Pérez (Mission Operations, ESA)
 Stephan Thürey (Lead Avionics System Engineer, ESA)
 Luis Sanchez (Science Operations, ESA)

ESA planning and coordination office:

Fabio Favata
 Philippe Escoubet

We wish to acknowledge the important contribution of the Organizing Committees of the four Solar Orbiter Workshops, in particular: Eckart Marsch, Valentin Martinez Pillet (chair, 1st Solar Orbiter Workshop), Kanaris Tsinganos (chair, 2nd Solar Orbiter Workshop), Ester Antonucci (chair, 3rd Solar Orbiter Workshop), Don Hassler and Chris St.Cyr (co-chairs, 4th Solar Orbiter Workshop). These workshops were essential in defining the mission's science and for maintaining the community involvement over the years.

Richard G. Marsden (Study Scientist, ESA)
 Daniel Müller (Deputy Study Scientist, ESA)

1 Executive Summary

We live in the extended atmosphere of the Sun, a region of space known as the heliosphere. Understanding the connections and the coupling between the Sun and the heliosphere is of fundamental importance to addressing one of the major scientific questions of Cosmic Vision 2020: “How does the Solar System work?” The heliosphere also represents a uniquely accessible domain of space, where fundamental physical processes common to solar, astrophysical and laboratory plasmas can be studied under conditions impossible to reproduce on Earth, or to study from astronomical distances. The results from missions such as Helios, Ulysses, Yohkoh, SOHO, TRACE, RHESSI, Hinode, STEREO, as well as the recently launched Solar Dynamics Observatory (SDO) mission, have formed the foundation of our understanding of the solar corona, the solar wind, and the three-dimensional heliosphere. Each of these missions had a specific focus, being part of an overall strategy of coordinated solar and heliospheric research. However, an important element of this strategy has yet to be implemented. None of these missions have been able to fully explore the interface region where the solar wind is born and heliospheric structures are formed with sufficient instrumentation to link solar wind structures back to their source regions at the Sun. For example, Helios 1 and 2 carried no imaging instruments. With previously unavailable observational capabilities provided by the powerful combination of in-situ and remote-sensing instruments and the unique inner-heliospheric mission design specifically tailored for the task, Solar Orbiter will address the central question of heliophysics: ***How does the Sun create and control the heliosphere?***

This primary, overarching scientific objective can be broken down into four interrelated scientific questions, all of which have strong, direct relevance to the Cosmic Vision theme “How does the Solar System work?” The four top-level scientific questions being addressed by Solar Orbiter are:

- How and where do the solar wind plasma and magnetic field originate in the corona?
- How do solar transients drive heliospheric variability?
- How do solar eruptions produce energetic particle radiation that fills the heliosphere?
- How does the solar dynamo work and drive connections between the Sun and the heliosphere?

These are outstanding fundamental questions in solar and heliophysics today. By addressing them, we will make major breakthroughs in our understanding of how the inner solar system works and is driven by solar activity.

To answer these questions, it is essential to make in-situ measurements of the solar wind plasma, fields, waves, and energetic particles close enough to the Sun that they are still relatively pristine and have not had their properties modified by subsequent transport and propagation processes. This is one of the fundamental drivers for the Solar Orbiter mission, which will approach the Sun to 0.28 AU.

Relating these in-situ measurements back to their source regions and structures on the Sun requires simultaneous, high-resolution imaging and spectroscopic observations of the Sun in and out of the ecliptic plane. The resulting combination of in-situ and remote-sensing instruments on the same spacecraft, together with the new, inner-heliospheric perspective, distinguishes Solar Orbiter from all previous and current missions, enabling breakthrough science which can be achieved in no other way.

Mission Design. A mission profile for Solar Orbiter has been developed that will, for the first time, make it possible to study the Sun with a full suite of in-situ and remote-sensing instruments from as close as 0.28 AU and provide imaging and spectral observations of the Sun’s polar regions from out of the ecliptic. This proximity to the Sun will also have the advantage that the spacecraft will have periods of reduced angular velocity of the spacecraft with respect to the solar surface, allowing observations of solar surface features and their connection to the heliosphere for significantly longer periods than from near-Earth vantage points.

The baseline mission is planned to start in January 2017 with a launch on a NASA-provided launch vehicle from Cape Canaveral, placing the spacecraft on a ballistic trajectory that will be combined with planetary gravity assist manoeuvres (GAM) at Earth and Venus. The second Venus GAM places the spacecraft into a 4:3 resonant orbit with Venus at a perihelion radius of 0.284 AU. The first perihelion at this close distance to the Sun is reached 3.5 years after launch. This orbit is the start of the sequence of resonances 4:3-4:3-3:2-5:3 that is used to raise gradually the solar inclination angle at each Venus GAM. The resulting operational orbit has a period of 168 days during the nominal mission with a minimum perihelion radius of 0.28 AU. The end of the

nominal mission occurs 7 years after launch, when the orbit inclination relative to the solar equator reaches 25°. The inclination may be further increased during an extended mission phase using additional Venus GAMs, to reach a maximum of 34° for the January 2017 baseline and 36° for a launch in March 2017.

Scientific Payload. The majority of the scientific payload elements of Solar Orbiter will be provided by ESA member states, NASA and ESA, and has already been selected and funded for the definition phase through a competitive AO selection process. These are:

The in-situ instruments:

- The Solar Wind Analyser (SWA) instrument suite (C. J. Owen, PI, UK) will fully characterize the major constituents of the solar wind plasma (protons, alpha particles, electrons, heavy ions) between 0.28 and 1.4 AU.
- The Energetic Particle Detector (EPD) experiment (J. R. Pacheco, PI, Spain) will measure the properties of suprathermal ions and energetic particles in the energy range of a few keV/n to relativistic electrons and high-energy ions (100 MeV/n protons, 200 MeV/n heavy ions).
- The Magnetometer (MAG) experiment (T. S. Horbury, PI, UK) will provide detailed in-situ measurements of the heliospheric magnetic field.
- The Radio and Plasma Waves (RPW) experiment (M. Maksimovic, PI, France) will measure magnetic and electric fields at high time resolution and determine the characteristics of electromagnetic and electrostatic waves in the solar wind from almost DC to 20 MHz.

The remote-sensing instruments:

- The Polarimetric and Helioseismic Imager (PHI, S. K. Solanki, PI, Germany) will provide high-resolution and full-disk measurements of the photospheric vector magnetic field and line-of-sight velocity as well as the continuum intensity in the visible wavelength range.
- The Extreme Ultraviolet Imager (EUI, P. Rochus, PI, Belgium) will provide image sequences of the solar atmospheric layers from the photosphere into the corona.
- The Spectrometer/Telescope for Imaging X-rays (STIX) (A. O. Benz, PI, Switzerland) provides imaging spectroscopy of solar thermal and non-thermal X-ray emission from ~4 to 150 keV.
- The Multi Element Telescope for Imaging and Spectroscopy (METIS) Coronagraph (E. Antonucci, PI, Italy) will perform broad-band and polarized imaging of the visible K-corona, narrow-band imaging of the UV and EUV corona and spectroscopy of the most intense lines of the outer corona.
- The Solar Orbiter Heliospheric Imager (SoloHI, R. A. Howard, PI, U.S.) will image both the quasi-steady flow and transient disturbances in the solar wind over a wide field of view by observing visible sunlight scattered by solar wind electrons.
- A European-lead extreme ultraviolet imaging spectrograph with contributions from ESA member states and ESA. This instrument will remotely characterize plasma properties of regions at and near the Sun, based on the previously selected Spectral Imaging of the Coronal Environment (SPICE) investigation. For simplicity, this payload element will be referred to as SPICE in this document.

Spacecraft. The Solar Orbiter spacecraft is a Sun-pointed, 3-axis stabilized platform, with a dedicated heat shield to provide protection from the high levels of solar flux near perihelion. Feed-throughs in the heat shield (with individual doors) provide the remote-sensing instruments with their required fields-of-view to the Sun. Two-sided solar arrays provide the capability to produce the required power throughout the mission over the wide range of distances from the Sun using rotation about their longitudinal axis to allow switching between faces, as well as control of the solar aspect angle to allow management of the array temperature throughout the mission, particularly during closest approach to the Sun. An articulated high-temperature high-gain antenna provides nominal communication with the ground station, and a medium gain antenna and two low gain antennas are included for use as backup. The design drivers for the Solar Orbiter spacecraft come not only from the need to satisfy the mission's technical and performance requirements, but also from the need to minimize the total cost of the mission. The adopted philosophy is therefore to avoid technology development as far as possible, in order to maintain the cost-cap of the mission in keeping with its M-class status. The design of Solar Orbiter has therefore incorporated BepiColombo technology items where appropriate. Furthermore, design

heritage from the Express series of missions, with their goal of rapid and streamlined development, has also featured heavily in the Solar Orbiter spacecraft design.

Mission Operations. One of the strengths of the Solar Orbiter mission is the synergy between in-situ and remote-sensing observations, and each science objective requires coordinated observations between several in-situ and remote-sensing instruments. Another unique aspect of Solar Orbiter, in contrast to near-Earth observatory missions like SOHO, is that Solar Orbiter will operate much like a planetary encounter mission, with the main scientific activity and planning taking place during the near-Sun encounter part of each orbit. Specifically, observations with the remote-sensing instruments will be organized into three 10-day intervals centered around perihelion and either maximum latitude or maximum corotation passages. As a baseline, the in-situ instruments will operate continuously during normal operations. Another important aspect of this mission, from a science operations standpoint, is that every science orbit is different, with different orbital characteristics (Sun-spacecraft distance, Earth-spacecraft distance, etc.). Science and operations planning for each orbit is therefore critical, with specific orbits expected to be dedicated to specific science problems. This will be similar to what has been used successfully in the ESA/NASA SOHO mission's Joint Observation Programs (JOPs).

Science Management and Data Archiving. Planning for Solar Orbiter is already quite mature, with science planning in particular already under way. Science teams have been formed for each science problem, which includes representatives from each instrument team, as well as theorists and modelers from the broader international scientific community. Data archiving will follow the same model as previous ESA PI-led solar and heliospheric missions, such as SOHO, with data made available to the scientific community through the ESA science data archive.

International Cooperation. Solar Orbiter is an ESA-led mission with strong NASA participation. Specifically, NASA will provide the launch on an evolved expendable launch vehicle (EELV), and parts (1 complete instrument, 1 sensor) of the scientific payload. The mission also has important synergies with NASA's Solar Probe Plus mission, and coordinated observations are expected to enhance greatly the scientific return of both missions. In the overall international context, Solar Orbiter is ESA's primary contribution to the International Living With a Star (ILWS) initiative, and joint studies incorporating data from all missions operating in the inner heliosphere (or providing remote-sensing observations of the near-Sun environment) will contribute greatly to our understanding of the Sun and its environment.

Conclusion. Solar Orbiter is a mature mission with focused and timely scientific objectives directly relevant and important to the Cosmic Vision science programme. Its powerful combination of in-situ and remote-sensing instruments and unique mission design make Solar Orbiter ideally suited to answer several of the outstanding, fundamental questions in solar and heliophysics today. By addressing them, Solar Orbiter will achieve major breakthroughs in our understanding of how the inner solar system works and how it is driven by solar activity, as well as improve our understanding of fundamental physical processes common to all solar, astrophysical, and laboratory plasmas.

2 Science Objectives

Solar Orbiter's mission is to address the central question of heliophysics: *How does the Sun create and control the heliosphere?* This, in turn, is a fundamental part of the second science question of ESA's Cosmic Vision: *"How does the solar system work?"*¹ Solar Orbiter is specifically designed to identify the origins and causes of the solar wind, the heliospheric magnetic field, solar energetic particles, transient interplanetary disturbances, and even the Sun's magnetic field itself.

The supersonic solar wind, driven by dynamic plasma and magnetic processes at the Sun's surface, expands to surround the solar system's planets and the space far beyond. Below the surface, the solar dynamo drives magnetic fields whose buoyancy brings them to the surface where they form huge arcades of loops which contain enormous amounts of stored energy. These magnetic loops are stretched and sheared by the Sun's differential rotation and unknown surface processes, eventually erupting in explosions which eject magnetic structures that fly into the solar system, occasionally impacting the Earth and its magnetic shield with disruptive effects on space and terrestrial systems. Understanding the complex physical processes at work in this system is the central goal of heliophysics. Since the Sun and presumably the heliosphere are typical of less massive stars and their stellar spheres, these studies are relevant to astrophysics, but are unique since the Sun alone is close enough for detailed study.

Over the past 20 years, an international effort to understand the Sun and heliosphere has been undertaken with an array of spacecraft carrying out both remote observations at visible, UV, and X-ray wavelengths, as well as in-situ observations of interplanetary plasmas, particles, and fields. Combined and coordinated observations from missions such as Ulysses, Yohkoh, SOHO, TRACE, RHESSI, Hinode, STEREO and SDO have resulted in an enormous advance in our understanding of the Sun and heliosphere and have proven that critical progress in understanding the physics underlying the Sun-heliosphere connection requires both remote and in-situ observations working together.

Although our vantage point at 1 AU is close by astrophysical measures, it has been long known that much of the crucial physics in the formation and activity of the heliosphere takes place much closer to the Sun, and that by the time magnetic structures, shocks, energetic particles and solar wind pass by Earth they have already evolved and in many cases mixed so as to blur the signatures of their origin (Figure 2.1). With the proven effectiveness of combined remote and in-situ studies on the missions cited above, it is clear that *the critical new advances will be achieved by flying a spacecraft combining remote and in-situ observations into the inner solar system*. From this inner heliospheric vantage point, solar sources can be identified and studied accurately and combined with in-situ observations of solar wind, shocks, energetic particles, etc., before they evolve significantly. The expertise gained by the international scientific community on our existing missions has been used to design Solar Orbiter to provide the complete set of required measurements. Solar Orbiter is the next critical step in our exploration of the Sun and heliosphere.

Here we outline the major physical problems that Solar Orbiter will address; subsequent sections expand on each major question and demonstrate how Solar Orbiter will address them.

How and where do the solar wind plasma and magnetic field originate in the corona? The solar corona continuously expands and develops into a supersonic wind that extends outward, interacting with itself and with the Earth and other planets, to the heliopause boundary with interstellar space, far beyond Pluto's orbit. The solar wind has profound effects on planetary environments and on the planets themselves – for example, it is responsible for many of the phenomena in Earth's magnetosphere and is thought to have played a role in the evolution of Venus and Mars through the erosion of their upper atmospheres.

Two classes of solar wind – 'fast' and 'slow' – fill the heliosphere, and the balance between them is modulated by the 11-year solar cycle. The fast solar wind (~700 km/s and comparatively steady) is known to arise from coronal holes. The slow solar wind (~400-500 km/s) permeates the plane of the ecliptic during most of the solar cycle so it is important to Earth's space environment. The slow solar wind shows different mass flux and composition than the fast wind, consistent with confined plasma in the solar corona. The specific escape mechanism through the largely closed magnetic field is not known since candidate sites and mechanisms

¹ Solar Orbiter also has direct relevance to Cosmic Vision Goal #3 ("What are the fundamental physical laws of the Universe?").

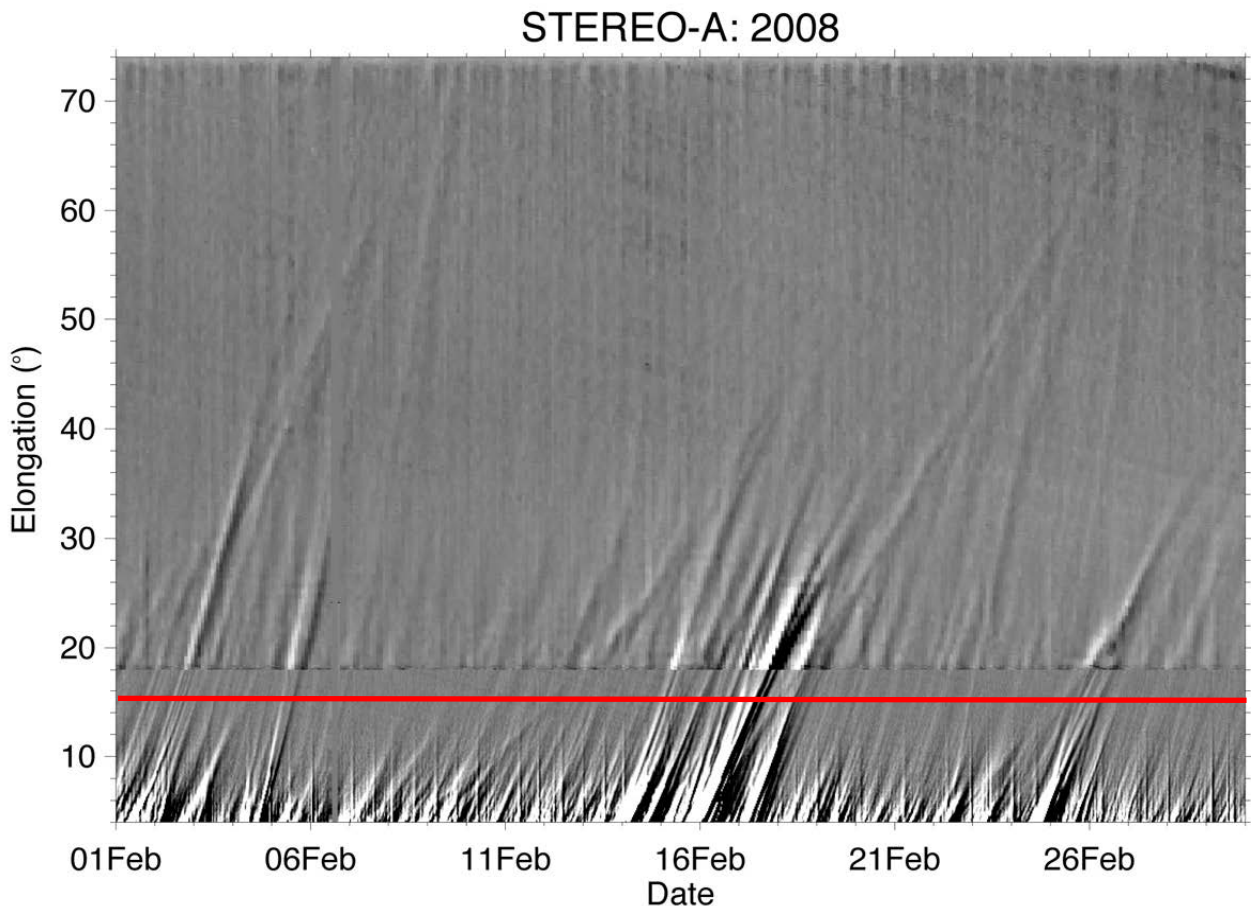


Figure 2.1. Small-scale structures flowing in the solar wind are visible as diagonal lines in this plot from the STEREO Heliospheric Imager instrument, moving further from the Sun (elongation) with time. Structures moving at different speeds collide and merge, smoothing out the flow and removing information about their relative origins. Solar Orbiter will travel to 0.28 AU, corresponding to an elongation of 15.6° (red horizontal line), making it possible to measure unevolved small-scale solar wind structures for the first time. (Figure courtesy J. Davies, Rutherford Appleton Laboratory, UK.)

cannot be resolved from 1 AU. Fast and slow wind carry embedded turbulent fluctuations, and these also display different properties compatible with different solar origins. It is thought that such fluctuations may be responsible for the difference in heating and acceleration between different solar wind streams.

Understanding the physics relating the plasma at the solar surface and the heating and acceleration of the escaping solar wind is crucial to understanding both the effects of the Sun on the heliosphere and how stars in general lose mass and angular momentum to stellar winds.

How do solar transients drive heliospheric variability? The largest transient events from the Sun are coronal mass ejections (CMEs), large structures of magnetic field and material that are ejected from the Sun at speeds up to 3000 km/s. CMEs are also of astrophysical interest since they are the dominant way that stars shed both magnetic flux and magnetic helicity that build up as a result of the stellar dynamo. Interplanetary CMEs (ICMEs) are the major cause of interplanetary shocks, but the locations and mechanisms by which shocks form around them is not known since this occurs in the inner solar system. Similarly, the longitudinal structure of ICMEs is not observable from the ecliptic, while its extent has a large impact on the acceleration of energetic particles. ICMEs are a major cause of geomagnetic storms but their effectiveness at disrupting the magnetosphere is only loosely related to the parent CME, because the evolution of the propagating cloud with the surrounding heliosphere is complex and has not been well studied. These unknowns have direct impact on our ability to predict transient ‘space weather’ events that affect Earth.

How do solar eruptions produce energetic particle radiation that fills the heliosphere? Like many astrophysical systems, the Sun is an effective particle accelerator. Large solar energetic particle (SEP) events

produce highly energetic particles that fill the solar system with ionizing radiation. CME driven shocks can produce relativistic particles on time scales of minutes, and many CMEs convert $\sim 10\%$ of their kinetic energy into energetic particles. Other processes produce high-energy particles on magnetic loops without involving shocks. The multiple processes operating in SEP events are not well understood or distinguishable from observations at 1 AU. In particular, particles accelerated in the corona and inner heliosphere are scattered by inhomogeneities in the interplanetary magnetic field (IMF) before they arrive at Earth, destroying much of the information they carry about the processes that accelerated them. Particle transport and scattering in the inner solar system are poorly understood since the turbulence properties cannot be determined from 1 AU. The actual seed population of particles energized by CME-driven shocks in the inner solar system is unexplored, and needs to be understood to construct a complete picture of particle acceleration in shock-related events.

How does the solar dynamo work and drive connections between the Sun and the heliosphere? The Sun's magnetic field connects the interior of the star to interplanetary space and its evolution is dominated by a quasi-periodic 11-year activity cycle that modulates the form of the heliosphere and strongly affects the space environment throughout the solar system. The large-scale solar field is generated in the Sun's interior, within the convection zone, by a dynamo driven by complex three-dimensional mass flows that transport and process magnetic flux. Despite notable advances in our knowledge and understanding of solar magnetism made possible by Ulysses, SOHO, and Hinode observations as well as by recent theoretical models and numerical simulations, fundamental questions remain about the operation of the solar dynamo and the cyclic nature of solar magnetic activity. Of paramount importance to answering these questions is detailed knowledge of the transport of flux at high latitudes and the properties of the polar magnetic field. To date, however, the solar high latitudes remain poorly known owing to our dependence on observations made from the ecliptic. In addition to questions about the global dynamo and the generation of the large-scale field, there are unanswered questions about the origin of the small-scale internetwork field observed in the quiet photosphere. Is this weak field produced by turbulent local dynamo action near the solar surface?

2.1 How and where do the solar wind plasma and magnetic field originate in the corona?

Significance of the question. Hot plasma in the Sun's atmosphere flows radially outward into interplanetary space to form the solar wind, filling the solar system and blowing a cavity in the interstellar medium known as the heliosphere. During solar minimum, large-scale regions of a single magnetic polarity in the Sun's atmosphere – polar coronal holes – open into space and are the source of high speed (~ 700 km/s), rather steady solar wind flows (Figure 2.2). There is also a slow wind (300-500 km/s) that emanates from magnetically complex regions at low latitudes and the periphery of coronal holes. It is highly variable in speed, composition, and charge state. The origin of the slow wind is not known. At solar maximum, this stable bimodal configuration gives way to a more complex mixture of slow and fast streams emitted at all latitudes, depending on the distribution of open and closed magnetic regions and the highly tilted magnetic polarity inversion line.

The fast wind from the polar coronal holes carries magnetic fields of opposite polarity into the heliosphere, which are then separated by the heliospheric current sheet (HCS) embedded in the slow wind. Measurements over a range of latitudes far from the Sun show that this boundary is not symmetric around the Sun's equator, but is on average displaced southward. This offset must reflect an asymmetry on the Sun; but since there cannot be a mismatch between the inward and outward magnetic flux on the Sun, its origin is unclear. In situ, the HCS is warped and deformed by the combined effects of solar rotation and inclination of the Sun's magnetic axis, effects that are even more prominent at solar maximum.

The energy that heats the corona and drives the wind comes from the mechanical energy of convective photospheric motions, which is converted into magnetic and/or wave energy. In particular, both turbulence and magnetic reconnection are implicated theoretically and observationally in coronal heating and acceleration. However, existing observations cannot adequately constrain these theories, and the identity of the mechanisms that heat the corona and accelerate the solar wind remains one of the unsolved mysteries of solar and heliospheric physics. How the coronal plasma is generated, energized, and the way in which it breaks loose from the confining coronal magnetic field are fundamental physical questions with crucial implications for

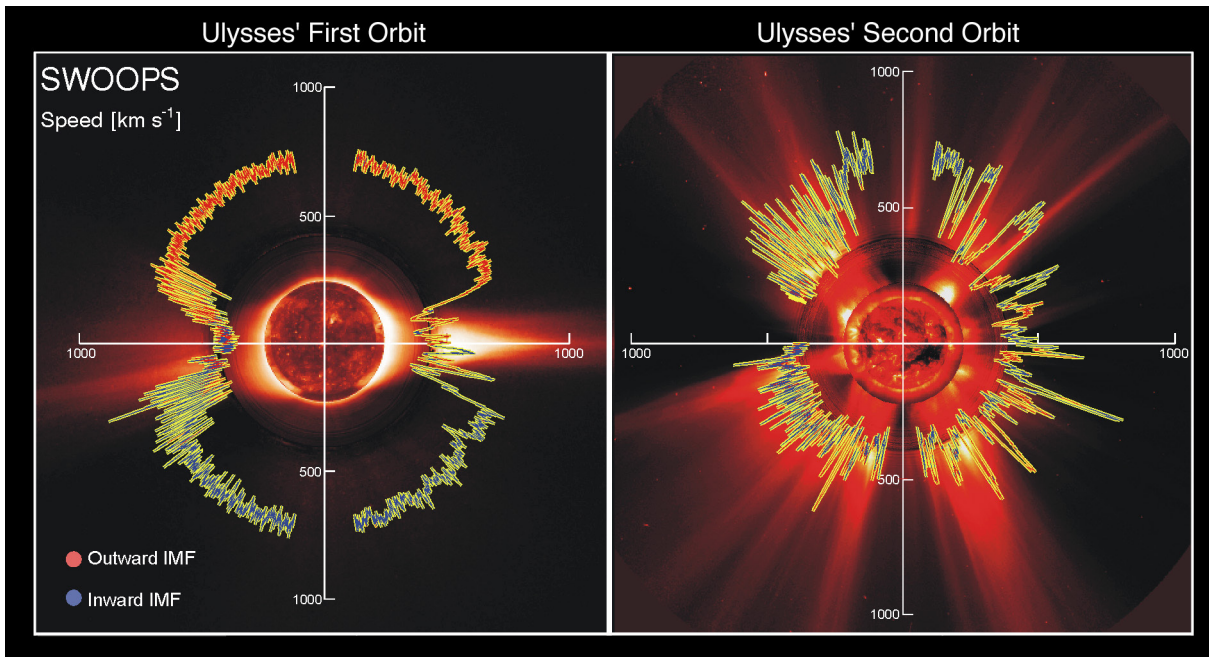


Figure 2.2. Polar plots of the solar wind speed, colored by the interplanetary magnetic field (IMF) polarity for Ulysses' first two polar orbits. The earliest times are on the left (nine o'clock position) and progress around counterclockwise. The characteristic solar images for solar minimum for cycle 22 (left), solar maximum for cycle 23 (right) are from SOHO EIT and C2 coronagraph and the Mauna Loa K coronameter. Through a unique combination of remote-sensing and in-situ measurements, Solar Orbiter will map structures measured in the inner heliosphere to features observed in the corona. (Figure from McComas et al. 2008)

predicting our own space environment, as well as for the understanding of the natural plasma physics of other astrophysical objects, from other stars, to accretion disks and their coronae, to energetic phenomena such as jets, X- and gamma-ray bursts, and cosmic-ray acceleration.

The solar wind contains waves and turbulence on scales from millions of kilometres to below the electron gyroradius. The turbulence scatters energetic particles, affecting the flux of particles that arrives at the Earth; local kinetic processes dissipate the turbulent fluctuations and heat the plasma. Properties of the turbulence vary with solar wind stream structure, reflecting its origins near the Sun, but the turbulence also evolves as it is carried into space with the solar wind, blurring the imprint of coronal conditions and making it difficult to determine its physical origin. The inner heliosphere, where Solar Orbiter will conduct its combination of remote-sensing and in-situ observations, provides the ideal laboratory for understanding the magnetohydrodynamic turbulence of natural plasmas expected to be ubiquitous in astrophysical environments.

Below we discuss in more detail three interrelated questions which flow down from this top-level question: What are the source regions of the solar wind and the heliospheric magnetic field? What mechanisms heat and accelerate the solar wind? What are the sources of turbulence in the solar wind and how does it evolve?

2.1.1 What are the source regions of the solar wind and the heliospheric magnetic field?

Present state of knowledge. At large scales, the structure of the solar wind and heliospheric magnetic field and their mapping to the solar corona are reasonably well understood. However, extending this global understanding of the overall connection between the corona and the solar wind deeper into the solar atmosphere and to the photosphere where the magnetic field can be measured has been difficult due to the dynamically evolved state of the plasma measured in situ at 1 AU and to the lack of simultaneous in-situ measurements and high-cadence, high-resolution remote sensing of solar plasma. A number of fundamental questions remain unanswered both about the source of the fast and slow solar wind and about the source of the magnetic field that the solar wind carries into the heliosphere.

Source regions of the solar wind. The speed of the solar wind is empirically anti-correlated with the (modelled) expansion rate of the magnetic field with radial distance close to the Sun (Wang and Sheeley 2006),

where central areas of polar coronal holes give rise to the fastest solar wind streams, while regions closer to the coronal hole boundary give rise to progressively slower wind. Within coronal holes, strong outflows are well correlated with the intense flux elements found at the intersection of the photospheric supergranular cells; these expand into the corona as ‘funnels,’ preferentially from regions dominated by flux of the dominant hole polarity (Tu et al. 2005; McIntosh et al. 2006).

The source region of the wind, at chromospheric and transition region heights, is extremely structured and dynamic (Figure 2.3). The chromosphere is permeated by spicules, cool and dense jets of chromospheric plasma. Spicules have been thought to be too slow and cold to contribute significantly to the solar wind, but a more dynamic type of spicule, with shorter lifetimes, faster motions, and a hotter plasma component has recently been discovered by Hinode. Such spicules also support waves, possibly with sufficient energy to accelerate fast wind streams in coronal holes (De Pontieu et al. 2009, 2011).

Hinode has also observed the frequent occurrence of very small-scale X-ray jets in polar coronal holes (Cirtain et al., 2007). Given the high velocities and frequency of these events, it has been suggested that they contribute to the fast solar wind. Their relation to the photospheric magnetic field, however, has not been established as the high latitudes at which they are observed hamper the accurate determination of their photospheric footpoints from the ecliptic plane. Other fine-scale ray-like structures – coronal plumes – permeate coronal holes and are correlated with small-scale bipolar structures inside the hole. Ultraviolet measurements show that these structures are cooler than the surrounding background hole plasma, and have slower, but denser outflows. In-situ measurements reveal the existence of faster and slower microstreams within the fast wind (Neugebauer et al. 1995) as well as other fine-scale structures (Thieme et al. 1990), but the two have not been unambiguously linked to coronal features.

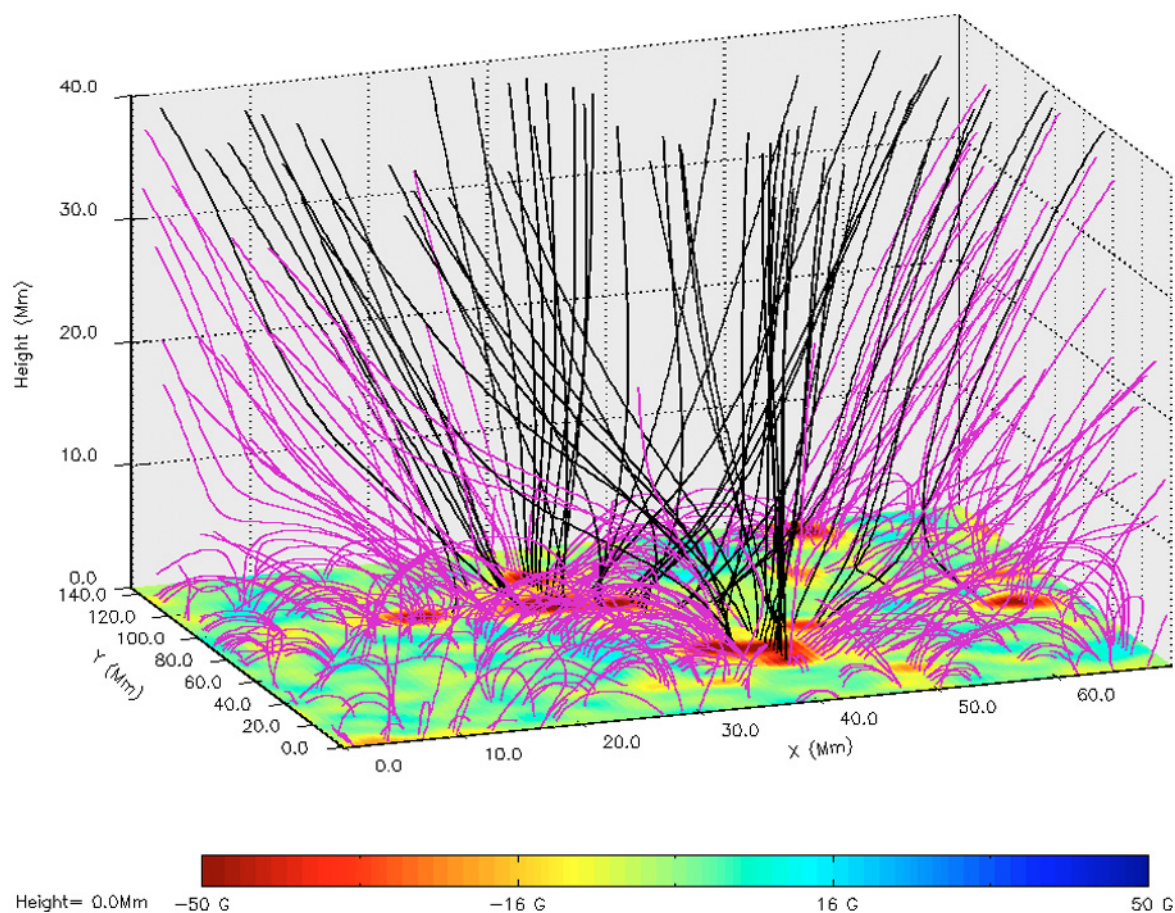


Figure 2.3. The modelled magnetic field of the transition region and lower corona in a polar coronal hole based on measurements of the photospheric magnetic field strength. The figure illustrates the complex connections between the solar surface and space: only the black field lines extend far from the surface. A central goal of Solar Orbiter is to establish the links between the observed solar wind streams and their sources back on the Sun. Understanding the dynamics of the Sun’s magnetic atmosphere and its signatures in the measured solar wind holds the key to understanding the origin of all solar wind flows. (Figure from Marsch et al. 2006)

The anticorrelation of expansion/wind speed suggests that the slow wind is accelerated along those open field lines with the greatest expansion rate, notably corresponding to the bright rays at the coronal hole-streamer interface (e.g., Wang et al. 2007) and to outflows from coronal hole boundaries (Antonucci et al. 2005). However, composition measurements tend to call this notion into question: a significant elemental fractionation is observed in the solar wind plasma relative to that of the photosphere (e.g., Geiss and Bochsler 1985), which scales with the first ionization potential (FIP). Metallic ions, with low FIP, are more abundant in the solar wind than mid- or high-FIP elements, when compared with their photospheric compositions (von Steiger et al. 1997). Ulysses has revealed a systematic difference in the degree of fractionation depending on the solar wind type. Fast wind associated with coronal holes has a composition similar to that of the photosphere, whereas the slow solar wind is characterized by a substantially larger degree of fractionation.

The alternative is that magnetic reconnection between closed and open field lines plays a fundamental role in slow wind generation. Closed magnetic field lines close to the Sun confine the plasma in loops, where the compositional differentiation occurs, but these are continuously destroyed when neighbouring open field lines are advected into them. Interchange reconnection between the open and closed field allows the plasma to flow outwards into space (Figure 2.4). This process should occur predominantly at the coronal hole boundary, but may also be active in the intermediate areas of quiet Sun.

Additional contributions to the slow wind could arise from the opening of previously closed field lines in the middle and lower corona, from the tops of helmet streamers or the complex magnetic fields around active regions (Figure 2.5), for example, releasing plasma blobs or plasmoids into the heliosphere. White-light coronagraph observations show streamer blobs that might be plasmoids or might be pile-up from reconnection high in the corona. Finally, there might be a continuous outward leakage of plasma from high in the solar corona where the plasma pressure becomes comparable to the magnetic pressure in the weak field at the apex of closed loops.

Source regions of the heliospheric magnetic field. Our current knowledge of the surface magnetic field of the Sun and its extension into the solar atmosphere and interplanetary space is based on measurements of the photospheric line-of-sight – and recently, vector – magnetic field, coupled with spacecraft measurements of the field in situ. The vast majority of the magnetic flux from the Sun closes in the lower layers of the solar atmosphere, within the chromosphere and lower corona, in multiple small scale bipolar regions with strong local fields, and it is only a small fraction which extends high enough in the solar atmosphere to be dragged out into the heliosphere by the solar wind. In addition, the intense magnetic fields in the lower atmosphere are highly variable and dynamic at scales extending down to instrument resolution limits in both time and space, continuously reconnecting and contributing to the intense activity, spicules and jets in the chromosphere and lower corona. The magnetic connection between the solar wind and the solar source therefore hinges on

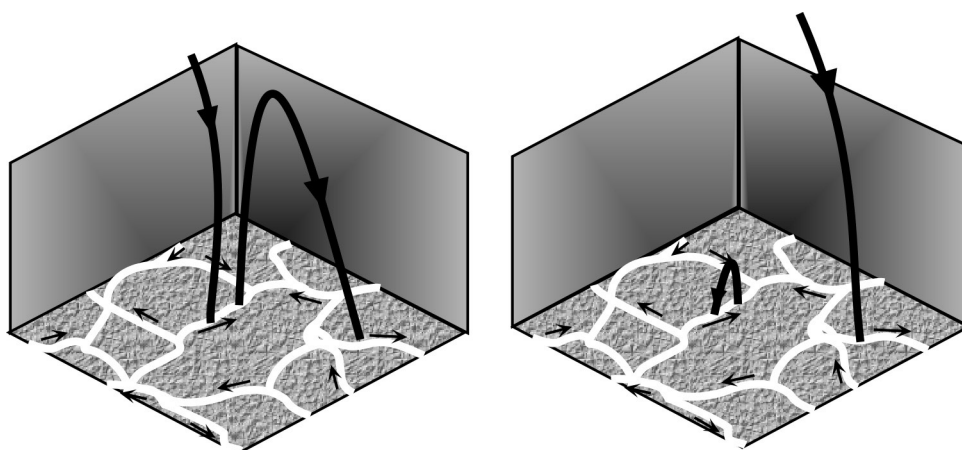


Figure 2.4. Convective cells (white lines) in the photosphere can bring together oppositely directed magnetic field lines (left). These can undergo ‘interchange reconnection,’ altering which field lines open into space and which close back to the surface (right). This process is thought to be important in generating the slow solar wind flow, as well as moving magnetic flux over the solar cycle, but observational evidence for it is currently weak. Solar Orbiter will combine high resolution observations of photospheric motion and magnetic fields with measurements of the solar wind and magnetic field flowing outward to determine the quantitative effects of interchange reconnection for the first time. (Figure from Fisk and Zurbuchen 2006)

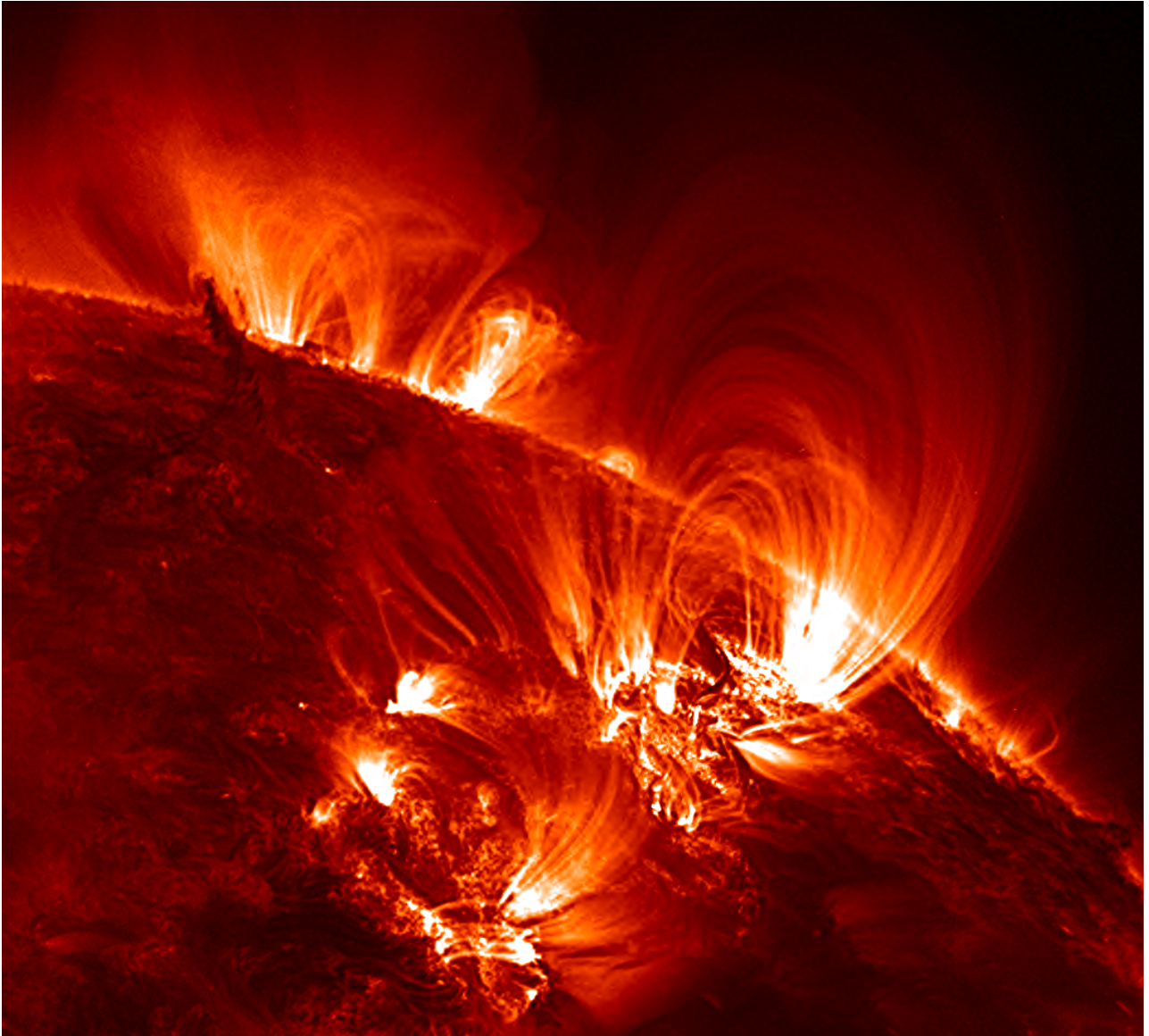


Figure 2.5. Ultraviolet emission from plasma in the Sun's atmosphere, revealing the complex magnetic field structures around active regions. Solar Orbiter will test theories of solar wind plasma emerging from such regions. (SDO AIA image)

understanding what determines the amount of open flux from the Sun, how open field lines are distributed at the solar surface at any given time, and how these open field lines reconnect and change their connection across the solar surface in time, processes which are controlled by interchange reconnection.

The HCS is embedded in slow solar wind and, like the slow wind, is full of small-scale structure. The origin of fine-scale structure in the magnetic field is therefore directly related to the origin of the slow solar wind. One of the most surprising results regarding the heliospheric current sheet is that it is not symmetric around the equator, but appears to be displaced southward by around 10° (Smith et al. 2000) during solar minima, causing a difference in cosmic ray fluxes between hemispheres. Similar asymmetries exist in the Sun's polar magnetic fields and even sunspot numbers, but what is the origin of this asymmetry, and how does the Sun produce it in space?

How Solar Orbiter will address the question. Solar Orbiter will measure the solar wind plasma and magnetic field in situ while simultaneously performing remote-sensing measurements of the photosphere and corona, thus allowing the properties of the solar wind measured in situ to be correlated with structures observed in the source regions at the Sun. During the perihelion segments of the orbit when the spacecraft is in near-corotation with the Sun, Solar Orbiter will determine the plasma parameters and compositional signatures of the solar wind, which can be compared directly with the spectroscopic signatures of coronal ions with differing charge-

to-mass ratios and FIP. Solar Orbiter will determine magnetic connectivity by measuring energetic electrons and the associated X-rays and radio emissions and using these measurements to trace the magnetic field lines directly to the solar source regions. Photospheric magnetic field measurements, together with those made in situ, will allow the coronal magnetic field to be reconstructed by extrapolation with well-defined boundary conditions. Extreme ultraviolet imaging (EUV) imaging and spectroscopy will provide the images and plasma diagnostics needed to characterize the plasma state in the coronal loops, which can erupt and deliver material to solar wind streams in the outer corona. As Solar Orbiter observes different source regions, from active regions to quiet Sun to coronal holes, hovering for substantial amounts of time in each during the near-corotation periods, it will be able to answer the question of the origin of the solar wind.

EUV spectroscopy and imaging are needed to detect magnetic reconnection in the transition region and corona – e.g., by the observation of plasma jets or of explosive events as seen in the heavy-ion Doppler motions believed to mark the reconnection-driven plasma outflow. These events appear to be associated with impulsive energetic particle bursts observed near 1 AU. The study of the time evolution of such events, and of their particle and radiation outputs, can reveal whether reconnection is quasi-steady or time-varying, and a comparison with magnetic field data will indicate the locations of the reconnection sites with respect to the overall magnetic field structure and topology. Solar Orbiter’s coronagraph and imager will construct global maps of the H and He outflow velocity and measure the degree of correlation of wind speed and He fraction.

Using the coronagraph to measure the velocity, acceleration, and mass density structures in the accelerating wind, Solar Orbiter will simultaneously provide images of solar structure from the chromosphere to the corona. Within the solar wind, the plasma and fields instrument suites will measure the radial, latitudinal, and longitudinal gradients of plasma and field parameters in the inner heliosphere, providing information fundamental to diagnosing the connection of the solar wind with the coronal structure. Combining Solar Orbiter data from the in-situ and remote-sensing instruments taken at different intervals will make it possible to determine the relative contributions of plumes, jets, and spicules to the fast wind.

2.1.2 What mechanisms heat and accelerate the solar wind?

Present state of knowledge. Despite more than a half-century of study, the basic physical processes responsible for heating the million-degree corona and accelerating the solar wind are still not known. Identification of these processes is important for understanding the origins and impacts of space weather and to make progress in fundamental stellar astrophysics.

Ultimately, the problem of solar wind acceleration is a question of the transfer, storage, and dissipation of the abundant energy present in the solar convective flows. The key question is to establish how a small fraction of that energy is transformed into magnetic and thermal energy above the photosphere. Both emerging magnetic flux and the constant convective shaking and tangling of magnetic field lines already threading the corona contribute to the processing of the energy in what is an extremely structured, highly dynamic region of the solar atmosphere, the route to dissipation involving cascading turbulence, current sheet collapse and reconnection, shocks, high-frequency waves, and wave-particle interactions. The advent of high-cadence high-resolution observations has demonstrated the extremely complex phenomenology of the energy flux in the lower atmosphere, including many types of transient events discovered and classified by Yohkoh, SOHO, TRACE, RHESSI, Hinode and, most recently, SDO.

Energy deposited in the corona is lost in the form of conduction, radiation (negligible in coronal holes), gravitational enthalpy, and kinetic energy fluxes into the accelerating solar wind plasma. Transition region pressures, coronal densities and temperatures, and the asymptotic solar wind speed are sensitive functions of the mode and location of energy deposition. The mass flux is not, however, as it depends only on the amplitude of the energy flux (Hansteen and Leer 1995). A relatively constant coronal energy flux therefore explains the small variations in mass flux between slow and fast solar wind found by Ulysses during its first two orbits, although the dramatic decrease in mass flux over the present cycle points also to a decreased efficiency of coronal heating and therefore to its dependence on the solar magnetic field (McComas et al. 2008; Schwadron and McComas 2008).

One of the fundamental experimental facts that has been difficult to account for theoretically is that the fast solar wind originates in regions where the electron temperature and densities are low, while the slow solar wind comes from hotter regions of the corona. The anticorrelation of solar wind speed with electron temperature is

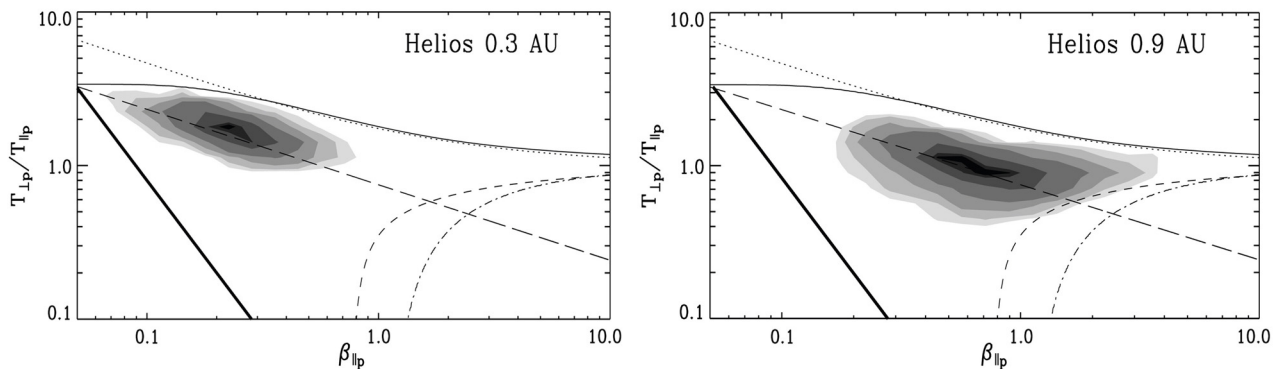


Figure 2.6. Histograms of the solar wind proton temperature anisotropy (ratio of perpendicular to parallel temperatures) versus the plasma pressure parallel to the field (parallel plasma beta) in the fast solar wind measured at two different radial distances by Helios. The dark line shows the decrease of anisotropy expected if the wind were expanding adiabatically without heating (dark continuous), and the actual distribution function contours with best fit of the run of anisotropy. Instability threshold conditions for the ion-cyclotron (solid), the mirror (dotted), the parallel (dashed) and oblique (dash-dotted) fire hose instabilities are also shown. Distribution functions display perpendicular heating and evolve towards marginal stability with distance from the Sun. Solar Orbiter will determine initial conditions for the perpendicular anisotropies and help determine the nature of the plasma-wave interactions responsible for this heating. (From Matteini et al. 2007)

confirmed by the anti-correlation between wind speed and ‘freezing in’ temperature of the different ionization states of heavy ions in the solar wind (Geiss et al. 1995) and implies that the electron pressure gradient does not play a major role in the acceleration of the fast wind. On the other hand, the speed of the solar wind is positively correlated with the in-situ proton temperature, and the fastest and least collisionally coupled wind streams also contain the largest distribution function anisotropies. Observations of the very high temperatures and anisotropies of coronal heavy ions suggest that other processes such as magnetic mirror and wave-particle interactions should also contribute strongly to the expansion of the fast wind (Li et al. 1998; Kohl et al. 1997, 1998, 2006; Doderio et al. 1998). In particular, either the direct generation of high-frequency waves close to the cyclotron resonance of ions or the turbulent cascade of energy to those frequencies should play an important role (Figure 2.6).

Theoretical attempts to develop self-consistent models of fast solar wind acceleration have followed two somewhat different paths. First, there are models in which the convection-driven jostling of magnetic flux tubes in the photosphere drives wave-like fluctuations that propagate up into the extended corona. The waves partially reflect back toward the Sun, develop into strong turbulence, and/or dissipate over a range of heights. These models also tend to attribute the differences between the fast and slow solar wind not to any major differences in the lower boundary conditions, but to the varying expansion factor of magnetic field lines in different areas of coronal holes (Cranmer et al. 2007, and references therein).

In the second class of models, the interchange reconnection models, the energy flux usually results from magnetic reconnection between closed, loop-like magnetic flux systems (which are in the process of emerging, fragmenting, and being otherwise jostled by convection) and the open flux tubes that connect to the solar wind. Here the differences between fast and slow solar wind result from qualitatively different rates of flux emergence, reconnection, and coronal heating in different regions on the Sun (Axford and McKenzie 1992; Fisk et al. 1999; Schwadron and McComas, 2003).

It has been difficult to evaluate competing models of fast wind acceleration and to assess observationally the relative contributions of locally emerging magnetic fields and waves to the heat input and pressure required to accelerate the wind largely because of the absence of measurements of the solar wind close to the Sun where they can be mapped with sufficient precision to a solar source region.

How Solar Orbiter will address the question. Solar Orbiter’s combination of high-resolution measurements of the photospheric magnetic field together with images and spectra at unprecedented spatial resolution will make it possible to identify plasma processes such as reconnection/shock formation and wave dissipation in rapidly varying surface features, observe Doppler shifts of the generated upflows, and determine compositional

signatures. Whatever the scale, magnetic reconnection leads to particle dissipative heating and acceleration and wave generation, which have the net effect of a local kinetic energy increase in the lower solar atmosphere that can be revealed through high-resolution extreme ultraviolet (EUV) imaging and spectroscopy. Wave propagation will be traced from the source site to the region of dissipation through observations of EUV-line broadening and Doppler shifts.

Global maps of the H and He outflow velocity, obtained by applying the Doppler dimming technique to the resonantly scattered component of the most intense emission lines of the outer corona (H I 121.6 and He II 30.4 nm), will provide the contours of the maximum coronal expansion velocity gradient for the two major components of the solar wind, and the role of high-frequency cyclotron waves will be comprehensively assessed by measuring spectroscopically the particle velocity distribution across the field and determining the height where the maximum gradient of outflow velocity occurs (Telloni et al. 2007).

Solar Orbiter's heliospheric imager will measure the velocity, acceleration, and mass density of structures in the accelerating wind, allowing precise comparison with the different acceleration profiles of turbulence-driven and interchange reconnection-driven solar wind models.

As it is performing imaging and spectroscopic observations of the corona and photosphere, Solar Orbiter will simultaneously measure in situ the properties of the solar wind emanating from the source regions. The in-situ instrumentation will determine all of the properties predicted by solar wind acceleration models: speed, mass flux, composition, charge states, and wave amplitudes. Moving relative slowly over the solar surface near perihelion, Solar Orbiter will measure how properties of the solar wind vary depending on the changing properties of its source region, as a function of both space and time, distinguishing between competing models of solar wind generation.

2.1.3 What are the sources of turbulence in the solar wind and how does it evolve?

Present state of knowledge. The solar wind is filled with turbulence and instabilities. At large scales, the fast solar wind is dominated by anti-sunward propagating Alfvén waves thought to be generated by photospheric motions. At smaller scales, these waves decay and generate an active turbulent cascade, with a spectrum similar to the Kolmogorov hydrodynamic scaling of $f^{5/3}$. In the slow solar wind, turbulence does not have a dominant Alfvénic component, and it is fully developed over all measured scales. There is strong evidence that the cascade to smaller scales is anisotropic, but it is not known how the anisotropy is generated or driven (Horbury et al. 2008). What do the differences between the turbulence observed in the fast wind and that observed in the slow wind reveal about the sources of the turbulence and of the wind itself?

Little is known about what drives the evolution of solar wind turbulence. Slow-fast wind shears, fine-scale structures, and gradients are all candidate mechanisms (Tu and Marsch 1990; Breech et al. 2008). To determine how the plasma environment affects the dynamical evolution of solar wind turbulence it is essential to measure the plasma and magnetic field fluctuations in the solar wind as close to the Sun as possible, before the effects of mechanisms such as velocity shear become significant, and then to observe how the turbulence evolves with heliocentric distance.

The dissipation of energy in a turbulent cascade contributes to the heating of the solar wind plasma. However, while measurements of the properties of solar wind turbulence in near-Earth orbit largely agree with observed heating rates (Smith et al. 2001; Marino et al. 2008), the details are controversial and dependent on precise models of turbulent dynamics. In order to establish a full energy budget for the solar wind, the heating rates as a function of distance and stream properties must be determined, including turbulence levels before the cascade develops significantly.

The statistical analysis of the fluctuating fields also reveals pervasive fine-scale structure (e.g., discontinuities and pressure balanced structures). The origin of these structures is uncertain: are they the remnant of complex coronal structuring in the form of strands of small-scale flux tubes advected by the solar wind flow (Borovsky 2008; Bruno et al. 2001), or are they generated locally by turbulent fluctuations?

At scales around the proton gyroradius and below, turbulent fluctuations interact directly with the solar wind ions. The precise nature of the turbulent cascade below the proton gyroradius is poorly understood and might even vary depending on local plasma conditions. Below the electron gyroradius, conditions are even less certain and the partitioning of turbulent energy into electron or ion heating is unknown at this time. In addition, solar wind expansion constantly drives distribution functions toward kinetic instabilities, where fluctuations

with characteristic signatures are generated (e.g., Marsch 2006). What physical role do kinetic effects play with distance from the Sun? What role do wave-particle interactions play in accelerating the fast solar wind? What contribution do minor ions make to the turbulent energy density in near-Sun space?

How Solar Orbiter will address the question. Solar Orbiter will measure waves and turbulence in the solar corona and solar wind over a wide range of latitudes and distances, including closer to the Sun than ever before, making it possible to study turbulence before it is significantly affected by stream-stream interactions. By travelling over a range of distances, the spacecraft will determine how the turbulence evolves and is driven as it is carried anti-sunward by the solar wind flow.

Detailed in-situ data will make it possible to distinguish between competing theories of turbulent dissipation and heating mechanisms in a range of plasma environments and are thus of critical importance for advancing our understanding of coronal heating and of the role of turbulence in stellar winds.

By entering near-corotation close to the Sun, Solar Orbiter will be able to distinguish between the radial, longitudinal, and temporal scales of small-scale structures, determining whether they are the signatures of embedded flux tubes or are generated by local turbulence.

Solar Orbiter's magnetic and electric field measurements, combined with measurement of the full distribution functions of the protons and electrons will fully characterize plasma turbulence over all physically relevant time scales from very low frequencies to above the electron gyrofrequency. Because Solar Orbiter is a three-axis stabilized spacecraft, it can continuously view the solar wind beam with its proton instrument, measuring proton distributions at the gyroperiod and hence making it possible directly to diagnose wave-particle interactions in ways that are not possible on spinning spacecraft. By travelling closer to the Sun than ever before, it will measure wave-particle interactions before the particle distributions have fully thermalized, studying the same processes that occur in the corona. By measuring how the distributions and waves change with solar distance and between solar wind streams with different plasma properties, Solar Orbiter will make it possible to determine the relative effects of instabilities and turbulence in heating the plasma.

The solar wind is the only available plasma 'laboratory' where detailed studies of magnetohydrodynamic (MHD) turbulence can be carried out free from interference with spatial boundaries, and in the important domain of very large magnetic Reynolds numbers. Detailed comparison between experimental in-situ data and theoretical concepts will provide a more solid physical foundation for MHD turbulence theory, which will be of critical importance for understanding the solar (stellar) coronal heating mechanism and the role of turbulence in the solar (a stellar) wind.

2.2 How do solar transients drive heliospheric variability?

Significance of the question. The dynamic Sun exhibits many forms of transient phenomena, such as flares, CMEs, eruptive prominences, and shock waves. Many directly affect the structure and dynamics of the outflowing solar wind and thereby also eventually affect Earth's magnetosphere and upper atmosphere, with significant consequences for society through hazards to, for example, space-based technology systems and surface power systems. Understanding these impacts, with the ultimate aim of predicting them, has received much attention during the past decade and a half under the banner of 'space weather.' However, many fundamental questions remain about the physics underpinning these phenomena and their origins, and these questions must be answered before we can realistically expect to be able to predict the occurrence of solar transients and their effects on geospace and the heliosphere. These questions are also pertinent, within the framework of the 'solar-stellar connection,' to our understanding of other stellar systems that exhibit transient behaviour such as flaring (e.g., Getman et al. 2008).

Solar Orbiter will provide a critical step forward in understanding the origin of solar transient phenomena and their impact on the heliosphere. Located close to the solar sources of transients, Solar Orbiter will be able both to determine the inputs to the heliosphere and to measure directly the heliospheric consequences of eruptive events at distances close enough to sample the fields and plasmas in their pristine state, prior to significant processing during their propagation to 1 AU. Solar Orbiter will thus be a key augmentation to the chain of solar-terrestrial observatories in Earth orbit and at the libration points, providing a critical perspective from its orbit close to the Sun and out of the ecliptic.

Below we discuss in more detail three interrelated questions which flow down from this top-level question:

How do CMEs evolve through the corona and inner heliosphere? How do CMEs contribute to solar magnetic flux and helicity balance? How and where do shocks form in the corona and inner heliosphere?

2.2.1 How do CMEs evolve through the corona and inner heliosphere?

Present state of knowledge. Following earlier observations by space-based white-light coronagraphs, considerable progress in understanding CMEs has been achieved using data from the ESA-NASA SOHO mission, which provides continuous coverage of the Sun and combines coronagraphs with an EUV imager and off-limb spectrometer. Other spacecraft, such as ACE, WIND and Ulysses, which carried comprehensive in-situ instrumentation, have contributed significantly to our understanding of the interplanetary manifestation of these events. With a full solar cycle of CME observations, the basic features of CMEs are now understood. CMEs appear to originate from highly-sheared magnetic field regions on the Sun known as filament channels, which support colder plasma condensations known as prominences. Eruptions develop in the low corona within 10-15 minutes, while the associated shocks cross the solar disk within 1 hour. CMEs reach speeds of up to 3000 km/s and carry energies (kinetic, thermal and magnetic) of $\sim 10^{25}$ J ($= 10^{32}$ ergs). They can also accelerate rapidly during the very early stages of their formation, with the CME velocity being closely tied, in time, to the associated flare's soft X-ray light profile (Zhang and Dere 2006). High-resolution SOHO coronagraph images (Figure 2.7) have provided evidence for a magnetic flux rope structure in some CMEs as well as for post-CME

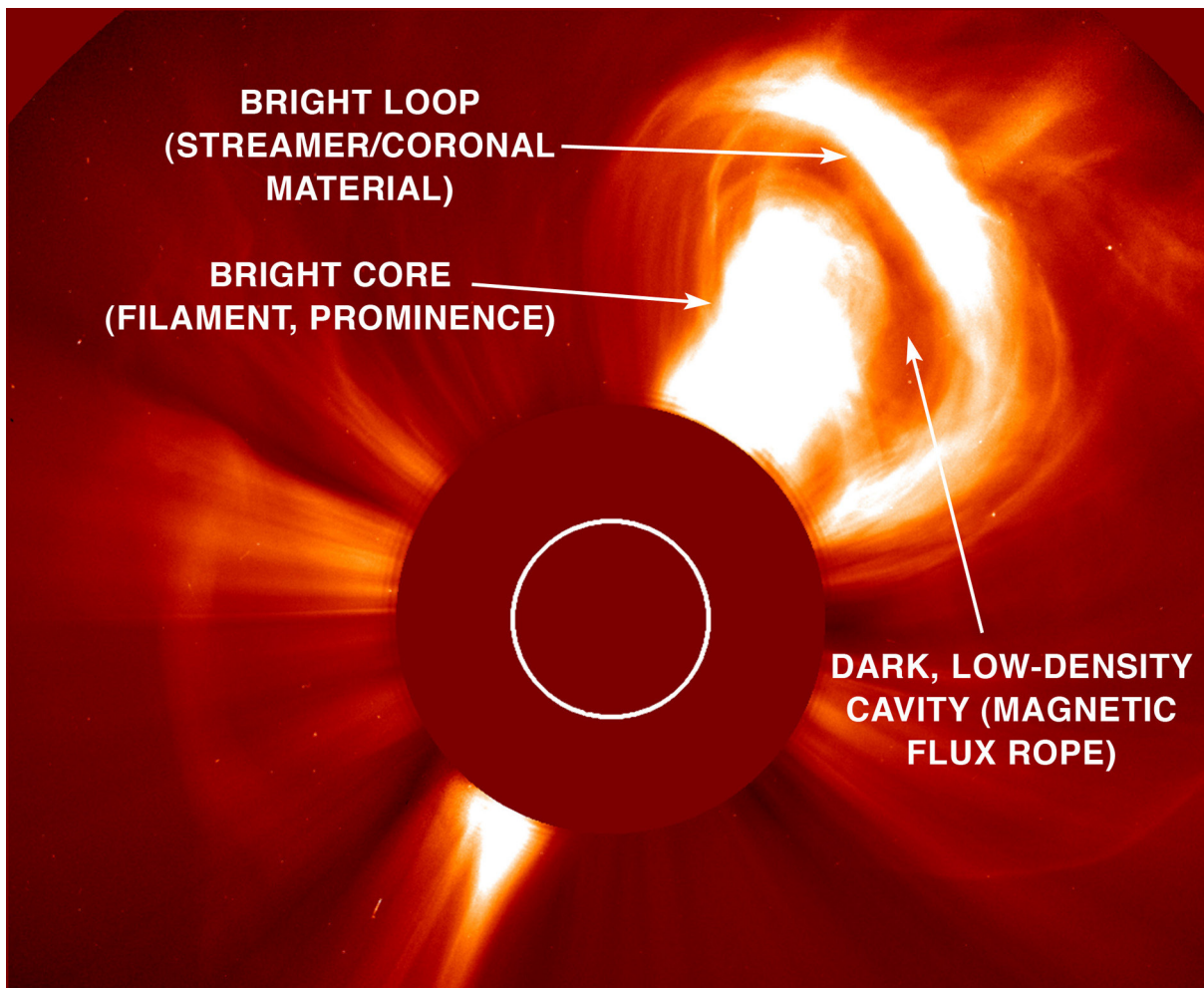


Figure 2.7. A coronal mass ejection (CME) on the solar limb as viewed by LASCO on SOHO in December, 2002. The dark, low-density region inside the structure formed by the bright loop of streamer material is thought to be the magnetic flux rope predicted by current CME initiation models. CMEs are believed to originate from prominence eruptions, yet in ICMEs observed at 1 AU prominence plasma (the bright core in this image) is very rarely detected. Solar Orbiter will, with its unique orbit, enable in-situ measurements of the ejecta and their radial (and out-of-the-ecliptic) evolution in much more detail than possible from Earth orbit, where many features have been washed out. (Adapted from the HELEX report)

current sheets. Both features are predicted by CME initiation models (e.g., Lin & Forbes 2000; Lynch et al. 2004).

STEREO observations are making it possible to chart in three dimensions the trajectories of CMEs in the corona and heliosphere, thereby improving our understanding of CME evolution and propagation. STEREO data have supported detailed comparison both of in-situ measurements with remote-sensing observations and of MHD heliospheric simulations with observations. The combination of high-cadence coronagraphic and EUV imaging simplifies the separation of the CME proper from its effects in the surrounding corona (Patsourakos and Vourlidas 2009) and allows a more accurate determination of its dynamics.

Despite the advances in our understanding enabled by SOHO and STEREO, very basic questions remain unanswered. These concern the source and initiation of eruptions, their early evolution, and the heliospheric propagation of CMEs. All current CME models predict that the topology of ICMEs is that of a twisted flux rope as a result of the flare reconnection that occurs behind the ejection. Observations at 1 AU, however, find that less than half of all ICMEs, even those associated with strong flares, have a flux rope structure (Richardson and Cane 2004). Many ICMEs at 1 AU appear to have a complex magnetic structure with no clearly-defined topology. Moreover, for ICMEs that do contain flux ropes, the orientation is often significantly different from that expected on the basis of the orientation of the magnetic fields in the prospective source region. CMEs are believed to originate from prominence eruptions, yet in ICMEs observed at 1 AU prominence plasma is very rarely detected. These major disconnects between theoretical models (of prominence eruption and CME propagation) and observations (remote and in situ) need to be resolved if any understanding of the CME process is to be achieved.

How Solar Orbiter will address the question. To advance our understanding of the structure of ICMEs and its relation to CMEs at the Sun beyond what has been achieved with SOHO and STEREO requires a combination of remote-sensing and in-situ measurements made at close perihelion and in near-corotation with the Sun. Through combined observations with its magnetograph, imaging spectrograph, and soft X-ray imager, Solar Orbiter will provide the data required to establish the properties of CMEs at the Sun and to determine how coronal magnetic energy is released into CME kinetic energy, flare-associated thermal/non-thermal particle acceleration, and heating. Observations with the imaging spectrograph will be used to determine the composition of CMEs in the low corona and to establish how they expand and rotate and will also provide vital clues to the energy partition within a CME once it is released. Solar Orbiter will make comprehensive in-situ measurements of the fields and plasmas (particularly composition) of ICMEs following their release and, critically, prior to their processing during propagation in the heliosphere. These measurements will allow the properties of an ICME to be related to those of the CME at the Sun and to the conditions in the CME source region as observed by Solar Orbiter's remote-sensing instruments and will make it possible to examine the evolution of CMEs in the inner heliosphere. Solar Orbiter's combination of remote-sensing and in-situ observations will also establish unambiguously the magnetic connectivity of the ICME and reveal how the magnetic energy within flux ropes is dissipated to heat and accelerate the associated particles. Solar Orbiter data will also reveal how the structure of the magnetic field at the front of a CME evolves in the inner heliosphere – a critical link in understanding, and eventually predicting, how transient events on the Sun may determine the geoeffective potential of the event.

To fully understand the physical system surrounding CME ejection, the temporal evolution of active regions and CME-related shocks and current sheets must be tracked from their formation in the corona to their expulsion in the solar wind. During the mission phases when the spacecraft is in near-corotation with the Sun, Solar Orbiter will continuously observe individual active regions, free from projection complications, over longer periods than are possible from Earth orbit. Solar Orbiter will thus be able to monitor the development of sheared magnetic fields and neutral lines and to trace the flux of magnetic energy into the corona. Observations from the vantage point of near-corotation will make it possible to follow the evolution of the current sheet behind a CME with unprecedented detail and to clarify the varying distribution of energy in different forms (heating, particle acceleration, kinetic).

2.2.2 How do CMEs contribute to the solar magnetic flux and helicity balance?

Present state of knowledge. Magnetic flux is transported into the heliosphere both by the solar wind, in the form of open flux carried mostly by the fast wind from polar coronal holes, and by coronal mass ejections, which drag closed flux with them as they propagate into the heliosphere. At some point the closed flux introduced by CMEs must be opened to avoid an unsustainable buildup of magnetic flux in the heliosphere. Measurements of the magnetic flux content of the heliosphere from near the Earth (covering more than 40 years and 4 cycles) show that the total amount of magnetic flux in the solar system changes over the solar cycle (Figure 2.8). Longer-term variations are also known to occur. Proxies such as geomagnetic activity and cosmic ray fluxes provide evidence that the average IMF strength has increased substantially in the last 100 years, perhaps by as much as a factor of 2. Surprisingly, however, during the recent solar minimum the IMF strength is lower than at any time since the beginning of the space age.

The relative contribution of the solar wind and CMEs to the heliospheric magnetic flux budget is an unresolved question, as is the process by which the flux added by the CMEs is removed. Models to explain the solar cycle variation assume a background level of open flux, to which CMEs add extra flux during solar maximum, increasing the intensity of the IMF. The exceptionally low intensity of the IMF during the current minimum has been attributed to the low rate of CME occurrence [Owens et al. 2008]. Alternatively, there may simply be no ‘background’ open flux level.

There is evidence that the flux introduced into the heliosphere by CMEs may be removed by magnetic reconnection within the trailing edges of CMEs, which disconnects the CME from the Sun or by interchange reconnection closer to the solar surface [e.g., Owens and Crooker 2006]. Recent observations show that the reconnection process occurs quite often in the solar wind, even when the magnetic field is not under compression. However, the rate and/or locations at which reconnection generally removes open flux are not at present known.

Together with magnetic flux, the solar wind and CMEs carry magnetic helicity away from the sun. Helicity is a fundamental property of magnetic fields in natural plasmas, where it plays a special role because it is conserved not only by the ideal dynamics, but also during the relaxation which follows instabilities and dissipation. Helicity is injected into the corona when sunspots and active regions emerge, via the twisting and braiding of magnetic flux. During the coronal heating process the overall helicity is conserved and tends to accumulate at the largest possible scales. It is natural to assume that critical helicity thresholds may be involved in the triggering of CMEs, but how solar eruptions depend on the relative amounts of energy and helicity injection during active region emergence and evolution is unknown. Yet this understanding could be a crucial element in the prediction of large solar events.

How Solar Orbiter will address the question. Fundamental to the question of contribution of CMEs to the heliospheric flux budget is the flux content of individual events. Encountering CMEs close to the Sun before

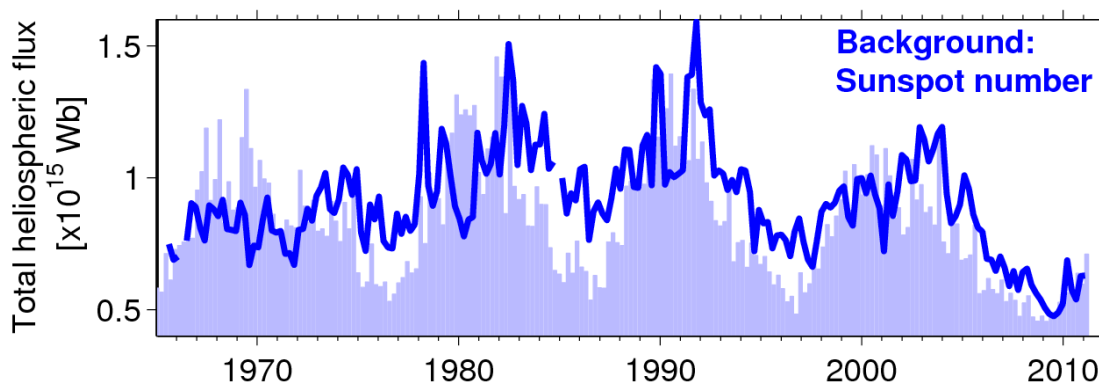


Figure 2.8. Near-Earth interplanetary magnetic field strength (thick line) for the last 45 years, with the sunspot number (background filled values). The magnetic field strength varies over the solar cycle, but was lower during the recent minimum than at any time since the beginning of the space age. The depth, as well as the length of this minimum was not predicted and is not understood. Solar Orbiter will investigate the evolving links between solar and interplanetary magnetic fields. (From M. Owens, University of Reading)

interplanetary dynamics affects their structure, Solar Orbiter will measure their magnetic flux content directly; comparisons with remote-sensing measurements of their source regions will clarify the relation between CME flux and the eruption process. As Solar Orbiter moves through the inner heliosphere, it will encounter CMEs at different solar distances, making it possible to quantify the effect of interplanetary dynamics on their apparent flux content.

The flux carried outwards by CMEs must eventually disconnect completely from the Sun, or interchange reconnect with existing open field lines. Solar Orbiter will diagnose the magnetic connectivity of the solar wind and CME plasma using suprathermal electron and energetic particle measurements. These particles, which stream rapidly along the magnetic field from the Sun, indicate whether a magnetic flux tube is connected to the Sun at one end, at both ends, or not at all. These particles disappear when the field is completely disconnected, or may reverse their flow direction as a result of interchange reconnection. However, scattering and reflection due to curved, tangled, or compressed magnetic field lines act to smear out these signatures with increasing solar distance, leading to ambiguity in connectivity measurements. Solar Orbiter, by travelling close to the Sun before this scattering is significant, will determine the original level of magnetic connectivity; covering a wide range of distances in the inner heliosphere, the spacecraft will measure how the connectivity changes as field lines are carried away from the Sun.

Solar Orbiter will also directly sample reconnection regions in the solar wind as they pass the spacecraft, determining their occurrence rates in the inner heliosphere as a function of distance and testing theories of CME disconnection by searching for reconnection signatures in the tails of CMEs.

The contribution to the heliospheric magnetic flux of small scale plasmoids, ejected from the tops of streamers following reconnection events, is unclear. Solar Orbiter, slowly moving above the solar surface during perihelion passes, will determine the magnetic structure, connectivity, and plasma properties including composition of these ejecta, using spectroscopic imaging observations to unambiguously link them to their source regions.

To assess the role of CMEs in maintaining the solar magnetic helicity balance, Solar Orbiter will compare the helicity content of active regions as determined from remote sensing of the photospheric magnetic field with that of magnetic clouds measured in situ. Such a comparison requires both extended remote-sensing observations of the same active region over the region's lifetime and in-situ measurements of magnetic clouds from a vantage point as close to the solar source as possible. Around its perihelia, Solar Orbiter will 'dwell' over particular active regions and observe the emergent flux for a longer interval (more than 22 days) than is possible from 1 AU, where perspective effects complicate extended observations. The resulting data will be used to calculate the helicity content of an active region, track its temporal variation, and determine the change in helicity before and after the launch of any CMEs. Should a magnetic cloud result from an eruptive event in the active region over which Solar Orbiter is dwelling, the relatively small heliocentric distances between the solar source and the spacecraft will make it highly probable that Solar Orbiter will directly encounter the magnetic cloud soon after its release. Determination of the cloud's properties and connectivity through Solar Orbiter's in-situ particle-and-fields measurements will enable the first-ever comparison of a magnetic cloud in a relatively unevolved state with the properties of the solar source, an impossibility with measurements made at 1 AU. The comparison of the helicity change in the source region with the value measured in the magnetic cloud will provide insight into the role of CMEs in the helicity balance of the Sun.

2.2.3 How and where do shocks form in the corona and inner heliosphere?

Present state of knowledge. The rapid expulsion of material during CMEs can drive shock waves in the corona and heliosphere. Shocks in the lower corona can also be driven by flares, and in the case of CME/eruptive flare events it may be difficult to unambiguously identify the driver (Vršnak and Cliver 2008). CME-driven shocks are of particular interest because of the central role they play in accelerating coronal and solar wind particles to very high energies in SEP events (see Section 2.3).

Shocks form when the speed of the driver is super-Alfvénic. The formation and evolution of shocks in corona and the inner heliosphere thus depend (1) on the speed of the driving CME and (2) on the Alfvén speed of the ambient plasma and its spatial and temporal variations. According to one model of the radial distribution of the Alfvén speed in the corona near active regions, for example, shocks can form essentially in two locations, in the middle corona ($1.2\text{-}3 R_{\text{Sun}}$), where there is an Alfvén speed minimum, and distances beyond an Alfvén

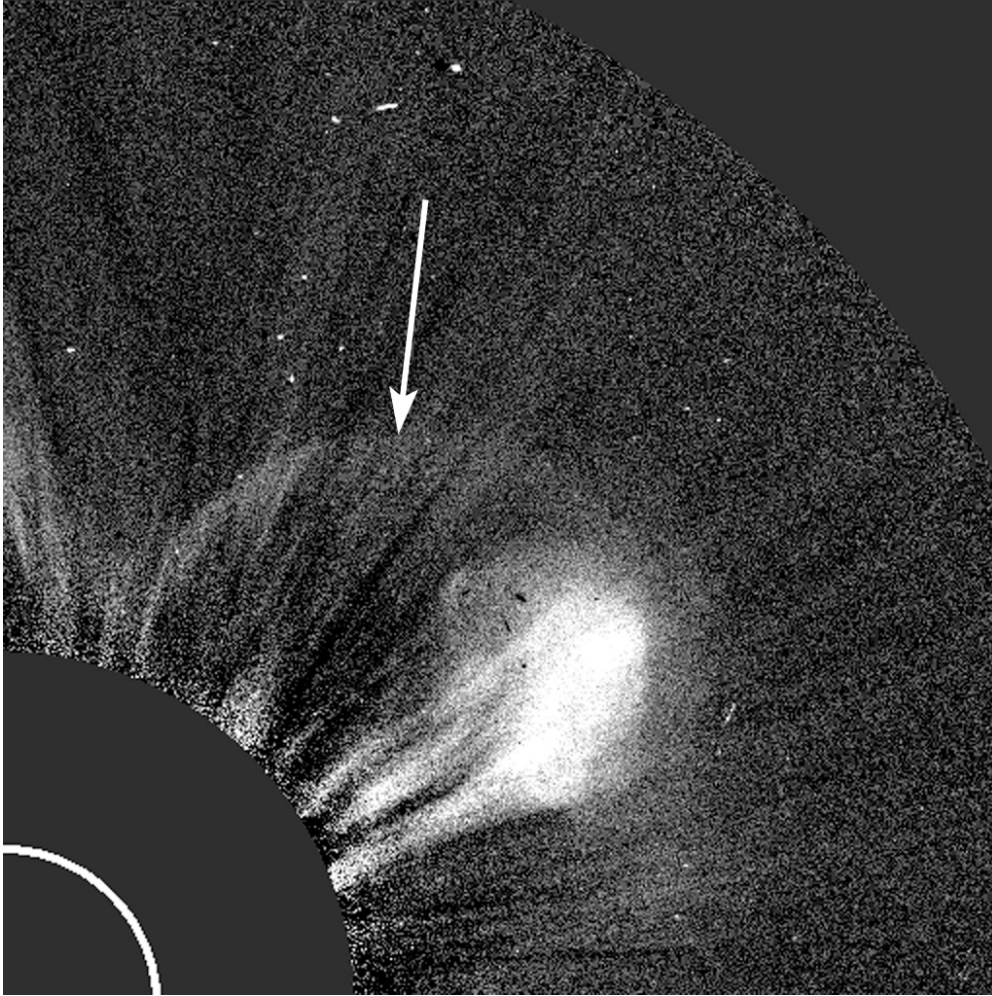


Figure 2.9. Example of a CME-driven shock signature in a coronagraph white light image. The image was taken by the LASCO/C2 coronagraph on 12/18/2000 at 02:06 UT. The CME is narrow and the shock appears as a parabolic front extending to the NW of the CME front. The occulter edge is at $2.2 R_{\text{Sun}}$ and the solar disk is marked by a white circle. With its remote-sensing instruments, Solar Orbiter will be able to observe the formation and evolution of shocks in the lower corona, and the in-situ instruments will measure the properties of the shock as it propagates through the inner heliosphere. This powerful combination of remote-sensing and in-situ measurements will help constrain models of shock formation and provide valuable insight into the role of CME-driven shocks in SEP acceleration. (From A. Vourlidas, NRL)

speed maximum at $\sim 4 R_{\text{Sun}}$ (Mann et al. 2003). A recent study of CMEs with and without type II radio bursts (indicative of shock formation) has shown that some of the fast and wide CMEs observed produced no shock or only a weak shock because they propagated through tenuous regions in the corona where the Alfvén velocity exceeded that of the CME (Gopalswamy et al. 2008). CME shock formation/evolution can also be affected by the interaction between an older, slower-moving CME and a faster CME that overtakes it. Depending on the Alfvén speed in the former, the interaction may result in the strengthening or weakening of an existing shock driven by the overtaking CME or, if there is no existing shock, the formation of one (Gopalswamy 2001; 2002).

Recent studies of LASCO images obtained during the rising phase of solar cycle 23 have demonstrated the feasibility of detecting CME-driven shocks from a few to $\sim 20 R_{\text{Sun}}$ and of measuring their density compression ratio and propagation direction (Vourlidas et al. 2003; Ontiveros and Vourlidas 2009) (Figure 2.9). This development has opened the way for the investigation of shock formation and evolution in the lower corona and heliosphere through Solar Orbiter’s combination of remote-sensing observations and in-situ measurements.

How Solar Orbiter will address the question. Understanding shock generation and evolution in the inner heliosphere requires knowledge of the spatial distribution and temporal variation of plasma parameters (density, temperature, and magnetic field) throughout the corona. Solar Orbiter’s remote-sensing measurements – in particular electron density maps derived from the polarized visible-light images and maps of the density and

outflow velocity of coronal hydrogen and helium – will provide much improved basic plasma models of the corona, so that the Alfvén speed and magnetic field direction can be reconstructed over the distance range from the Sun to the spacecraft. Remote sensing will also provide observations of shock drivers, such as flares (location, intensity, thermal/non-thermal electron populations, time-profiles), and manifestations of CMEs (waves, dimmings, etc.) in the low corona with spatial resolution of a few hundred kilometres and cadence of a few seconds. It will measure the acceleration profile of the latter and then track the CMEs through the crucial heights for shock formation ($2-10 R_{\text{Sun}}$) and provide speed, acceleration, and shock compression ratio measurements.

Type II bursts, detected by Solar Orbiter, will indicate shock-accelerated electron beams produced by the passage of a CME and thus provide warning of an approaching shock to the in-situ instruments. These in-situ plasma and magnetic field measurements will fully characterize the upstream and downstream plasma and magnetic field properties and quantify their microphysical properties, such as turbulence levels and transient electric fields (while also directly measuring any SEPs - cf. Section 2.3). Spacecraft potential measurements also allow for rapid determinations of the plasma density, and of electric and magnetic field fluctuations, on microphysical scales, comparable to the Doppler-shifted ion scales, which are characteristic of the spatial scales of shocks. The evolution of such parameters will provide insight into the processes dissipating shock fronts throughout the range of magnetic/velocity/density and pressure parameter space. Because of Solar Orbiter's close proximity to the Sun, the measurements of the solar wind plasma, electric field, and magnetic field will be unspoiled by the dynamical wind interaction pressure effects due to solar rotation and will provide the first reliable data on the magnetosonic speed, the spatial variation of the plasma pressure and magnetic field in the inner heliosphere. A recent MHD modelling study has shown that interactions among recurring CMEs and their shocks occur typically in the distance range around 0.2-0.5 AU (Lugaz et al. 2005). Solar Orbiter will spend significant time in the regions of recurring CME interactions and so will be able to investigate the effects of such interactions on the evolution of CME-driven shocks.

2.3 How do solar eruptions produce energetic particle radiation that fills the heliosphere?

Significance of the Question. Astrophysical sites throughout the solar system and galaxy have the universal ability to accelerate ions and electrons to high speeds, forming energetic particle radiation. Detected remotely from radio and light emission around supernovae remnants, the Sun, and planets, or directly from particles that reach our detectors, this radiation arises from the explosive release of stored energy that can cause magnetic fields to rearrange, or can launch shock waves which accelerate particles by repeatedly imparting many small boosts to their speed. The nearly universal occurrence of energetic particle radiation, along with the effects it can have on planetary environments, evolution of life forms, and space systems has fostered a broad interest in this phenomenon that has long made it a high priority area of investigation in space science. Since remote sites in the galaxy cannot be studied directly, solar system sources of energetic particles give the best opportunity for studying all aspects of this complex problem.

The Sun is the most powerful particle accelerator in the solar system, routinely producing energetic particle radiation at speeds close to the speed of light, sufficiently energetic to be detected at ground level on Earth even under the protection of our magnetic field and atmosphere. SEP events can severely affect space hardware, disrupt radio communications, and cause re-routing of commercial air traffic away from polar regions. In addition to large events, which occur roughly monthly during periods of high sunspot count, more numerous, smaller solar events can occur by the thousands each year, providing multiple opportunities to understand the physical processes involved. Below we discuss in more detail three interrelated questions that flow down from this top-level question: How and where are energetic particles accelerated at the Sun? How are energetic particles released from their sources and distributed in space and time? What are the seed populations for energetic particles?

2.3.1 How and where are energetic particles accelerated at the Sun?

Present state of knowledge. One of the two major physical mechanisms for energizing particles involves particles interacting with moving or turbulent magnetic fields, gaining small amounts of energy at each step

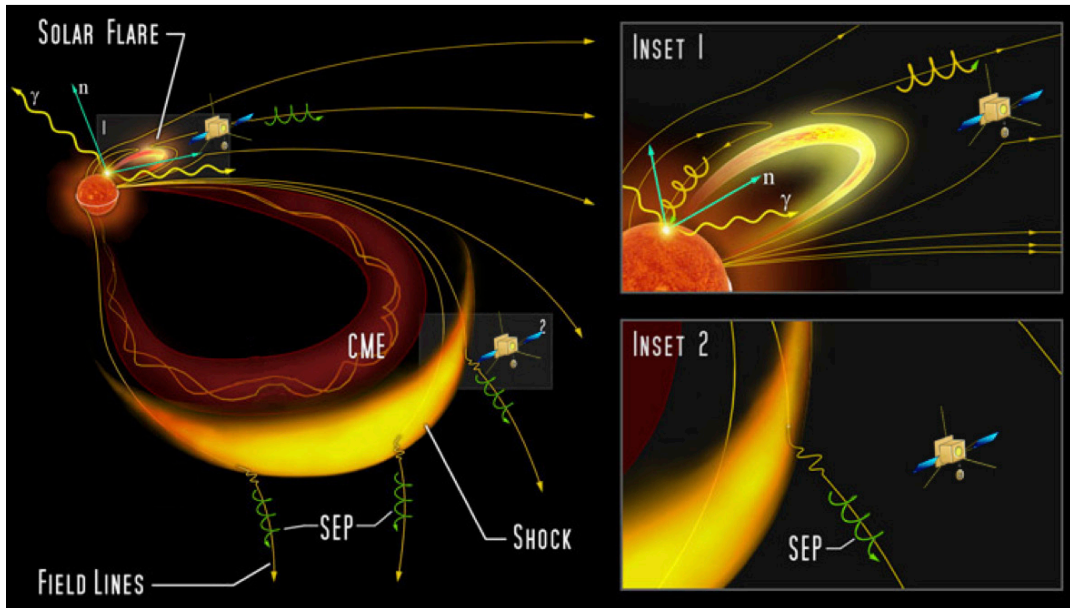


Figure 2.10. Sketch showing a solar flare and CME driving an interplanetary shock. Both the solar flare source and shock may contribute to the interplanetary energetic particle populations. However, the relative importance of acceleration processes due to flares and CME-driven shocks cannot be determined at 1 AU because of particle mixing. Solar Orbiter will allow tests of the relative importance of the different acceleration mechanisms because it goes close to the Sun. There, the shock will pass over Solar Orbiter while still in the early phases of particle acceleration, making it possible for the first time to directly compare the energetic particles with shock properties such as mach number, turbulence level, and with the local seed population. Simultaneous in-situ observations of magnetic field lines connecting back to flare sites and to shock fronts driven by CMEs, together with concurrent remote imaging of flares, wide field-of-view imaging of CMEs and spectroscopic identification of the CME-driven shocks from Solar Orbiter, will make it possible to determine the relative importance of the associated acceleration processes. (Adapted from NASA's Solar Sentinels STDT report)

and eventually reaching high energies. Called Fermi or stochastic acceleration, this mechanism is believed to operate in shock waves and in turbulent regions such as those associated with reconnecting magnetic fields or in heated coronal loops. The second major physical mechanism is a magnetic field whose strength or configuration changes in time, producing an electric field which can directly accelerate particles in a single step. At the Sun, such changes occur when large magnetic loop structures reconnect, or are explosively rearranged due to the stress from the motion of their footpoints on the solar surface (e.g., Aschwanden 2006; Giacalone and Kota 2006).

Multiple processes may take place in SEP events, and while it is not possible to cleanly separate them, they can be split into two broad classes, the first being events associated with shock waves. Figure 2.10 shows a sketch wherein an instability in coronal magnetic loops has resulted in an eruption that launches a CME. As it moves into space, it drives a shock creating turbulence that accelerates SEPs from a seed population of ions filling the interplanetary medium (inset 2). Mixed into this may be particles from an associated solar flare (inset 1). CMEs often accelerate particles for hours as they move away from the Sun, and in some cases are still accelerating particles when they pass Earth orbit in a day or two (Figure 2.11). Since CMEs can be huge as shown in the LASCO image, it is easy to see how they can fill a large portion of the heliosphere with SEPs. However, the correlation of the observed radiation intensities with CME properties is poor, indicating that additional aspects of the mechanism such as seed populations or shock geometry must play important roles that are not yet well understood (Gopalswamy 2006; Desai et al. 2006; Mewaldt 2006).

The second class of events is associated with plasma and magnetic field processes in loops and active regions that accelerate particles. Reconnecting magnetic loops, and emerging magnetic flux regions provide sites for stochastic energetic particle acceleration or acceleration by electric fields. Because these regions are relatively small, the acceleration process is quick: on the order of seconds or minutes, but the resulting event is small and often difficult to observe. Since the energized particles are in the relatively high-density regions of the corona, they collide with coronal plasma, producing ultraviolet (UV) and X-ray signatures that make it possible to locate their acceleration sites and probe the local plasma density. Most of these particles remain

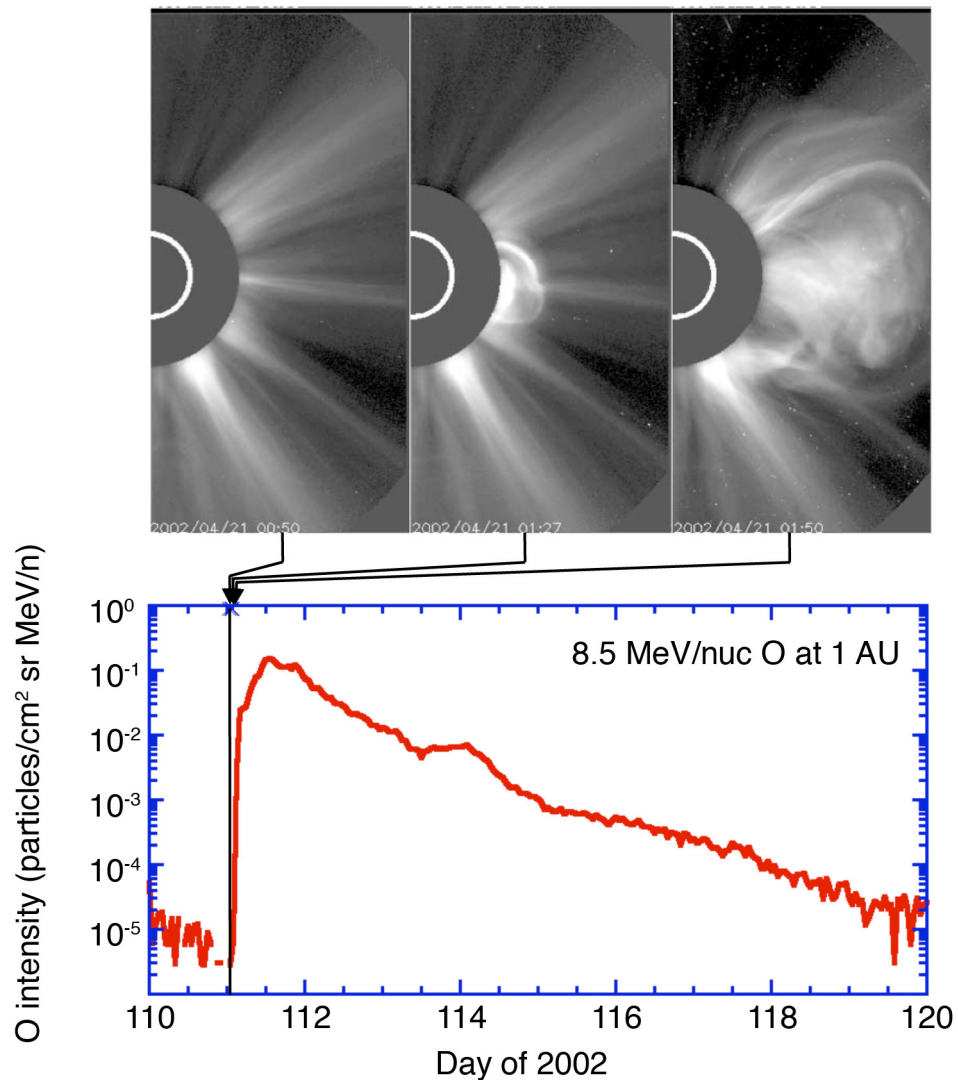


Figure 2.11. Upper panel: SOHO LASCO observations of a CME erupting from the Sun's western hemisphere, with exposure times at 00:50, 01:27, and 01:50. The CME reached a speed of 2700 km/s at $18 R_{\text{Sun}}$, and the associated interplanetary shock passed Earth around ~ 0415 UT on April 23, about 51 hours after the lift-off. Lower panel: ACE observations of high energy SEP O nuclei showing an increase in intensity of nearly 5 orders of magnitude beginning shortly after the CME lift-off. Note that, while the CME photos are all taken near the intensity onset, the ACE intensities remained elevated for days, long after the shock had passed the Earth. Solar Orbiter will provide much more accurate timing and particle distribution measurements because of its much shorter magnetic connection to the acceleration sites. This will pinpoint the acceleration mechanisms and determine the importance of interplanetary transport processes. (Adapted from Emslie et al. 2004)

trapped on their parent loops, travelling down the legs to the solar surface where they lose their energy to ambient material, producing X- and gamma-rays. A few escape on magnetic field lines leading to interplanetary space, traceable by their ('type III') radio signatures, electrons, and highly fractionated ion abundances where the rare ^3He can be enhanced by 1000-10,000 times more than in solar material. Figure 2.12 illustrates another site where reconnection can accelerate particles: in the current sheet behind a CME lift-off. In this case, particles can be accelerated for hours, and may 'leak' around the CME structure and become mixed with the shock accelerated particles. (Lin 2006; Cargill et al. 2006; Drake et al. 2009)

The energetic particles from these events reach our detectors at Earth orbit after spiralling around the IMF, which is an Archimedes spiral on average. But since the IMF meanders, and has many kinks, the length of the particle's path has a good deal of uncertainty, and the particles themselves scatter and mix, smearing and blurring signatures of the acceleration at the Sun. Although we can enumerate candidate mechanisms for producing SEPs, a critical question is: what actually happens in nature? Which processes dominate? How can shocks form fast enough to accelerate ions and electrons to relativistic energies in a matter of minutes, as

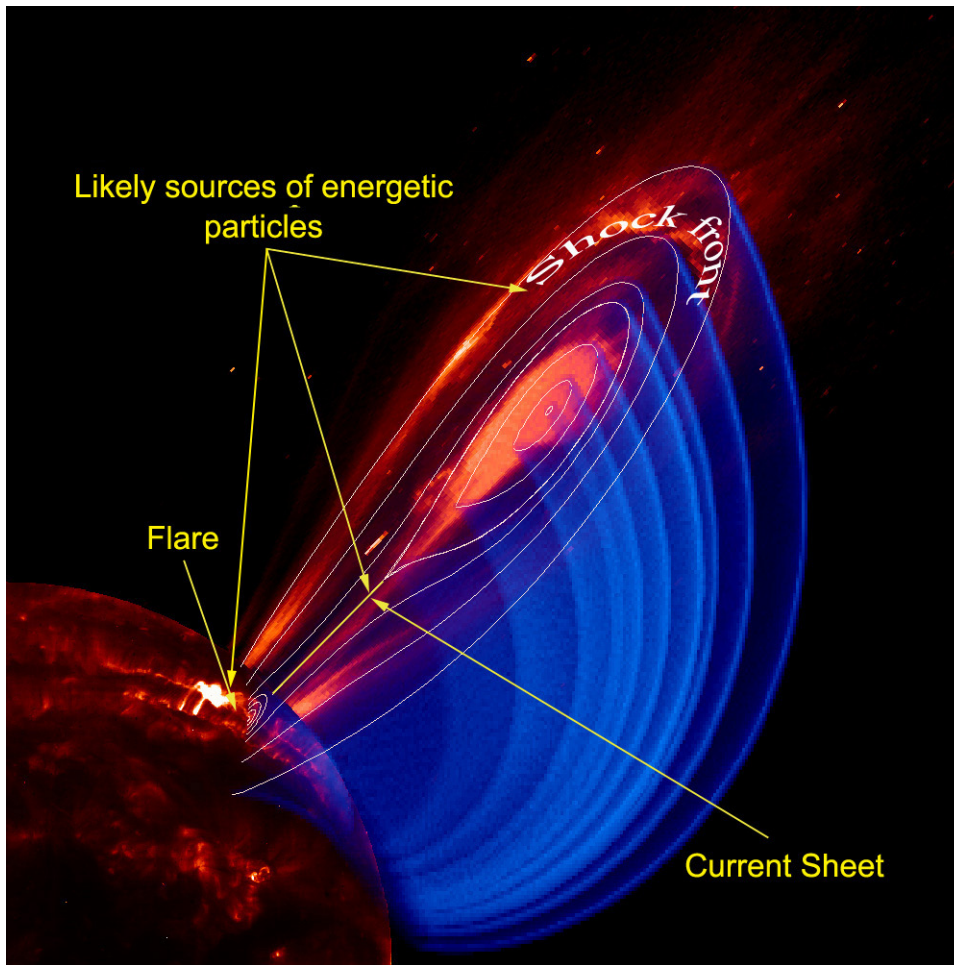


Figure 2.12. Composite illustration of a unified flare/CME system showing potential solar energetic particle source regions. The coronagraph image (red image off the limb) shows the CME with a trailing current sheet seen nearly head-on. A cutaway of the modeled magnetic field structure is shown by the blue overlap. Post flare loops are shown on the UV disk image. By going closer to the Sun, Solar Orbiter will be able to distinguish between the timing and release signatures from the shock front vs. the connection region at the current sheet. (Figure from NASA's Solar Sentinels STDT report)

happened in the January 20, 2005 SEP event?

How Solar Orbiter will address the question. Solar Orbiter will make decisive progress on the origins of SEPs by going close to Sun, thus enabling precise determination of the sequences of events, along with comprehensive in-situ determination of the field and plasma properties and the suprathermal ion pool in the inner heliosphere. Recent progress at 1 AU has relied on combining remote and in-situ observations from different missions such as ACE, SOHO, Wind, RHESSI, TRACE, Hinode, and SDO – where using multiple spacecraft is possible since they are all at virtually the same vantage point. But to do this in close to the Sun, where there is an enormous observational advantage due to proximity, it is necessary to carry the whole suite on one spacecraft, since the probe's trajectory is not in synchronization with Earth. Almost the entire Solar Orbiter payload contributes to unravelling the question of SEP origins: visible, UV, and X-ray imaging of loops, flares, and CMEs with their location and timing; X-ray signatures of energetic particle interactions at loop footpoints, or on loops themselves; radio signatures of coronal shocks and escaping electrons; magnetic field, plasma wave and solar wind measurements to determine turbulence levels and identify shock passages; seed population specification from the heavy ion composition of solar wind and suprathermals in the inner heliosphere; finally, the accelerated energetic particles themselves: their timing, velocity distributions, scattering characteristics, and composition.

CME and shock associated SEPs. Moving from the lower corona to the interplanetary medium, shocks evolve rapidly since the sound speed drops as plasma density and magnetic field strength decline as $\sim 1/r^2$. Solar Orbiter's coronagraphs will remotely identify shock front location, speed, and compression ratios through this

critical region within $\sim 10 R_{\text{Sun}}$. Combining this information with local electron densities as well as coronal ion velocities given by Solar Orbiter radio and light polarization observations will provide critical constraints on shock evolution models in regions too close to the Sun for direct sampling.

In the regions explored by Solar Orbiter close to the Sun, the IMF is almost radial with much less variation (uncertainty) in length than is the case at 1 AU, so the knowledge of the actual path length improves by a factor of 3-5 as the length shortens. Having observed the CMEs and their radio signatures in the corona and the X-ray signatures of the energetic particles near the Sun, Solar Orbiter will then determine subsequent arrival time of the particles in situ that can be accurately compared to CME position. As the shock then rolls past the spacecraft, Solar Orbiter will measure the shock speed and strength as well as the associated plasma turbulence, electric, and magnetic field fluctuations. This will give a complete description of the acceleration parameters in the inner heliosphere where much of the particle acceleration takes place. Indirect evidence from 1 AU indicates that shock acceleration properties depend on the longitude of the shock compared to the observer; close to the Sun, Solar Orbiter can cleanly test this property since the IMF is nearly radial, the CME lift-off site is known, and the accelerated particles will have little chance to mix. In the high-latitude phase of the mission, Solar Orbiter will be able to look down on the longitudinal extent of CMEs in visible, UV, and hard X-rays, allowing first direct observations of the longitudinal size of the acceleration region. This will make it possible to test currently unconstrained acceleration and transport models by using measured CME size, speed, and shape to specify the accelerating shock.

SEPs associated with coronal loops and reconnection regions. As Solar Orbiter approaches the Sun, the photon and particle signatures from small events will increase by $1/r^2$, making it possible to observe events 15-20 times smaller than ever before, in effect opening a new window for SEP processes. We may detect for the first time energetic particle populations from X-ray microflares, a candidate mechanism for coronal heating that cannot be studied further away from the Sun due to background problems. For the small flares that produce X-ray, electron, and ^3He -enrichments we will observe with great accuracy events that at 1 AU are not far above the level of detection: the timing of particle and radio signatures, the composition and spectra, etc., providing strong new constraints on the process operating in these events. Particle acceleration on coronal loops will have new insights since the $1/r^2$ sensitivity advantage and viewing geometry will make it possible to view the X-ray emission from the tops of loops in numerous cases where the much stronger footpoint sources are occulted behind the solar limb. These studies of faint coronal sources that are only rarely observable from 1 AU will give crucial information about the location and plasma properties of suspected electron acceleration sites in the high corona.

2.3.2 How are energetic particles released from their sources and distributed in space and time?

Present state of knowledge. SEPs associated with CME driven shocks have been long known to often arrive at Earth orbit hours later than would be expected based on their velocities. There are two alternate processes that might cause this. (1) The acceleration may require significant time to energize the particles since they must repeatedly collide with the shock to gain energy in many small steps, so the process may continue for many hours as the shock moves well into the inner solar system. Or (2) the particle intensities near the shock may create strong turbulence that traps the particles in the vicinity of the shock, and their intensity observed at earth orbit depends on the physics of the particles escaping from the trapping region. Once free of the vicinity of the shock, SEPs may spiral relatively freely on their way to earth orbit, or more usually will be scattered repeatedly from kinks in the IMF, delaying their arrival further. The amount of scattering in the interplanetary space varies depending on other activity such as recent passage of other shocks or solar wind stream interactions. By the time the particles reach Earth orbit, they are so thoroughly mixed that these effects cannot be untangled. (Gopalswamy et al. 2006; Cohen et al. 2007)

Particles accelerated on magnetic loops can reach very high energies in seconds after the onset of flaring activity, and then collide with the solar surface where they emit gamma radiation. There is a poor correlation between the intensity of the gamma radiation and the SEP intensities observed at earth orbit, so most particles from this powerful acceleration process do not escape. Much more common are flare events observed in UV and X-rays that produce sudden acceleration of electrons, sketched in Figure 2.13. The electrons can escape from the corona, producing nonthermal radio emission as they interact with the local plasma. Moving from higher to lower

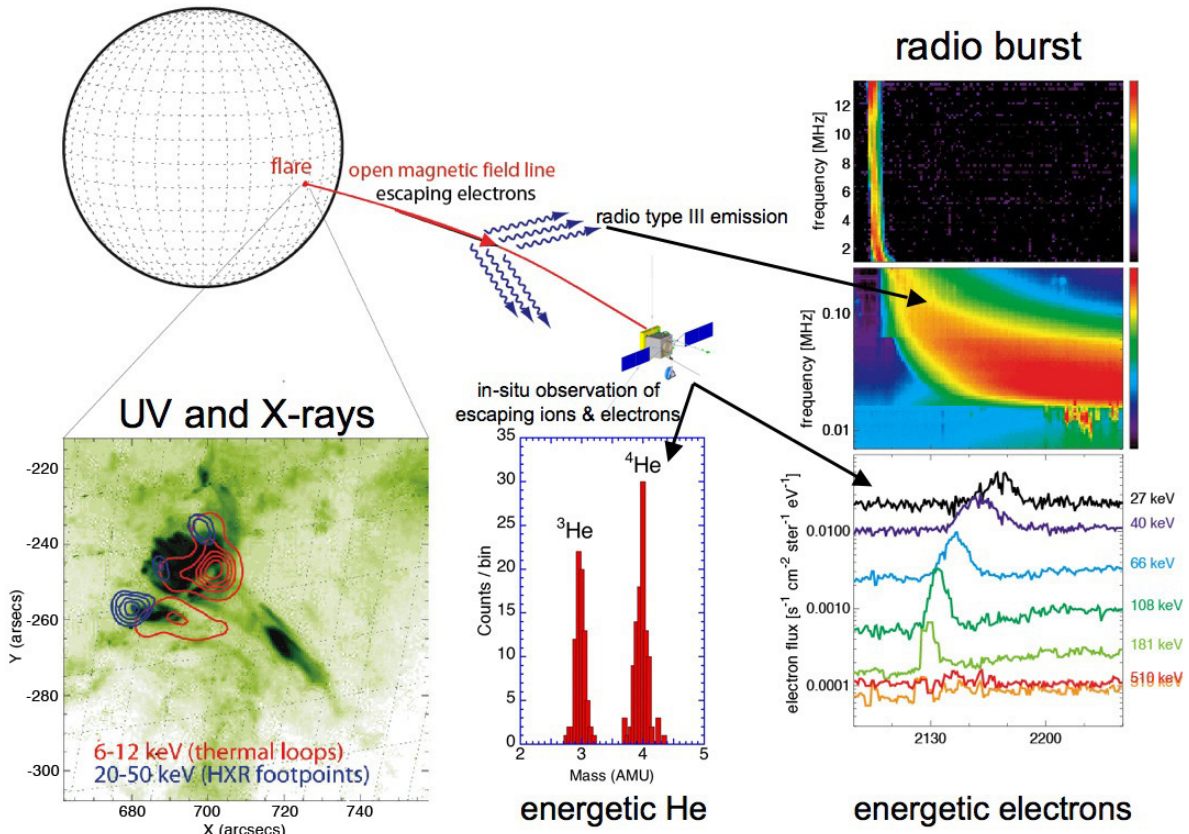


Figure 2.13. Coordinated remote and in-situ observations of a flare source (lower left) producing a jet seen in UV and X-rays which outline the loops and interactions at loop footpoints (blue). Escaping electrons produce a radio burst (upper right) whose frequency depends on coronal height of the emitting particles. At the Solar Orbiter spacecraft, prompt arrival of energetic electrons time the arrival of escaping particles, and energetic ions provide signatures of extreme fractionation produced by the acceleration mechanism. The prompt arrival of the particles establishes that Solar Orbiter is magnetically connected to the X-ray source, allowing comparison with coronal magnetic field models in the region of the active region. (Figure adapted from A. Benz, 3rd Solar Orbiter Workshop, Sorrento)

frequencies as the local plasma density decreases with altitude, the (type III) radio emission makes it possible to track the energetic electron burst into interplanetary space where it may pass by the observer. Energetic ions, greatly enriched in ^3He and heavy nuclei, accompany these electron bursts (Lin 2006; Mason 2007).

Key open questions in shock associated events are whether particle arrival delays at 1 AU are due to the length of time needed to accelerate the particles, or due to trapping in the turbulence near an accelerating shock, or a combination of both? For particles accelerated on loops, are the electrons and ions accelerated from sites low in the corona or at higher altitudes, and how are they related to the X- and gamma-ray signatures?

How Solar Orbiter will address the question. Solar Orbiter will revolutionize our understanding of SEP acceleration associated with CME driven shocks by probing the inner heliospheric sites where particle acceleration and release take place. Solar Orbiter will observe how shocks evolve, and whether they are still accelerating particles as they pass by the spacecraft. If particle arrivals are controlled by the time it takes the shock to accelerate them, then the highest energy particles will be delayed since they require many more interactions with the shock. If trapping and release controls the timing, then as the shock moves by the faster and slower particles will have similar intensity changes. Since Solar Orbiter will simultaneously measure the turbulence properties in the shock acceleration region, it will be possible to construct a complete theory and models of the acceleration process, and its radial dependence in the inner heliosphere.

For SEPs accelerated on loops or in reconnection regions, Solar Orbiter will see the coronal location from UV and X-rays, and then trace the progress of released electrons by radio emission that will drift to the plasma frequency at the spacecraft for those bursts that pass by. This unambiguously establishes that the magnetic field line at Solar Orbiter connects to the coronal UV and X-ray emission site. Since Solar Orbiter can be connected

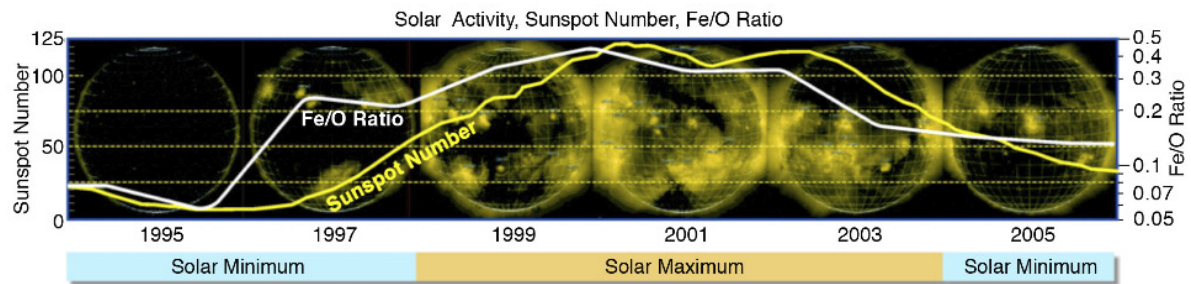


Figure 2.14. The seed population for SEP shock accelerated particles is the suprathermal ion pool. At 1 AU this pool has large variations over the solar cycle as shown above for the Fe/O ratio: the average pool composition goes from domination by flare activity at solar maximum (high Fe/O), to interplanetary sources at solar minimum (low Fe/O). Day-to-day variations in the pool's composition can be larger than shown here because of other transient activity such as interplanetary shock passages. Inside 1 AU, where almost all shock acceleration of particles takes place, the suprathermal ion pool is completely unexplored, and will be mapped for the first time by Solar Orbiter. (Figure from M. Desai, 2nd Solar Orbiter Workshop, Athens)

to active regions for periods of days, this will provide multiple tracings between the heliospheric magnetic field and its origin in the corona. The corotation phase of Solar Orbiter will considerably lengthen the periods of connection to active regions, greatly increasing the number of field line origin sites that can be determined from a single active region. X-ray emission from the flaring sites can be used to derive the energetic electron spectrum at the flare site, which in turn can be compared with the escaping population to see if most of the accelerated electrons are released (usually most do not escape). Thanks to the $1/r^2$ intensity advantage, Solar Orbiter will observe thousands of these cases and thereby permit detailed mapping of coronal sources and the trapping properties of the acceleration sites.

2.3.3 What are the seed populations for energetic particles?

Present state of knowledge. The low-energy particles accelerated by CME-driven shocks to SEP energies are called the seed population. The observed ionization states of SEP ions show temperatures typical of the corona, ruling out hot material on flare loops as the seeds. But SEPs also show significant abundances of ions such as ^3He and singly ionized He, which are virtually absent from the solar wind. The observed energetic particle abundances indicate that the suprathermal ion pool, composed of ions from a few to a few 10 s the speed of the solar wind, is the likely source. At 1 AU the suprathermal ion pool is ~ 100 times more variable in intensity than the solar wind, and varies in composition depending on solar and interplanetary activity. The suprathermal ions are continuously present at 1 AU (Figure 2.14), but it is not known if there is a continuous solar source, or if these ions are from other activities such as acceleration in association with fast- and slow-solar wind streams. Inside 1 AU, the suprathermal ion pool is expected to show significant radial dependence due to the different processes that contribute to the mixture, but it is unexplored (Desai et al. 2006; Mewaldt et al. 2007; Lee 2007; Fisk and Gloeckler 2007).

For SEPs accelerated on loops or in reconnection regions that give rise to electron and type-III radio bursts, ionization states are coronal-like at lower energies and change over to much hotter flare-like at high energies. This may be evidence for a complex source, or, more likely, of energetic particle stripping as the ions escape from a low coronal source. For SEPs accelerated at reconnection sites behind CMEs (Figure 2.12) abundances and ionization states would be coronal (Klecker et al. 2006).

Critical questions in this area are: what is the suprathermal ion pool in the inner heliosphere, including its composition and temporal and spatial variations? What turbulence or stochastic mechanisms in the inner heliosphere accelerate particles to suprathermal energies? Are the source locations and arrival times of electrons from SEPs on loops or reconnection regions consistent with a low or high coronal source?

How Solar Orbiter will address the question. By systematically mapping the suprathermal ion pool in the inner heliosphere with spectroscopic and in-situ data, Solar Orbiter will provide the missing seed particle data for models of SEP acceleration associated with shocks. Together with the shock and turbulence parameters also measured on Solar Orbiter there will be the first well-constrained models. Since the suprathermal ion pool

composition varies, different shock events will be expected to produce correspondingly different energetic particle populations that can be examined on a case-by-case basis. The *high-latitude phase* of the mission will add an important third dimension to the suprathermal pool mapping, since it will be more heavily influenced by, e.g., mid-latitude streamer belts, making it possible to probe the solar and interplanetary origins of the seed particle populations. Taken together, these observations will make it possible to construct the first complete physics-based theory and models of particle acceleration close to the Sun.

For SEPs accelerated on loops or in reconnection regions the $1/r^2$ advantage of Solar Orbiter will again provide a decisive advantage since particle properties will be accurately measured and comparable with much more precise information on the coronal location. This will permit distinguishing between low coronal sources that result in stripping of escaping particles vs. higher sources which could mimic stripping properties. SEPs accelerated from reconnection regions in back of CME lift-offs will be identified by comparing energetic particle timing with the location of the CME, and energetic particle composition with that determined spectroscopically for the remote coronal source.

2.4 How does the solar dynamo work and drive the connections between the Sun and heliosphere?

Significance of the question. The Sun's magnetic field dominates the solar atmosphere. It structures the coronal plasma, drives much of the coronal dynamics, and produces all the observed energetic phenomena. One of the most striking features of solar magnetism is its ~ 11 -year activity cycle, which is manifest in all the associated solar and heliospheric phenomena. Similar activity cycles are also observed in a broad range of stars in the right half of the Hertzsprung-Russell diagram, and the Sun is an important test case for dynamo models of stellar activity.

The Sun's global magnetic field is generated by a dynamo generally believed to be seated in the tachocline, the shear layer at the base of the convection zone. According to flux-transport dynamo models (e.g., Dikpati and Gilman 2008), meridional circulation, and other near-surface flows transport magnetic flux from decaying active regions to the poles. There subduction carries it to the tachocline to be reprocessed for the next cycle. This 'conveyor belt' scenario provides a natural explanation for the sunspot cycle, and characterizing the flows that drive it will provide a crucial test of our models and may also allow us to predict the length and amplitude of future cycles. However, current models fail miserably at predicting actual global solar behaviour. For example, the current sunspot minimum has been far deeper and longer than predicted by any solar modelling group, indicating that crucial elements are missing from current understanding.

A major weakness of current global dynamo models is poor constraint of the meridional circulation at high latitudes. The exact profile and nature of the turnover from poleward flow to subduction strongly affects behaviour of the resulting global dynamo (e.g., Dikpati and Charbonneau 1999), but detecting and characterizing the solar flow is essentially impossible at shallow viewing angles in the ecliptic plane.

In addition to the global dynamo, turbulent convection may drive a local dynamo that could be responsible for generating the observed weak, small-scale internetwork field, which is ubiquitous across the surface and appears to dominate the emergent unsigned flux there.

A key objective of the Solar Orbiter mission is to measure and characterize the flows that transport the solar magnetic fields: complex near-surface flows, the meridional flow, and the differential rotation at all latitudes and radii. Of particular and perhaps paramount importance for advancing our understanding of the solar dynamo and the polarity reversal of the global magnetic field is a detailed knowledge of magnetic flux transport near the poles. Hinode, peering over the Sun's limb from a heliographic latitude of 7° , has provided a tantalizing glimpse of the Sun's high-latitude region above 70° ; however, observations from near the ecliptic lack the detail, coverage, and unambiguous interpretation needed to understand the properties and dynamics of the polar region. Thus, Solar Orbiter's imaging of the properties and dynamics of the polar region during the out-of-the-ecliptic phase of the mission (reaching heliographic latitudes of 25° during the nominal mission and as high as 34° during the extended mission) will provide urgently needed constraints on our models of the solar dynamo.

Most of the open magnetic flux that extends into the heliosphere originates from the Sun's polar regions, from polar coronal holes. The current solar minimum activity period, which is deeper and more extended than previously measured minima, demonstrates the importance of this polar field to the solar wind and heliosphere.

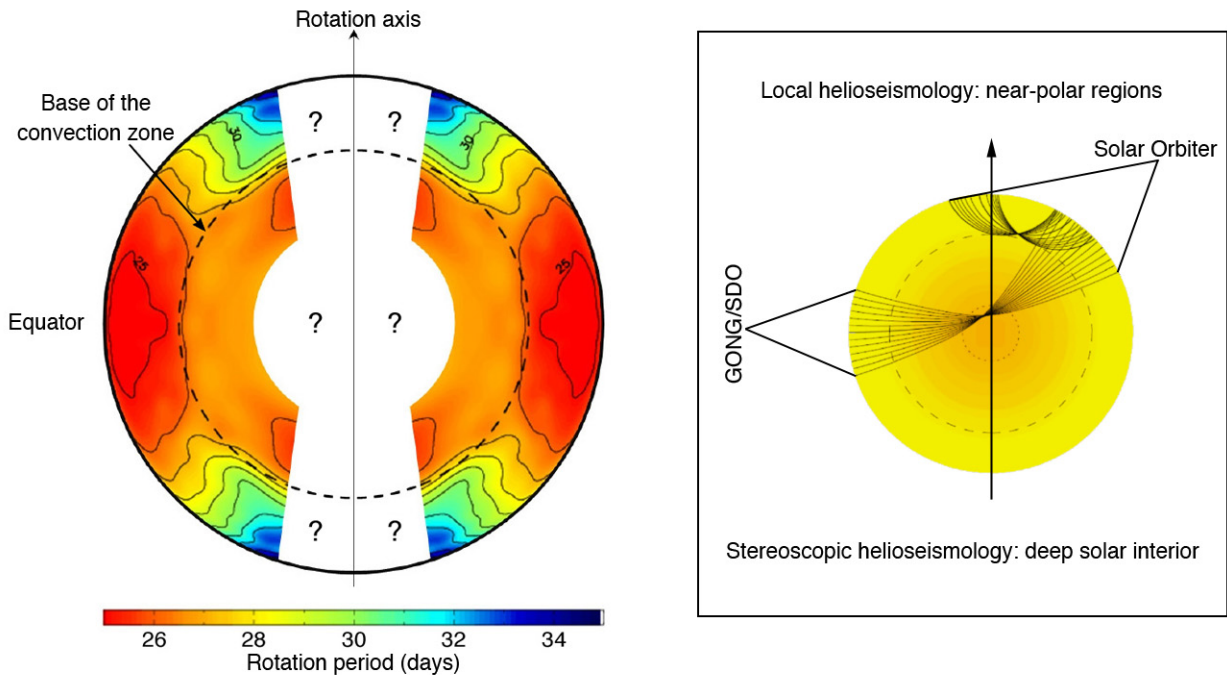


Figure 2.15. Left: Rotation profile in the solar interior as derived from GONG and MDI data. By traveling to high latitudes, Solar Orbiter will use local helioseismology to determine the currently unknown properties of the solar interior below the poles (Corbard 1998). Right: Solar Orbiter's helioseismology capabilities: (i) probing near polar regions with local helioseismology and (ii) probing the deep solar interior with stereoscopic helioseismology in combination with near-Earth observations (e.g., GONG or SDO). (Roth 2007)

There is evidence that the solar wind dynamic pressure, composition and turbulence levels, as well as the strength of the heliospheric magnetic field, have all changed in the last few years in ways that are unprecedented in the space age. None of these changes were predicted, and current solar conditions present a challenge to our understanding of the solar dynamo and its effects on the solar system at large and the Earth in particular.

Below we discuss in more detail three interrelated questions that flow down from this top-level question: How is magnetic flux transported to and reprocessed at high solar latitudes? What are the properties of the magnetic field at high solar latitudes? Are there separate dynamo processes in the Sun?

2.4.1 How is magnetic flux transported to and reprocessed at high solar latitudes?

Present state of knowledge. In the last decade, the mapping of surface and subsurface flow fields at low and middle latitudes has seen major advances, largely due to the availability of high-quality data from the SOHO's Michelson Doppler Imager (MDI) instrument. These data have provided accurate knowledge of differential rotation, the low latitude, near-surface part of the meridional flows, and the near-surface torsional oscillations, which are rhythmic changes in the rotation speed that travel from mid-latitudes both equatorward and poleward (Howe et al. 2006). Local helioseismic techniques have also reached a level of maturity that allows the three-dimensional structure of the shallow velocity field beneath the solar surface to be determined.

Despite these advances, progress in understanding the operation of the solar dynamo depends on how well we understand differential rotation and the meridional flows near the poles of the Sun. However, because of the lack of out-of-the ecliptic observations, the near-polar flow fields remain poorly mapped, as does the differential rotation at high latitudes (see Beck 2000; Thompson et al. 2003; and Figure 2.15). The meridional flow in particular, the very foundation of the flux transport dynamo, is not well characterized above $\sim 50^\circ$ latitude; it is not even certain that it consists of only one cell in each hemisphere. The return flow, believed to occur at the base of the convection zone, is entirely undetermined save for the requirement of mass conservation. All these flows must be better constrained observationally in order to help solve the puzzle of the solar cycle and to advance our understanding of the operation of the solar dynamo (and, more broadly, of stellar dynamos generally).

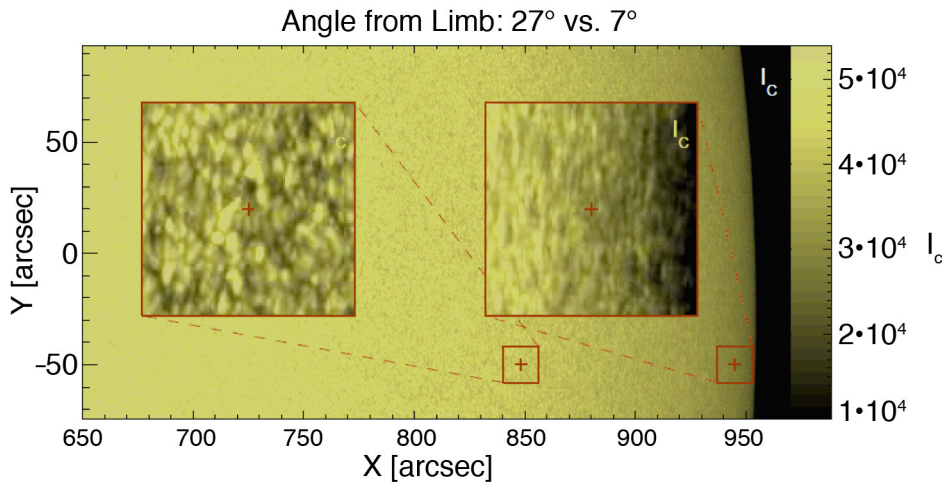


Figure 2.16. Comparison of solar granulation at the poles as viewed from 27° where the fine scale structure can be resolved with much higher fidelity than is obtained in the ecliptic plane twice a year (7°). The latter is the perspective used by the Hinode satellite to offer the first vector magnetic field imaging of the solar pole. Solar Orbiter will characterize the properties and dynamics of the polar regions for the first time, including magnetic fields, plasma flows, and temperatures.

How Solar Orbiter will address this question. Solar Orbiter will measure or infer local and convective flows, rotation, and meridional circulation in the photosphere and in the subsurface convection zone at all heliographic latitudes including, during the later stages of the nominal mission, at the critical near-polar latitudes. Solar Orbiter will reveal the patterns of differential rotation, the geometry of the meridional flow, the structure of subduction areas around the poles where the solar plasma dives back into the Sun, and the properties of convection cells below the solar surface. This will be achieved through correlation tracking of small features, direct imaging of Doppler shifts, and helioseismic observations (including the first from a high-latitude vantage point). By monitoring the temporal variations over the course of the mission, it will be possible to deduce solar cycle variations in the flows.

Solar Orbiter will resolve small-scale magnetic features near the poles, even within the nominal mission phase (Figure 2.16), and right up to the poles during the extended mission. It will determine the detailed surface flow field through tracking algorithms. Such algorithms provide only inconclusive results when applied to polar data obtained from near-Earth orbit due to the foreshortening. Doppler maps of the line-of-sight velocity component will complement the correlation tracking measurements and will also reveal convection, rotation, and meridional circulation flows.

Time series of Doppler and intensity maps will be used to probe the three-dimensional mass flows in the upper layers of the convection zone, at high heliographic latitudes. The flows will be inferred using the methods of local helioseismology (e.g., Gizon and Birch 2005): time-distance helioseismology, ring diagram analysis, helioseismic holography, and direct modelling. Using SOHO/MDI Dopplergrams, it was demonstrated that even complex velocity fields can be derived with a single day of data (e.g., Jackiewicz et al. 2008).

The deeper layers of the convection zone will be studied using both local and the global methods of helioseismology. Moreover, Solar Orbiter will provide the first opportunity to implement the novel technique of stereoscopic helioseismology to probe flows and structural heterogeneities deep in the convection zone, even reaching down to the tachocline. Combining Solar Orbiter observations with ground- or space-based helioseismic observations from 1 AU (e.g., GONG or SDO) will open new windows into the Sun. Looking at the Sun from two distinct viewing angles will increase the observed fraction of the Sun's surface and will benefit global helioseismology because the modes of oscillation will be easier to disentangle (reduction of spatial leaks). With stereoscopic helioseismology, new acoustic ray paths can be taken into account to probe deeper layers in the interior (Figure 2.15), including the bottom of the convection zone.

2.4.2 What are the properties of the magnetic field at high solar latitudes?

Present state of knowledge. Meridional circulation transports the surface magnetic flux toward the poles, where a concentration of magnetic flux is expected to occur. However, because of the directional sensitivity

of the Zeeman effect and magnetic polarity cancellation resulting from geometric foreshortening, present-day observations from the ecliptic at 1 AU can provide only a poor representation of the polar magnetic field. The high resolution of Hinode's Solar Optical Telescope (SOT) can partly overcome the second disadvantage (Tsuneta et al. 2008), but not the first. Consequently, an accurate quantitative estimate of the polar magnetic field remains a major and as yet unattained goal.

The polar field is directly related to the dynamo process, presumably as a source of poloidal field that is wound up by the differential rotation in the shear layer at the base of the convection zone. The distribution of the magnetic field at the poles drives the formation and evolution of polar coronal holes, polar plumes, X-ray jets, and other events and structures that characterize the polar corona. Polar coronal holes have been intensively studied from the non-ideal vantage point offered by the ecliptic, but never imaged from outside the ecliptic. Consequently the distribution of the polar field and the origin of polar structures are only poorly determined. The fast solar wind is associated with open field lines inside coronal holes, whereas at least parts of the slow solar wind are thought to emanate from the coronal hole boundaries. Understanding the interaction of open and closed field lines across these boundaries is of paramount importance for elucidating the connection between the solar magnetic field and the heliosphere.

The magnetic flux in the heliosphere varies with the solar cycle (Owens et al. 2008 and Figure 2.8). There is evidence that the heliospheric magnetic flux has increased substantially in the last hundred years, perhaps by as much as a factor of two (Lockwood et al. 1999; Rouillard et al. 2007), possibly due to a long-term change in the Sun's dynamo action. As noted earlier, however, the interplanetary magnetic field is dramatically lower than expected during the current solar minimum. Models based on the injection of flux into the heliosphere by coronal mass ejections (cf. Section 2.2.2) cannot explain this reduction, and it is becoming clear that the processes by which flux is added to and removed from the heliosphere are more complex than previously thought.

How Solar Orbiter will address this question. Solar Orbiter's comprehensive imaging instruments will characterize the properties and dynamics of the polar regions for the first time, including magnetic fields, plasma flows, and temperatures (Figure 2.16). Solar Orbiter will make the first reliable measurements of the amount of polar magnetic flux, its spatial distribution and its evolution (by comparing results from different orbits), providing an independent constraint on the strength and direction of the meridional flow near the pole. The evolution of Solar Orbiter's orbit to higher heliographic latitudes will make it possible to study the transport of magnetic flux from the activity belts toward the poles, which drives the polarity reversal of the global magnetic field (see Wang et al. 1989; Sheeley 1991; Makarov et al. 2003). From its viewpoint outside the ecliptic, Solar Orbiter will probe the cancellation processes that take place when flux elements of opposite polarity meet as part of the polarity reversal process. Joint observations from Solar Orbiter and spacecraft in the ecliptic will determine, with high accuracy, the transversal magnetic field, which is notoriously difficult to measure, along with derived quantities such as the electric current density.

Solar Orbiter will measure the photospheric magnetic field at the poles, while simultaneously imaging the coronal and heliospheric structure at visible and EUV wavelengths. In addition, as the spacecraft passes through the mid-latitude slow/fast wind boundary at around 0.5 AU, the field and plasma properties of the solar wind will be measured. With the help of magnetic field extrapolation methods these observations will, for the first time, allow the photospheric and coronal magnetic field in polar coronal holes to be studied simultaneously and the evolution of polar coronal hole boundaries and other coronal structures to be investigated. The images are complementary to those from low-latitude instruments (see Figure 2.17 for a simulated EUV image).

Solar Orbiter's observations from progressively higher heliographic latitudes (25° by the end of the nominal mission) will enable the first coordinated investigation (jointly with spacecraft in the ecliptic) of the three-dimensional structure of the inner heliosphere. These observations will reveal the links between the Sun's polar regions and the properties of the solar wind and interplanetary magnetic field, in particular the heliospheric current sheet, which is used as a proxy for the tilt of the solar magnetic dipole. In addition, Solar Orbiter will pass both north and south of the solar equatorial plane in each orbit, with repeated transits through the equatorial streamer belt and through the slow/fast wind boundary at mid-latitudes into the polar wind, making it possible to follow the evolution of the solar wind and interplanetary magnetic field as well as of the sources in the polar coronal holes. Ulysses has shown that poleward of the edge of coronal holes the properties of the solar wind are relatively uniform, so that Solar Orbiter only needs to reach heliographic latitudes just above the coronal hole edge to enter the high-speed solar wind. The orbital inclination of 25° reached during the nominal



Figure 2.17. Simulated EUV view of the ultraviolet corona from 35° heliolatitude. Solar Orbiter's remote-sensing instruments and unique high-latitude vantage point will enable the first-ever simultaneous measurements of the polar magnetic field and the associated structures in a polar coronal magnetic hole.

mission is sufficiently high to satisfy this constraint.

2.4.3 Are there separate dynamo processes acting in the Sun?

Present state of knowledge. MHD simulations indicate that a local turbulent dynamo should be acting in the Sun's turbulent convection zone (Brun et al. 2004) and even in the near-surface layers (Vögler and Schüssler 2007). Hinode/SOT has detected ubiquitous horizontal magnetic fields in quiet regions of the Sun (Lites et al. 2007), which are possibly generated by local dynamo action (Pietarila Graham et al. 2009). These small, weak features (inter-network fields; Zirin 1987) bring 100 times more magnetic flux to the solar surface than the stronger features that are known to be the product of the global dynamo, and have themselves shown to be in cross-scale turbulent equilibrium (Schrijver et al. 1997). Even the smallest observable features have been shown to be formed primarily by aggregation of yet smaller, yet more prevalent features too small to resolve with current instrumentation (Lamb et al. 2008, 2009). It is, however, still uncertain whether a separate local, turbulent dynamo really is acting on the Sun and how strongly it contributes to the Sun's magnetic flux (and magnetic energy). In particular, all solar magnetic features, from the smallest observable intergranular flux concentrations to the largest active regions, have been shown (Parnell et al. 2009) to have a power law (scale free) probability distribution function, suggesting that a single turbulent mechanism may be responsible for all observable scales of magnetic activity.

How Solar Orbiter will address this question. One way to distinguish between the products of a global and a local dynamo is to study the distribution of small elements of freshly emerging magnetic flux over heliographic latitude. The global dynamo, presumably owing to the structure of the differential rotation and the meridional flow near the base of the convection zone, leads to the emergence of large bipolar magnetic regions (active regions) at the solar surface at latitudes between 5° and 30° and of smaller ephemeral active regions over a larger range of latitudes, but concentrated also at low latitudes. In contrast, a local turbulent dynamo is expected to enhance field more uniformly across the surface.

Observations carried out from the ecliptic cannot quantitatively determine the latitudinal distribution of magnetic flux and in particular the emergence of small-scale magnetic features (inter-network fields) due to foreshortening and the different sensitivity of the Zeeman effect to longitudinal and transversal fields. Solar Orbiter, by flying to latitudes of 25° and higher above the ecliptic, will be able to measure weak magnetic features equally well at low and high latitudes (Martínez Pillet 2006). If the number and size (i.e., magnetic flux) distributions of such features are significantly different at high latitudes, then even the weak features are probably due to the global dynamo. If, however, they are evenly distributed, then the evidence for a significant role of a local dynamo will be greatly strengthened. Current work is confounded by viewing angle restrictions near the poles, by the ubiquitous seething horizontal field (e.g., Harvey et al. 2007), and by small deflections in near-vertical fields, which dominate observed feature distributions near the limb of the Sun.

3 Scientific Requirements

This chapter describes how the Solar Orbiter science investigations will be implemented and places special emphasis on demonstrating traceability: the flow down from the science objectives discussed in the previous chapter to the observations and measurements required to meet those objectives, to the instrumentation needed to provide the required measurements, and to the requirements placed by the science objectives on the design of the orbit. Tables 3.1-3.4 map the science questions to the required observations and instrumentation. Table 3.5 then traces in detail the flow down from required observations to specific measurement requirements to the capabilities of the selected payload. The chapter concludes with a brief discussion of the implications of the observational requirements and orbit design for the design of the spacecraft. The instruments that have been selected for Solar Orbiter are described in Chapter 4.

3.1 Observations, Measurements, and Orbital Characteristics

The overarching objective of the Solar Orbiter mission is to address the central question of heliophysics: *How does the Sun create and control the heliosphere?* Achieving this objective is the next critical step in an overall strategy to address one of the fundamental questions in the Cosmic Vision theme: *How does the Solar System work?* To this end, Solar Orbiter will use a carefully selected combination of in-situ and remote-sensing instrumentation, a unique orbit and mission design, and a well-planned observational strategy to explore systematically the region where the solar wind is born and heliospheric structures are formed.

As discussed in Chapter 2, the broad question that defines the overarching objective of the Solar Orbiter mission is broken down into four interrelated scientific questions:

1. How and where do the solar wind plasma and magnetic field originate in the corona?
2. How do transients drive heliospheric variability?
3. How do solar eruptions produce energetic particle radiation that fills the heliosphere?
4. How does the solar dynamo work and drive connections between the Sun and heliosphere?

Common to all of these questions is the requirement that Solar Orbiter make in-situ measurements of the solar wind plasma, fields, waves, and energetic particles close enough to the Sun that they are still relatively pristine and have not had their properties modified by dynamical evolution during their propagation. Solar Orbiter must also relate these in-situ measurements back to their source regions and structures on the Sun through simultaneous, high-resolution imaging and spectroscopic observations both in and out of the ecliptic plane.

3.1.1 Measurement Requirements and Instrument Capabilities

The measurement requirements for Solar Orbiter have been defined by two independent science definition teams. The Solar Orbiter Science Definition Team provided the input for the Solar Orbiter Science Requirements Document, taking into account the Payload Definition Document and the reports from the Payload Working Groups. The Joint ESA-NASA HELEX Science and Technology Definition Team subsequently refined Solar Orbiter's observation and measurement requirements in the context of the joint HELEX mission. These studies formed the basis for the competitive announcements of opportunity released by ESA and NASA and the initial instrument selection.

Tables 3.1-3.4 specify the observations required to address the science objectives and the science questions detailed in Chapter 2. The required observations are repeated in the first column of Table 3.5, which maps them to instruments and measurements in the second column. The third column gives the detailed measurement requirements for each of the observations, and fourth column gives the corresponding capabilities of the selected instruments.

Table 3.1 Required observations and instrumentation for Solar Orbiter Objective 2.1.

Objective 2.1 How and where do the solar wind plasma and magnetic field originate in the corona?
2.1.1 What are the source regions of the solar wind and heliospheric magnetic field?
<ul style="list-style-type: none"> • Composition of source regions from remote (SPICE) and in-situ (SWA) observations • Magnetic connectivity (STIX, SWA, RPW, EPD) • Full disk photospheric magnetic fields (PHI) • In-situ magnetic field (MAG) • Full Sun, high-resolution and spectral images of corona and chromosphere (EUI, SPICE, METIS) • Global maps of H and He flow velocities and He fractions (METIS, SoloHI)
2.1.2 What mechanisms heat and accelerate the solar wind?
<ul style="list-style-type: none"> • High-resolution images of the photospheric magnetic field (PHI) • High-resolution images of coronal loops and evolving structures (EUI, SPICE) • Wave propagation and heating (SPICE, SWA, MAG, RPW) • H and He flow velocities and velocity distributions (SPICE, METIS) • Velocities and mass density of evolving structures (SoloHI, METIS) • Composition and plasma properties of associated wind (SWA, MAG, RPW) • Distribution of smallest flares and solar particle events (STIX, EPD)
2.1.3 What are the sources of solar wind turbulence and how does it evolve?
<ul style="list-style-type: none"> • High-cadence measurements of the plasma microstate across a wide band of heliolatitudes for all relevant solar wind regimes and heliocentric distances (MAG, SWA, RPW) • Images of source regions in Doppler-broadened lines (SPICE) • H and He flow velocity distributions (METIS) • Identification of dropouts and measurement of SEP scattering by turbulence (EPD) • Time history of velocity and brightness of solar wind features and turbulence (METIS, SoloHI) • High-resolution, high-cadence maps of photospheric magnetic field (PHI)

Table 3.2 Required observations and instrumentation for Solar Orbiter Objective 2.2.

Objective 2.2 How do solar transients drive heliospheric variability?
2.2.1 How do CMEs evolve through the corona and inner heliosphere?
<ul style="list-style-type: none"> • High-resolution maps of photospheric magnetic field (PHI) • CME source location, expansion, rotation, and composition through corona (EUI, SPICE, STIX) • Link CME to in-situ properties (MAG, RPW, SWA, EPD) • Evolution of CME properties in the corona mapped to those measured in situ (SoloHI, METIS, MAG, RPW, SWA) • Distribution of energy into heat, particle acceleration, and bulk kinetic energy (SWA, MAG, EPD)
2.2.2 How do CMEs contribute to solar magnetic flux and helicity balance?
<ul style="list-style-type: none"> • In-situ properties of ejecta (SWA, MAG, RPW) • Full-disk maps of photospheric magnetic field to determine source region helicity (PHI) • Map source regions to in-situ properties magnetic connectivity, polarity, and helicity (EUI, METIS, SPICE, SoloHI, SWA, MAG, EPD)
2.2.3 How and where do shocks form in the corona and inner heliosphere?
<ul style="list-style-type: none"> • Global maps of electron density, H & He flow velocities (METIS) • Position and speed of shocks (SPICE, METIS, SoloHI, EUI, RPW, SWA) • Full-sun and high-resolution coronal and chromospheric images (EUI, STIX, METIS, SPICE) • Location, intensity, thermal/non-thermal distribution of erupting regions (SoloHI, RPW) • Timing of eruptions and coronal manifestations (EUI, SoloHI, METIS, EPD) • Plasma, electric and magnetic fields in situ (SWA, MAG, RPW, EPD)

Table 3.3 Required observations and instrumentation for Solar Orbiter Objective 2.3.

Objective 2.3 How do solar eruptions produce energetic particle radiation that fills the heliosphere?
2.3.1 How and where are energetic particles accelerated at the Sun?
<ul style="list-style-type: none"> • UV, white light and X-ray imaging of loops, flares, and CMEs (EUI, SPICE, STIX, METIS, SoloHI) • Global maps of electron densities, H, He flow velocities (METIS) • Imaging of coronal suprathermal seed population (SPICE) • Location, timing, and motion of CMEs and shocks (EUI, SoloHI, METIS, EPD) • X-ray signatures of energetic particle interactions at loop footpoints, or on loops themselves (STIX) • Radio signatures of coronal shocks and escaping electrons (RPW) • Magnetic field, plasma wave and solar wind measurements to determine turbulence levels and identify shock passages (MAG, RPW, SWA) • Seed population specification from the heavy ion composition of solar wind and suprathermals in the inner heliosphere timing (SWA, EPD) • Velocity distributions, scattering characteristics, spectra and composition of energetic particles (EPD) • Timing and properties of small events (STIX, EPD, RPW, EUI) • Images of longitudinal extent of CMEs in visible, UV, and hard X-rays (SoloHI, METIS, EUI, SPICE, STIX)
2.3.2 How are energetic particles released from their sources and distributed in space and time?
<ul style="list-style-type: none"> • Timing, location, and intensity profiles of EUV, radio, and X-ray emissions in relation to energetic-particle intensities at a wide range of energies (EUI, SPICE, RPW, STIX, EPD) • X-ray spectral images of flaring regions (STIX) • High-resolution, high-cadence maps of photospheric magnetic field (PHI) • Turbulence properties throughout the inner heliosphere and corona (MAG, SWA, RPW, SPICE, EPD, METIS) • Magnetic connectivity (SWA, MAG, EPD)
2.3.3 What are the seed populations for energetic particles?
<ul style="list-style-type: none"> • Map coronal suprathermal ion pool (METIS) • Map inner-heliosphere suprathermal ions (EPD, SWA) • Shock and turbulence parameters (MAG, SWA, RPW)

Table 3.4 Required observations and instrumentation for Solar Orbiter Objective 2.4.

Objective 2.4 How does the solar dynamo work and drive connections between the Sun and the heliosphere?
2.4.1 How is magnetic flux transported to and reprocessed at high solar latitudes?
<ul style="list-style-type: none"> • Full-disk & high-resolution maps of the photospheric magnetic field and local and convective flows, maps of rotation, differential rotation, and meridional circulation, structure of subduction areas, properties of sub-surface convection cells (PHI) • High-resolution images of small-scale magnetic features at the poles (EUI, SPICE, PHI)
2.4.2 What are the properties of the magnetic field at high solar latitudes?
<ul style="list-style-type: none"> • Amount, distribution, and evolution of polar photospheric magnetic flux transversal magnetic field (PHI) • Magnetic fields, plasma flows, and temperatures in polar regions (PHI, EUI, SPICE, METIS) • Images of coronal and heliospheric structure in visible, UV and EUV (EUI, METIS, SoloHI) • Properties of bulk solar wind (SWA, MAG) • Magnetic connectivity (SWA, MAG, EPD, EUI)
2.4.3 Are there separate dynamo processes acting in the Sun?
<ul style="list-style-type: none"> • Latitudinal distribution of small-scale, emerging magnetic flux (PHI)

Table 3.5 Measurement and instrument requirements.

Required Observations (cf. Tables 3.1 – 3.4)	Instrument: Measurement	Measurement Requirements and Coordinated Observation Plans	Selected Payload Capability
Global maps of H and He flow velocities and He fractions	METIS: coronal imaging in visible, H I and He II Ly-alpha lines, polarization brightness	<p><u>Polarized visible-light imaging:</u> Physical quantity: electron density FOV: ~ 1.5 to $3.0 R_{\text{Sun}}$ (at 0.28 AU); $4.3 - 11 R_{\text{Sun}}$ (at 0.8 AU) Spatial resolution: $< 10^4 \text{ km}$ at 0.28 AU Spectral coverage: $500\text{-}600 \text{ nm}$ Cadence: 5 min. (CMEs obs.)</p> <p><u>UV & EUV imaging:</u> Physical quantities: hydrogen and singly-ionized helium densities, and outflow velocities FOV: $\sim 1.5 - 3.0 R_{\text{Sun}}$ (at 0.28 AU); extendable to $4.3 - 11 R_{\text{Sun}}$ (at 0.8 AU) Spatial resolution: $< 10^4 \text{ km}$ at 0.28 AU Spectral coverage: H I Ly-α, 121.6 nm; He II Ly-α, 30.4 nm Spectral Resolution: $\Delta\lambda/\lambda \leq 10^{-1}$ Cadence: $15\text{-}20 \text{ min.}$</p> <p>Substantial coverage of the Solar Probe Plus Orbit</p>	<p>$1.5 - 3.0 R_{\text{Sun}}$ at 0.28 AU at $20''$ at $20 \text{ s}/20 \text{ min}/1 \text{ hr}$ cadence (vis/UV/EUV)</p>
Mapping of coronal features to inner heliosphere, evolution of velocities and mass densities of coronal structures	SoloHI: White light, polarization brightness imaging	<p><u>Visible-light (VL) imaging:</u> Physical quantity: electron distribution FOV: $5.5^\circ - 40.5^\circ$ Spatial res: $2.7'$ Stray-light rejection: $10^{-14} \text{ B/B}_{\text{Sun}}$ Cadence: $15\text{-}30 \text{ min.}$</p>	<p>FOV: $40^\circ \times 40^\circ$ at better than $1.9''/\text{pixel}$</p>

Table 3.5 Measurement and instrument requirements (cont'd).

Required Observations (cf. Tables 3.1 – 3.4)	Instrument: Measurement	Measurement Requirements and Coordinated Observation Plans	Selected Payload Capability
Composition of coronal source region	<p>SPICE: imaging EUV spectroscopy</p> <p>METIS (coronal imaging): visible, H I and He II Ly α lines, polarized brightness</p>	<p>On disk: SPICE: - Best spatial resolution 1'' - Instantaneous FOV = 16' x 1' - Rastered FOV = 16' x 4' - Two lines per temperature decade - Exposure time 5 s - Spectral cadence of 20 min - Compositional signatures</p> <p>Off disk: METIS: see above in table, He abundance</p>	<p>(1, 2, and 6)'' x 17' slits 1''/pixel and 76 mÅ/pixel</p> <p>Cadence: 16 min per raster</p>
Composition of solar wind and compositional changes at solar wind boundaries	SWA: mass, charge, energy of ions	Many heavy ion 1-D energy spectra (0.5 – 60 keV/q, 5% energy resolution); FOV = $\pm 25^\circ$, cadence: up to 1 min at 0.3 AU	METIS: see above in table SWA-HIS: 3-D VDFs, FOV = $(-30^\circ$ – $+66^\circ) \times (-17^\circ$ – $+22.5^\circ)$, 0.5 – 100 keV/e, 5.6% resolution, 5 min cadence, 30 s burst mode (heavy ions) 3 s (alpha particles) sensitivity $\sim 2 \cdot 10^{-5}$
Full-disk and high-resolution EUV images of chromosphere and corona	EUI: 174 and 304 Å and HI Ly-alpha	<p>FSI: 2 passbands (cool/hot), 5.5° FOV, 7.2''/pixel, 1 min maximum cadence, SNR > 2 in QS (dimming) and off limb (CME ejecta).</p> <p>HRI: 2 passbands, 17' FOV, > 1 k format, 5 s cadence in burst mode, SNR > 10 on AR loops (nanoflares).</p>	FSI: 5.2° x 5.2° at 9'' resolution, cool and hot passbands (He II 304 Å) and Fe IX/X 174 Å HRI: 1000'' at 1'' resolution Ly- α (1216 Å), Fe IX/X (174 Å)
In-situ magnetic field properties	MAG: magnetic field vector	± 1000 nT, 0.5 nT absolute precision; 0–20 Hz	Ranges: from ± 32 nT to ± 2048 nT at ~ 4 pT resolution, up to 128 vectors/s

Table 3.5 Measurement and instrument requirements (cont'd).

Required Observations (cf. Tables 3.1 – 3.4)	Instrument: Measurement	Measurement Requirements and Coordinated Observation Plans	Selected Payload Capability
High-cadence plasma properties	SWA: proton and electron E/q spectra MAG: magnetic field vectors	Solar wind protons: Detailed 3-D velocity distribution functions at 10 s time resolution; FOV: $\pm 45^\circ$ to Sun, $\pm 15^\circ$ north/south, angular resolution of 2° Solar wind electrons: 3-D velocity distribution functions (about 5 -5000 eV, 10% energy resolution); 10 s resolution MAG: already covered by previous requirements (see above in table) (MAG vectors will be used to derive reduced high-cadence VDFs by SWA)	SWA: up to 1/10 s (in burst mode), FOV = $(-24^\circ$ to $+42^\circ) \times (\pm 22.5^\circ)$, resolution $< 2^\circ$ SWA/EAS: FOV = $(360^\circ \times (\pm 45^\circ))$ on two orthogonal sensors for near 4π steradian total FOV, 1 eV - 5 kV, 10% resolution, 4 s/ 100 s cadence, 0.125 s in burst mode
Full-disk and high-resolution images of photospheric magnetic field	PHI: Stokes parameters of Fe I 617.3 nm line	High-Res Mode: Vector magnetic field with accuracy of 0.1 G (longitudinal), 20 G (transverse); $15' \times 15'$ FOV; resolution $\sim 1''$ (0.5'' pixel size) Cadence: 1 min over selected periods of time; Low-Res (full disk) Mode: Vector magnetic field with accuracy of 0.1 G (longitudinal), 2 G (transverse); Pixel size: $\sim 5''$; Capability: Cadence of 1 min over selected period of times on the whole orbit FOV: $> 150'$ (full apparent Sun)	PHI/HRT: accuracy: 0.1 G/14 G $16.8' \times 16.8'$ at 150 km (at 0.28 AU), $1.11''$ at 617.3 nm; cadence: 45-60 s PHI/FDT: accuracy same as for HRT cadence: 45-60 s FOV $> 156'$
High-resolution images of loops	EUI: high-resolution EUV images	EUI: already covered by previous requirements (see above in table)	See EUI/HRI resolution above
Wave propagation and heating	SPICE: Doppler broadening of lines; RPW: spectra and waveforms; METIS: coronal density fluctuations and Doppler broadening of He I and He II Ly α in a sector of the corona	SPICE: already covered by previous requirements (see above in table), plus motions to ± 5 km/s Radio waves: 3-axis electric and magnetic spectra and correlations; frequency range: 100 kHz to 20 MHz METIS (coronal imaging): see above in table; METIS (coronal spectroscopy): intensity, profile and Doppler shift of H I and He II Ly α lines at three radial positions (1.4° , 1.7° , 2.0°) from Sun center at equatorial latitudes around West limb (32° sector)	SPICE: see above in table; RPW: range from μ V/m to V/m, down to near-DC METIS (coronal spectroscopy): Slit radial position: 1.5° , 1.8° , 2.1° , slit extension 0.6° , spatial res.: $34''$, spectral res.: 0.054 nm (H I), 0.013 nm (He II), cadence: 30 s - 20 min

Table 3.5 Measurement and instrument requirements (cont'd).

Required Observations (cf. Tables 3.1 – 3.4)	Instrument: Measurement	Measurement Requirements and Coordinated Observation Plans	Selected Payload Capability
Magnetic connectivity	MAG: local field direction SWA: halo/strahl electron pitch-angle distribution	MAG: already covered by previous requirements (see above in table) SWA: electrons FOV at least 2π solid angle, ideally $\pm 180^\circ$ to Sun, $\pm 45^\circ$ north/south, angular resolution 10° , core-halo electron pitch-angle distributions with strahl population; While MAG provides B vector, strahl electrons and pitch-angle distributions give connectivity.	MAG: see above in table SWA/EAS: two orthogonal heads covering 2π each, 32 azimuth bins by (16-32) elevation bins
X-ray imaging of loops, flares	STIX: high-resolution energy-resolved X-ray images of loops and footpoints	Energy range: 3 to 150 keV; Energy resolution: $\Delta E/E \sim 0.2$ FWHM; Angular resolution: $< \sim 7'$; FOV for imaging: $> \sim 20'$; FOV for source centroid location: Full Sun at 0.28 AU, i.e. $\sim 150'$; Effective area ~ 15 cm ² ; time resolution (for flares) $< \sim 5$ s, ~ 1 s in burst mode	STIX: range: 4 – 150 keV, Resolution: 1 keV at 6 keV, 15 keV at 150 keV; imaging at scales from $7''$ to $8.8''$, field-of-view for imaging of 1.5° , source centroid location over full Sun at all radial distances, effective area 6.4 cm ² , < 0.1 s time resolution
Timing of radio emissions	RPW: magnetic/electric fields	3-axis electric and magnetic spectra and correlations; frequency range: 100 kHz to 20 MHz	From DC to 20 MHz/500 kHz (electric/magnetic) at up to 500 kS/s*
Timing of EUV emission	EUI: high-cadence imaging	10 s or better cadence	EUI: up to 2 s typical for EUV, sub-second in high-cadence mode for Ly α
Timing of energetic particles	EPD: proton/electron measurements: particle intensities in various energy ranges, velocity dispersion, different species	Electrons: Energy range: ~ 2 keV to ~ 1 MeV, energy resolution: $\Delta E/E \sim 0.2$, geometry factor $> \sim 0.1$ - 1 cm ² sr; time resolution 10 s at < 0.5 AU, 1 min > 0.5 AU Protons: Energy range: 0.005 to > 100 MeV; energy resolution: $\Delta E/E \sim 0.2$; geometry factor $> \sim 0.1$ - 1 cm ² sr; time resolution 20 s below 10 MeV at < 0.5 AU, 1 min > 0.5 AU	EPD/EPT: time resolution up to 1 s in burst mode, electrons 2 keV – 30 MeV ions: 3 keV – 100 MeV/nuc

* kS/s = kilosamples per second

Table 3.5 Measurement and instrument requirements (cont'd).

Required Observations (cf. Tables 3.1 – 3.4)	Instrument: Measurement	Measurement Requirements and Coordinated Observation Plans	Selected Payload Capability
Turbulence levels	MAG: high-cadence magnetic field RPW: high-cadence electric and magnetic field, power spectral densities	MAG: already covered by previous requirements (see above in table) Plasma wave electric spectra for thermal-noise spectroscopy; sensitivity: $3 \text{ nV/Hz}^{1/2}$; frequency range: 10 – 800 kHz. Electric and magnetic spectra and waveforms in an internal burst mode (triggered internally or on input), frequency range: near DC to 1 MHz; AC magnetic fields: 10Hz – 10kHz; waveform capture	MAG: see above in table RPW: see above in table, up to 500 kS/s*
Suprathermal seed population	SWA: high-cadence bulk ion and electron properties, EPD: electron and proton anisotropies	already covered by previous requirement (see above in table) Electrons: angular resolution 30° over 60° FOV as close to Sun as possible; Protons: two angular sectors from 0 - 90° as close to the Sun as possible up to 10 MeV	SWA: see above in table EPD: up to 1s (burst mode), EPT/HET 4 FOV, LET 6 FOV
Solar wind bulk properties	EPD: suprathermal particle composition	Heavy ions: He – Fe, energy range: 0.02 – 10 MeV/nucleon (species dependent) Composition: separate ^3He , ^4He , C, N, O and Fe as a minimum; energy resolution: $\Delta E/E \sim 0.2$; geometry factor $> \sim 0.1$ - $1 \text{ cm}^2 \text{ sr}$; time resolution 30 s $< 0.5 \text{ AU}$, 1 min $> 0.5 \text{ AU}$ SWA: already covered by previous requirements (see above in table)	EPD/SIS: $0.21 \text{ cm}^2 \text{ sr geom. factor}$; ^3He , major species He-Fe, $\Delta E/E < 0.1$; range 0.008 - 10 MeV/nuc SWA: $\sim 4 \text{ s cadence}$
Distribution of smallest flares and solar particle events	SWA: electron, proton, alpha-particle velocities, temperatures, densities EPD: small flux events STIX: low X-ray intensity	EPD: already covered by previous requirement (see above in table) STIX: already covered by previous requirements (see above in table) While STIX will observe bremsstrahlung emission in the X-ray range from energetic electrons at the Sun, EPD will measure the properties of the escaping particles to determine to determine the energy content in energetic particles.	EPD: Low-noise detectors & FEE, large geometric factors ($> 0.1 \text{ cm}^2 \text{ sr}$), LET up to $1.7 \text{ cm}^2 \text{ sr}$ in single-detector mode STIX: 6.4 cm^2 effective area

*kS/s = kilosamples per second

Table 3.5 Measurement and instrument requirements (cont'd).

Required Observations (cf. Tables 3.1 – 3.4)	Instrument: Measurement	Measurement Requirements and Coordinated Observation Plans	Selected Payload Capability
High-cadence measurements of the plasma micro state across a wide band of helio-latitudes for all relevant solar wind regimes and heliocentric distances	MAG: high-cadence magnetic field SWA: high-cadence 2-D electron/proton VDFs, composition RPW: high-cadence electric and magnetic field spectra, wave forms	MAG, SWA, RPW: already covered by previous requirements (see above in table) Accurate timing between the three instruments is ensured by SpaceWire time signal to in-situ payload. Occasional burst modes chosen such as to cover all solar wind regimes at all distances and latitudes. Burst mode coordinated between in situ instruments. Composition will be used to determine coronal origin of solar wind.	MAG: see above in table SWA: 0.125 s e ⁻ , 0.1 s protons, 3 s alpha articles, 30 s heavy ions RPW: low frequency (near DC up to local plasma frequency) and time-domain sampling, at up to 500 kS/s*
Images of source regions in Doppler-broadened lines	SPICE: on-disk imaging spectroscopy in UV METIS: off-limb imaging-spectroscopy in H I and He II Ly α lines	SPICE: already covered by previous requirements (see above in table) METIS: already covered by previous requirements (see above in table)	SPICE: see above in table METIS: see above in table
Identify dropouts and measure scattering of SEPs by turbulence	EPD: intensities and anisotropies of low-energy ions, protons and electrons MAG: B-vectors SWA: bulk solar wind	EPD: already covered by previous requirements (see above in table) at least 1st-order anisotropies (forward-backward) Use velocity dispersion plots in conjunction with pitch-angle distributions and correlate with solar wind turbulence levels and variations at the coronal source.	EPD/STEIN: few keV – 100 keV e ⁻ /p, 1 st order anisotropy EPD/EPT: 20 – 400 keV electrons, 20 – 7 MeV protons, 4 FOVs EPD/LET: low-energy protons in 6 FOV EPD/SIS: 0.01 – 10 MeV/nuc heavy ions
Time history of velocity and brightness of solar wind features and turbulence	METIS: high-cadence visible, H I and He II Ly α lines; SoloHI: white-light and pB	METIS: already covered by previous requirements (see above in table) Derive acceleration and heating properties from time-height and time-brightness plots. SoloHI: Provide density power spectra in selected regions along the ecliptic path of the s/c and compare with SWA measurements.	METIS: see above in table at 20 s cadence SoloHI: 2° x 5° FOV centered at 7, 15, 20 R _{sun} at 0.28 AU, 10 s – 2 min cadence with SNR > 16
High-resolution, high-cadence maps of photospheric magnetic field	PHI: Stokes parameters	PHI: already covered by previous requirements (see above in table)	PHI: see above in table at 1 hr cadence

* kS/s = kilosamples per second

Table 3.5 Measurement and instrument requirements (cont'd).

Required Observations (cf. Tables 3.1 – 3.4)	Instrument: Measurement	Measurement Requirements and Coordinated Observation Plans	Selected Payload Capability
Map CME source location, expansion, rotation, and composition through corona	<p>STIX: X-ray source location of associated flare</p> <p>EUI: high-resolution images of source region</p> <p>SPICE: on-disk and limb imaging spectroscopy</p> <p>METIS: H and He flow velocities, electron densities</p> <p>SoloHI: track to inner heliosphere</p> <p>RPW: radio emission</p>	<p>STIX, EUI, SPICE, METIS, SoloHI, RPW: already covered by previous requirements (see above in table)</p> <p>Coordinated observations focusing on promising active region. STIX/EUI measure associated flare, SPICE/METIS flow velocities, expansion of different ions, SoloHI tracks to interplanetary space, while RPW measures radio emission from accelerated electrons at local plasma frequency (compare with METIS e^- density)</p>	<p>STIX, EUI, SPICE, METIS, SoloHI: see above in table</p> <p>RPW: up to 20 MHz</p>
Map CMEs to in-situ properties	<p>PHI: high-resolution photospheric magnetic field</p> <p>EUI: high-resolution images of source region</p> <p>SPICE: composition of source region</p> <p>SWA: composition of in-situ CME</p> <p>RPW: time history of (type II) radio emission</p> <p>MAG: in-situ magnetic field rotation</p> <p>METIS: track CMEs in inner corona (coronal images in visible, H I and He II Ly α lines)</p> <p>SoloHI: image large-scale heliospheric structures, track CMEs to inner heliosphere</p>	<p>PHI, EUI, SPICE, METIS, SWA, RPW, MAG: already covered by previous requirements (see above in table)</p> <p>While EUI and STIX provide context and timing, SPICE gives composition, for comparison with SWA composition. Compare PHI and MAG field data, track evolution with RPW, METIS, SoloHI</p> <p>SoloHI: Use statistical properties of CMEs to link them to in-situ properties. When Solar Probe Plus is appropriately located, compare with in-situ data.</p>	<p>PHI, EUI, SPICE, METIS: see above in table</p> <p>SWA: elemental and charge-state composition</p> <p>RPW: up to 20 MHz</p> <p>MAG: see above in table</p>

Table 3.5 *Measurement and instrument requirements (cont'd).*

Required Observations (cf. Tables 3.1 – 3.4)	Instrument: Measurement	Measurement Requirements and Coordinated Observation Plans	Selected Payload Capability
Distribution of energy into heat, particle acceleration, and bulk kinetic energy	SWA: 3-D velocity distribution functions, bulk speed MAG: magnetic pressure EPD: particle spectra	SWA, MAG, EPD: already covered by previous requirements (see above in table) Measure directly, in-situ, the energy content in the various forms and acquire distribution as statistics build up.	SWA, MAG, EPD: normal operation mode
Energetic particle timing	EPD: particle intensities in different energy ranges and for different species	EPD: already covered by previous requirements (see above in table)	EPD: burst mode intervals
Image coronal suprathermal population	SPICE: imaging UV spectroscopy	SPICE: already covered by previous requirements (see above in table) excellent signal to noise ratio, low background Use intensity differences in highly Doppler-broadened lines	SPICE: see above in table
X-ray signatures of energetic particle interactions at loop footpoints or on loops themselves	STIX: high-cadence, energy resolved imaging	STIX: already covered by previous requirements (see above in table)	STIX: see above in table
Radio signatures of coronal shocks and escaping electrons	RPW: Type II and III radio	RPW: already covered by previous requirements (see above in table)	RPW: see above in table

Table 3.5 Measurement and instrument requirements (cont'd).

Required Observations (cf. Tables 3.1 – 3.4)	Instrument: Measurement	Measurement Requirements and Coordinated Observation Plans	Selected Payload Capability
Magnetic field, plasma wave, and solar wind measurements to determine turbulence levels and shock passage	MAG: high-cadence magnetic field RPW: high-cadence electric/magnetic field SWA: high-cadence bulk plasma properties, 2-D VDFs,	MAG: already covered by previous requirements (see above in table) RPW: already covered by previous requirements (see above in table) SWA: already covered by previous requirements (see above in table) Use RPW of MAG to trigger in-situ suite. MAG and SWA data provide Alfvén velocity and turbulence parameters such as Elsässer variables; RPW measures electric field properties which influence solar wind electron and proton VDFs.	MAG: burst mode (128 vectors/s) RPW, SWA: burst mode
Seed population specification from the heavy ion composition of solar wind and suprathermals in the heliosphere	SWA: heavy ion composition and long-term velocity distribution functions EPD: suprathermal particle population	SWA: already covered by previous requirements (see above in table) This drives upper range of HIS energy band (100 keV/e) EPD: already covered by previous requirements (see above in table) Cross calibrated SWA and EPD/SIS fluences over a wide range in latitudes and distance	SWA: normal operation mode EPD/SIS: normal operation mode high latitudes and full radial coverage
Timing, velocity distributions, scattering characteristics, spectra and composition of energetic particles, continuous spectra of multiple heavy ion species in energy range 0.1–100 MeV/n	EPD: full composition, anisotropies, energy coverage, occasional high-cadence studies; Resolution of ^3He and multiple heavy ion species	EPD: already covered by previous requirements (see above in table)	EPD: 2 keV – 20 MeV e^- , 3 keV – 100 MeV p; 8 keV/n – 200 MeV/n ions continuous coverage with geometric factors > 0.1 cm^2sr 4 – 20 keV neutrals, normal operation, occasional burst mode

Table 3.5 Measurement and instrument requirements (cont'd).

Required Observations (cf. Tables 3.1 – 3.4)	Instrument: Measurement	Measurement Requirements and Coordinated Observation Plans	Selected payload capability
<p>Timing of EUV, radio, and X-ray emissions in relation to energetic particle intensities at a wide range of energies</p>	<p>EUI, STIX: high-cadence imaging of active region, trigger to EPD RPW: type II and type III radio emission EPD: staggered high-cadence measurements of particle intensities</p>	<p>EUI, STIX, RPW, EPD: already covered by previous requirements (see above in table) EUI/STIX provide trigger to EPD. RPW gives shock location (if present) from radio emission, and EPD determines particle properties. HET and EPT (for electrons) are triggered first, lower energy LET later (velocity dispersion)</p>	<p>EUI, STIX, RPW, EPD: see above in table</p>
<p>Full-disk & high-resolution maps of the photospheric magnetic field and local and convective flows, maps of rotation, differential rotation, and meridional circulation, structure of subduction areas, properties of sub-surface convection cells;</p>	<p>PHI: full-disk and high-resolution Stokes parameters, Doppler shifts, intensity variations</p>	<p>High-Res. Mode: Vector magnetic field with accuracy of 0.1 G (longitudinal), 20 G (transverse); Doppler velocity with accuracy of 15 m/s; Continuum images with accuracy of 0.5% (flat field uniformity) 15'x15' FOV; resolution 1" (0.5" pixel size); Cadence: 1 min over selected periods of time; Low-Res. (Full Disk) Mode: Vector magnetic field with accuracy of 0.1 G (longitudinal), 20 G (transverse); Doppler velocity with accuracy of 15 m/s; Continuum images with accuracy of 0.5% (flat field uniformity) Pixel size: ~5"; Cadence: 1 min. over selected periods of time FOV: >150' (full apparent Sun)</p>	<p>PHI/HRT: Accuracy: 0.1 G/14 G; 7 m/s; 0.5% 16.8' x16.8' FOV, 1.11" resolution at 617.3 nm; 45-60 s cadence PHI/FDT: accuracy same as for HRT Cadence: 45 – 60 s FOV > 156'</p>
<p>High-resolution images of small-scale magnetic features at the poles</p>	<p>EUI: high-resolution EUV images SPICE: high-resolution spectroscopy PHI: high-resolution Stokes parameters</p>	<p>EUI, SPICE, PHI: already covered by previous requirements (see above in table) Coordinated high-resolution FOV</p>	<p>EUI, SPICE, PHI: normal operation mode</p>

Table 3.5 Measurement and instrument requirements. (cont'd)

Required Observations (cf. Tables 3.1 – 3.4)	Instrument: Measurement	Measurement Requirements and Coordinated Observation Plans	Selected Payload Capability
Amount, distribution, and evolution of polar photospheric magnetic flux	PHI: full-disk and high-resolution Stokes parameters	PHI: already covered by previous requirements (see above in table)	PHI: normal operation mode
Transversal magnetic field in the photosphere	PHI: high-resolution Stokes parameters other remote-sensing observations (e.g. SDO/HMI)	PHI: already covered by previous requirements (see above in table)	PHI: normal operation mode
Latitudinal distribution of small-scale, emerging magnetic flux in the photosphere	PHI: high-resolution Stokes parameters	PHI: already covered by previous requirements (see above in table)	PHI: normal operation mode
Position and speed of shocks	METIS: flow velocities, electron densities SoloHI: white-light coronagraphy SPICE: temperatures from Doppler-broadened lines RPW: radio emissions	METIS, SoloHI, SPICE: already covered by previous requirements (see above in table) Use METIS electro-density maps to pinpoint radio emission and compare with RPW type-II radio bursts. Compare speeds of features in METIS/SPICE with derived velocities, use temperatures and magnetic field extrapolations to determine magnetosonic speed and compare with shock speed. Follow shocks in SoloHI images and extract speed and density profile	METIS, SPICE, RPW: see above in table SoloHI: FOV 5.5° – 45.5°, cadence 6-15 min
High-cadence microphysics of plasma	SWA: burst mode 2-D velocity distribution functions MAG, EPD: burst mode RPW: burst mode trigger to in-situ	SWA, MAG, EPD, RPW: already covered by previous requirements (see above in table)	SWA, MAG, EPD, RPW: see above in table

Table 3.5 Measurement and instrument requirements. (cont'd)

Required Observations (cf. Tables 3.1 – 3.4)	Instrument: Measurement	Measurement Requirements and Coordinated Observation Plans	Selected Payload Capability
Timing and properties of small events	STIX: high-cadence, high-resolution EUI: high-cadence, high-resolution images EPD: energy spectra of electrons and protons RPW: high-cadence	STIX, EUJEPD: already covered by previous requirements (see above in table) RPW: already covered by previous requirements (see above in table), low background, low noise	STIX, EUI, EPD, RPW: see above in table
Images of longitudinal extent of CMEs in visible and UV	METIS: flow velocities SoloHI: white light EUI: UV images	METIS, SoloHI, EUI: already covered by previous requirements (see above in table)	METIS, SoloHI, EUI: see above in table
Magnetic fields, plasma flows, and temperatures of polar regions	PHI: high-resolution photospheric magnetic field EUI: high-resolution EUV images SPICE: high-resolution images, Doppler-broadened lines	PHI, EUI, SPICE: already covered by previous requirements (see above in table)	PHI, EUI, SPICE: see above in table
Images of coronal and heliospheric structure in visible and EUV	METIS: electron density, H, He flows SoloHI: white-light images of corona EUI: coronal images	METIS, SoloHI, EUI: already covered by previous requirements (see above in table)	METIS, SoloHI, EUI: see above in table
Images of evolution of coronal hole boundaries	EUI: full-disk images in EUV METIS: images of coronal boundaries in the inner corona SoloHI: images of the coronal boundaries in the inner heliosphere	EUI, METIS, SoloHI: already covered by previous requirements (see above in table) Make available as data product for comparison with in-situ data and observations from near-Earth assets.	EUI, METIS, SoloHI: see above in table

3.1.2 Orbit Requirements

The science objectives discussed in Chapter 2 specifically identify a set of orbit characteristics and mission design parameters that define the Solar Orbiter mission. In summary, the requirements on the orbit are to: 1) go close to the Sun (within 0.3 AU); 2) have periods of reduced angular velocity of the spacecraft with respect to the solar surface (keeping in sight individual solar surface features for ~20 days, the maximum length of a remote-sensing observing window); 3) achieve moderate out-of-ecliptic viewing (~25°) and latitudinal coverage; and 4) comprehensively characterize conditions in the inner heliosphere as a function of distance and latitude. The science working team and project scientists have worked closely with the ESA Project engineers to design a mission that is both feasible from an engineering point of view and will achieve the science objectives discussed in the preceding chapter. Critical factors that drive the mission and spacecraft design are the perihelion distance and the inclination of the orbit. The scientific rationale for these requirements is reviewed below.

Perihelion Distance Requirement. In order to measure the less processed, pristine solar wind streams and the ongoing interaction at their interfaces as well as the kinetic processes that accelerate and heat the wind, Solar Orbiter must have a minimum perihelion within 0.3 AU. Another driver to go close to the Sun is the measurement of energetic particles, which should be made within one or two scattering mean free paths (typically 0.2 AU; Palmer 1982) of their source in order to minimize propagation effects. Solar Orbiter must therefore spend sufficient time within 0.4 AU to pass over several active regions during several solar rotations.

Solar Orbiter's perihelion distance also determines the degree to which the spacecraft can track features on the solar surface for extended periods (so-called near-corotation). The main drivers for near-corotation are the need to observe solar features or source regions, while at the same time sampling in situ the solar wind and energetic particles emanating from them on time scales which are comparable to their growth and evolution. From Earth orbit, no region can be observed for more than 14 days, observations being further restricted by line-of-sight effects when the regions are near the solar limb.

Latitude Requirement. The principal driver for attaining an out-of-ecliptic vantage point is to resolve outstanding questions about the dynamics of the solar dynamo and to measure directly the fast/slow solar wind boundary emanating from the edges of high latitude coronal holes. The inclination of the heliospheric current sheet (HCS) means that this boundary must be sampled at a range of latitudes, comparable to the HCS inclination, resulting in a requirement to measure from $\pm 15^\circ$ solar latitude within 0.5 AU. In order to accurately measure the polar magnetic field and its dynamics and meridional transport, at least five consecutive days of observations above 25° are required. As is clearly visible in Figure 5.2, the 25° solar latitude reached at the end of the nominal science mission is sufficient to perform those crucial measurements.

Comprehensive Characterization of the Inner Heliosphere. Many of Solar Orbiter's science objectives require a comprehensive characterization of the properties of the inner heliosphere at a level of sophistication never previously achieved. The only other mission to explore the inner heliosphere between 0.3 and 1 AU, Helios, had a payload limited in many ways (measurements, cadence) compared to modern instrumentation and lacked several critical elements such as remote-sensing (imaging and spectroscopy) observations and composition measurements. Helios was also restricted to measurements in the ecliptic plane. Solar Orbiter will make critical, previously unavailable measurements that are essential to fully characterize the inner heliosphere and relate these properties out to near-Earth measurements at 1 AU.

The scientific measurement requirements detailed above place the following specific requirements on the spacecraft: (a) Solar Orbiter must be a three-axis stabilized spacecraft with a pointing accuracy sufficient to achieve the scientific objectives; (b) Solar Orbiter must satisfy electromagnetic cleanliness such that the magnetometer, particle detectors and radio and plasma waves instruments can accurately measure relevant physical parameters. (c) For each operational orbit, the Solar Orbiter spacecraft must allow full operations of the complete payload for a minimum of three continuous periods of 10 days each. Other, more general requirements can be found in Section 5.1.

4 Payload

The Solar Orbiter payload was selected from proposals submitted in response to the ESA AO for the Solar Orbiter Payload (released on 18 October 2007) and to the NASA SMEX/FOSO AO (released on 22 October 2007). Following a review of the 14 proposals submitted to ESA, the PRC issued a final report on 24 May 2008 recommending a payload for selection. ESA subsequently called for an independent review of the PRC's recommended payload in the context of a joint scientific programme with NASA's high-priority Solar Probe Plus mission.² The joint ESA-NASA review panel confirmed the validity of the recommended payload in its report of March 2009. As a result, the instrument selections as recommended by the PRC in 2008 were formally announced on 20 March 2009 (selection to be confirmed after mission approval). In parallel, NASA announced the results of the FOSO selection, and selected 2 instruments and portions of 2 instruments to be included in the Solar Orbiter payload.

The selected payload is described in the sections that follow, and Figure 4.1 illustrates the accommodation of the instruments on the spacecraft. An overview of the payload is shown in Table 4.1, and a summary of the payload resource requirements is shown in Table 4.2. The available payload resource envelope is 180 kg of mass and 180 W of power, and includes resources for several payload support elements. A summary of the overall payload resources can be found in Table 4.3. Complete, detailed information about the selected payload can be found in the individual Engineering Interface Documents, Parts B (EID-Bs).

In March 2011, NASA informed ESA that, as a consequence of budgetary pressures, it had become necessary to reduce its contribution to the payload to 1 full instrument and 1 sensor. Specifically, the Spectral Imaging of the Coronal Environment and Suprathermal Ion Spectrograph investigations would not be funded. Given the scientific importance of these investigations, their measurement capabilities will be recovered through the inclusion of European-lead instruments with contributions from member states and ESA.

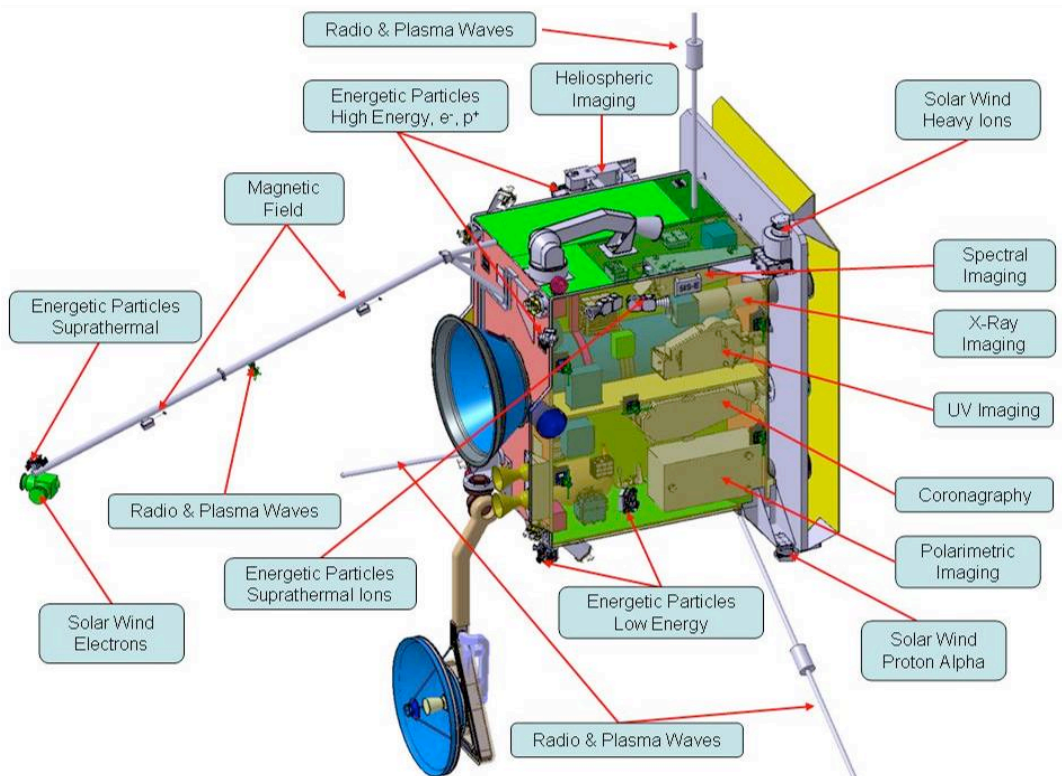


Figure 4.1. Payload accommodation onboard Solar Orbiter.

² The PRC's original payload recommendation was made in the context of the HELEX programme, a joint ESA-NASA programme involving both Solar Orbiter and the NASA Sentinels mission. During the course of 2008, however, NASA assigned higher priority to a redesigned Solar Probe mission, Solar Probe Plus, which is planned to be operating at the same time as Solar Orbiter and whose science objectives are strongly synergistic with those of Solar Orbiter (cf. Chapter 6).

4.1 In-Situ Instruments

4.1.1 Solar Wind Analyzer (SWA)

The Solar Wind Analyzer (SWA) instrument suite (Figure 4.2) comprises 3 sensors and a shared data processing unit (DPU), and will completely characterize the solar wind between 0.28 – 1.4 AU. The overarching objective of SWA is to provide comprehensive in-situ measurements of the solar wind to establish the fundamental physical links between the Sun's highly dynamic magnetized atmosphere and the solar wind in all its quiet and disturbed states. These measurements are vital to Solar Orbiter objectives addressing the origin of the solar wind, solar eruptions, shocks and the suprathermal ions that are the seed populations of hazardous solar particle events. To meet or exceed all the measurement requirements, SWA must be able to measure the three-dimensional velocity distribution functions of the major solar wind constituents: protons, alpha particles and electrons. The basic moments of the distributions, such as density, velocity, temperature tensor, and heat flux vector need to be obtained under all solar wind conditions and should be sampled sufficiently rapidly to characterize fully the fluid and kinetic state of the wind. In addition, measurements of representative high-FIP elements (the C, N, O group) and of low-FIP elements (such as Fe, Si or Mg) are required. These comprehensive and coordinated plasma measurements provided by SWA use simple, high-heritage components flown on previous missions, including Ulysses, ACE, Helios, STEREO, Wind, SOHO, Cluster and Cassini. The 3 sensors are:

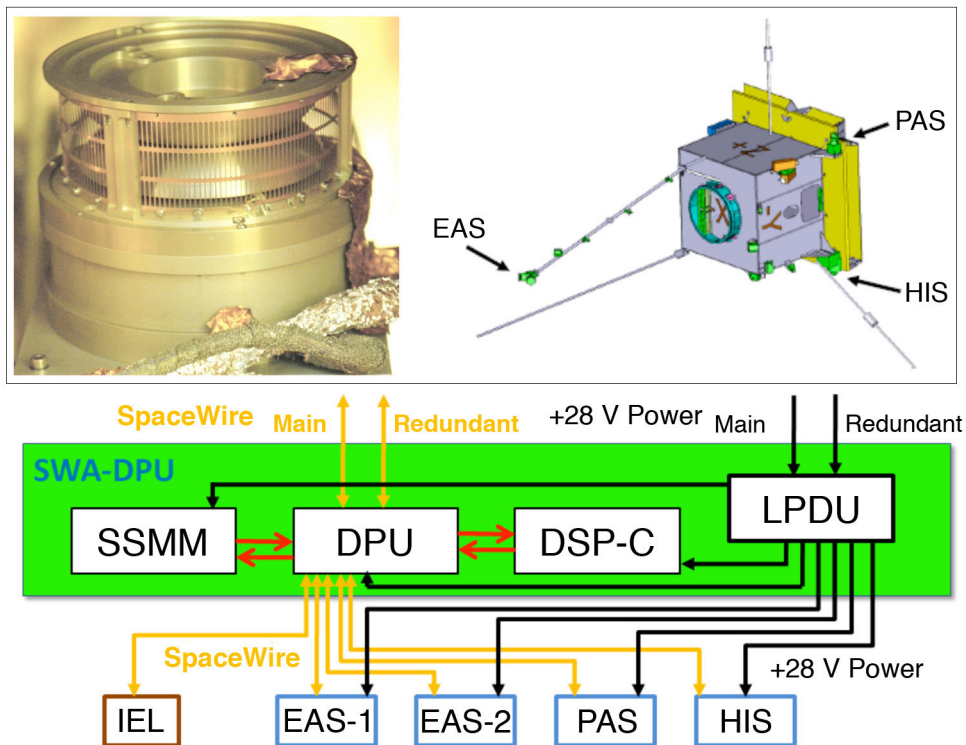


Figure 4.2. Solar Orbiter's Solar Wind Analyzer. Upper left: EAS prototype; upper right: location of the SWA sensors; bottom: SWA block diagram.

a) The Electron Analyzer System (SWA-EAS). SWA-EAS consists of a pair of top-hat electrostatic analysers with aperture deflection plates mounted in the shadow of the spacecraft at the end of the instrument boom. Orthogonal mounting of the 2 sensors and the $\pm 45^\circ$ aperture deflection provides an almost full 4π field-of-view subject only to minor blockage by the spacecraft and its appendages. The sensor will measure electron fluxes in the energy range from ~ 1 eV to ~ 5 keV with $\Delta E/E \sim 10$ -12% and an angular resolution $\leq 10^\circ$. Moments of the electron distribution will be returned with a cadence of 4 s, although the sensor will be capable of returning full 3-D distributions at lower cadence, and 2-D electron pitch angle distributions at ~ 0.125 s cadence during short periods of burst mode. A photo of the prototype EAS is shown in Figure 4.2 (upper left). The location of the two EAS sensors (along with PAS and HIS) sensors is also shown in Figure 4.2 (upper right).

Table 4.1 Overview of the Solar Orbiter payload.

Investigation	Principal Investigator	Collaborating countries (hardware)	Measurement	Technique
Solar Wind Analyzer (SWA)	C. Owen, MSSL, UK	UK, I, F, USA	Solar wind ion and electron bulk properties, ion composition (1 eV - 5 keV electrons; 0.2 - 100 keV/q ions)	Multiple sensors (electrons, proton/alpha, heavy ions); electrostatic deflection, time-of-flight measurement, solid state detectors
Energetic Particle Detector (EPD)	J. Rodriguez-Pacheco, Univ. of Alcalá, E	E, D, FI, S. Korea, USA, ESA	Composition, timing, and distribution functions of suprathermal and energetic particles (8 keV/n - 200 MeV/n ions; 20-700 keV electrons)	Multiple solid-state dE/dx vs E detector telescopes, time-of-flight measurement
Magnetometer (MAG)	T. Horbury, ICSTM, London, UK	UK	DC vector magnetic fields (0 - 64 Hz)	Dual fluxgate sensors
Radio & Plasma Waves (RPW)	M. Maksimovic, Obs de Meudon, Paris, F	F, SE, CZ, A	AC electric and magnetic fields (~DC - 20 MHz)	Electric antennas, Search Coil Magnetometer; Low-frequency and Thermal Noise/High-frequency receivers, Time-domain sampling
Polarimetric and Helioseismic Imager (PHI)	S. Solanki, MPS, Lindau, D	D, E, F	Vector magnetic field and line-of-sight velocity in the photosphere	High-resolution telescope: off-axis Ritchey-Chrétien, Full-disk telescope: refractor, Fabry-Pérot filtergraph
EUV Imager (EUI)	P. Rochus, CSL, Liege, B	B, UK, F, D, CH	Full-disk EUV and high-resolution EUV and Lyman- α imaging of the solar atmosphere	Full-Sun imager: dual-band EUV off-axis Herschelian, 2 High-res.. imagers: EUV + Ly α off-axis Ritchey-Chrétien
X-ray Spectrometer Telescope (STIX)	A. Benz, FHNW Windisch, CH	CH, PL, D, CZ, F	Solar thermal and non-thermal X-ray emission (4 - 150 keV)	Fourier transform imaging, CZT detectors
Coronagraph (METIS)	E. Antonucci, INAF-OATo, Turin, I	I, D, CZ	Visible, UV and EUV imaging of the solar corona	Externally-occulted coronagraph
Heliospheric Imager (SoloHI)	R. Howard, NRL, Washington DC, USA	USA	White-light imaging of the extended corona	Wide-angle lens with aperture stop
Spectral Imaging of the Coronal Environment (SPICE)	N/A (European-led instrument)	TBD	EUV spectroscopy of the solar disk and low corona	Off-axis paraboloid telescope, TVLS grating spectrograph

Table 4.2 Solar Orbiter selected payload resource summary.

Investigation	Basic Mass (kg)	Contin-gency (%)	Basic Power (W)	Contin-gency (%)	Contin-gency (%)	Dimensions	Telemetry (kpbs)	FOV	Heritage
Solar Wind Analyzer (SWA)	18.65	16.3	15.60	16.1		EAS: 11.6 cm x dia. 13.6 cm PAS: 30 x 20 x 20 cm HIS: 31 x 28 x 25 cm	14	EAS: 360° x ± 45° x 2 orthogonal sensors to provide 4- π ster FOV PAS: -24° to +42.5° Azimuth, -22.5° to +22.5° Elevation HIS: -30° to +66° Azimuth, -17° to +22.5° Elevation	Ulysses, ACE, STEREO
Energetic Particle Detector (EPD)	15.68	24.5	29.95	20.5		EPT1,2: 11 x 7 x 12 cm SIS: 35 x 13 x 11 cm LET 1,2: 22 x 15 x 11 cm HET: 13.6 x 17 x 16.2 cm STEIN: 10 x 13 x 13 cm CDPU/LVPS: 15 x 15 x 10 cm	3.1	EPT1,2: 30° cones SIS: 22° cone LET1,2: 40° cone (3x) HET: 50° cone (x2) STEIN: 60° x 70° (2x)	STEREO, SOHO, ACE
Magnetometer (MAG)	1.94	9.8	4.39	31.4		Fluxgate sensor (2x): 9.75 x 4.9 x 6.7 cm Electronics: 15.9 x 16.2 x 9.8 cm	0.9 (normal) 6.8 (burst mode)	N/A	VEX, Themis, Rosette Lander, Double Star
Radio & Plasma Waves (RPW)	13.45	18.4	18.07	16.7		Antenna (3x): 650 cm long SCM: 13.6 x dia. 10.4 cm Electronics: 24 x 21 x 15 cm	5	N/A	STEREO
Polarimetric and Helioseismic Imager (PHI)	29.90	23.4	28.30	14.8		Optical unit: 79.5 x 40 x 29 cm Electronics: 20 x 40 x 29 cm	20	HRT: 16.8 x 16.8' FDT: 2.6° cone	SUNRISE/IMaX
EUV Imager (EUI)	16.32	28.5	28.24	25.0		Optical bench: 83 x 54.5 x 22.8 cm Electronics: 120x300x250 mm	20	FSI: 5.2° x 5.2° HRI: 1000 x 1000"	SOHO, STEREO, TRACE, PROBA2
X-ray Spectrometer Telescope (STIX)	4.88	10.0	3.63	20.1		Imager Module: 55 x dia. 18 cm Spectrometer: 18 x 20 x 22 cm Electronics: 16 x 20 x 22 cm	0.2	2.5° for spectroscopy 1.5° for imaging	RHESSI
Coronagraph (METIS)	19.20	20.0	18.08	25.0		Optical Bench: 90 x 44 x 25 cm Electronics: 22 x 25 x 10 cm	10	1.5°-3° annular, off-limb corona	SCORE/HERSCHEL
Heliospheric Imager (SoloHI)	12.35	27.0	9.78	22.7		Optical unit: 425x140x180 mm Electronics: 100x100x50 mm	20	40° x 40°, offset 5° from Sun centre	STEREO
Spectral Imaging of Coronal Environment (SPICE)	16.72	16.7	26.60	25.2		Optical bench: 91.1 x 34.9 x 17.7 cm Electronics: 20 x 18.6 x 12.4 cm	17	1" x 17' slit	SOHO, SUMER, CDS, Hinode

Payload Element	Estimated Mass (kg)	Basic Power (W)
In-Situ Instruments	59.26	68.01
Remote Sensing Instruments	121.49	114.63
TOTAL	180.75	182.64

Table 4.3 Payload resource summary: Estimated mass (basic mass + contingency) and basic power.

b) The Proton-Alpha Sensor (SWA-PAS). SWA-PAS comprises a top-hat electrostatic analyser (EA) designed to measure the full 3-D velocity distribution functions of major solar wind species, protons and alpha particles in the energy range $\leq 0.2 - 20$ keV/q, with $\Delta E/E \sim 7.5\%$, an angular resolution $\leq 2^\circ$ across a field of view of -24° to $+42.5^\circ$ by $\pm 22.5^\circ$ about the solar direction and a cadence of 4 s. Reduced distribution functions (1.5-D) of the solar wind protons and alpha particles over a similar energy range will be returned at higher cadence (0.125 s or better) during burst modes.

c) The Heavy Ion Sensor (SWA-HIS). SWA-HIS consists of an electrostatic analyser module with ion steering to achieve the required extent of the HIS field-of-view (-30° to $+66^\circ$ by -17° to $+22.5^\circ$), coupled with a time-of-flight (TOF) telescope with solid state detectors for total ion energy measurements. HIS will measure five key properties for all ions: mass in the range 2 - 56 amu/q, charge (q), energy in the range 0.5 - 100 keV/q (for azimuth) and 0.5 - 16 keV/q (for elevation), $\Delta E/E \sim 6\%$ and direction of incidence (θ , φ) with $6^\circ \times 6^\circ$ pixel resolution. The time resolution for 3-D distribution measurements is 5 minutes for a full scan in normal mode and 30 s for heavy ions or 3 s for alphas in burst mode.

The HIS and PAS sensors require fields of view containing the Sun-direction and therefore require apertures in the spacecraft heat shield or (preferably) mounting at the edge of the heat shield in such a way that they can protrude beyond its edge. The SWA plasma sensors are integrated into a suite, and serviced by a common DPU, which provides a single power, telemetry, and control interface to the spacecraft as well as power, switching, commanding, data handling and data compression functions for all of the sensors (see electrical block diagram, Figure 4.2 bottom panel).

4.1.2 Energetic Particle Detector (EPD)

The Energetic Particle Detector (EPD) experiment will measure the composition, timing, and distribution functions of suprathermal and energetic particles. Scientific topics to be addressed include the sources, acceleration mechanisms, and transport processes of solar energetic particles; magnetic connectivity through the use of suprathermal particles as field-line tracers; the radial dependence of CME-driven shocks and associated particle populations. EPD covers the energy range from just above the solar wind (a few keV/n) to relativistic electrons and high-energy ions (100 MeV/n protons, 200 MeV/n heavy ions). The overall energy coverage achieved with the EPD sensors is 0.002 MeV to 20 MeV for electrons, 0.003 MeV to 100 MeV for protons, 0.008 MeV/n to 200 MeV/n for heavy ions (species-dependent).

EPD consists of 5 separate sensors sharing a common data processing unit and low voltage power supply (CDPU/LVPS). Each sensor has specific measurement tasks to cover the required range of particles and energies. Multiple sensor heads at different locations on the spacecraft and/or multiple view directions relative to the magnetic field direction are required for measuring pitch angle distributions of particles. The sensors apply solid state charged particle detectors of various types, electrostatic deflection and time-of-flight systems, microchannel plates, thin foils, and magnets. The sensors and their measured particle species and energies are:

a) The SupraThermal Electrons Ions and Neutrals Telescope (STEIN). STEIN is a double-ended telescope, utilizing passively cooled silicon semiconductor detectors (SSDs) to measure suprathermal particles from $\sim 3 - 100$ keV. STEIN utilizes an electrostatic deflection system to separate electrons and ions up to ~ 40 keV, and neutrals up to ~ 10 keV. STEIN is mounted on the magnetometer boom, with back-to-back $70^\circ \times 60^\circ$ fields of view covering both directions along the Parker spiral.

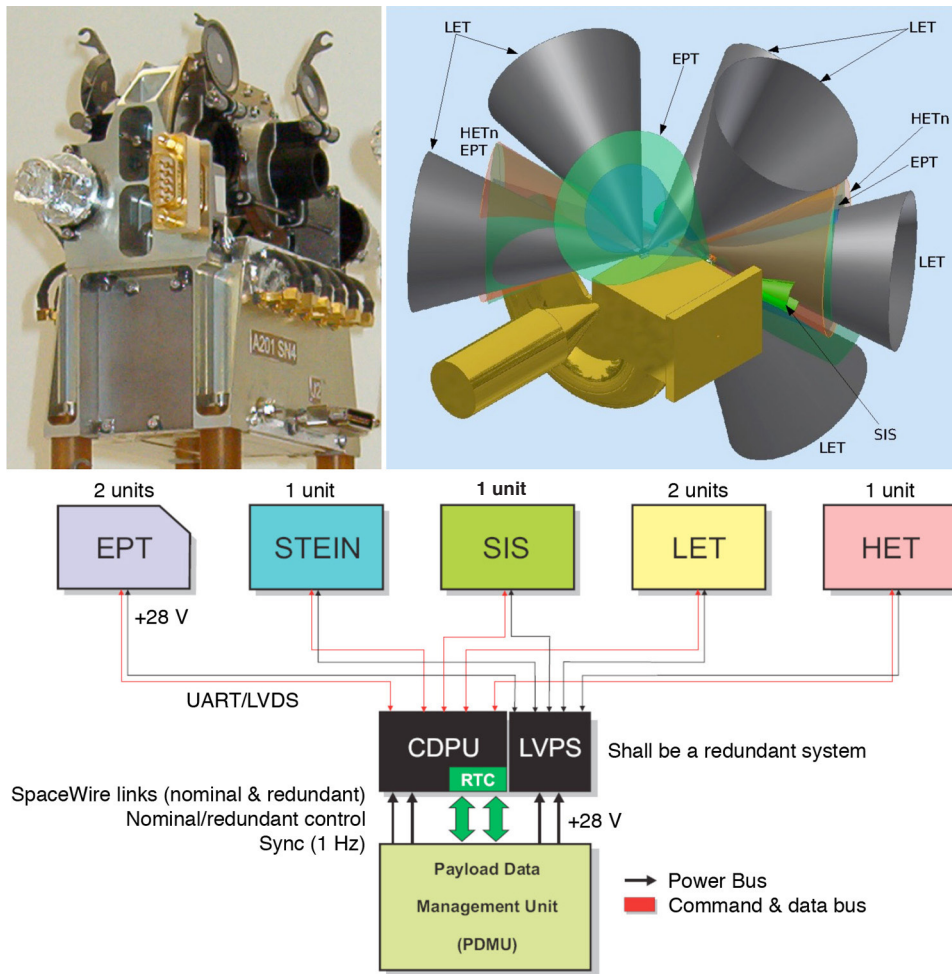


Figure 4.3. Solar Orbiter's Energetic Particle Detector. Upper left: the Electron Proton Telescope; upper right: the fields-of-view for each of the EPD sensors; bottom: EPD block diagram.

b) The Electron Proton Telescope (EPT). EPT (see Figure 4.3 upper left) measures electrons (20 keV to 700 keV) and protons (20 keV to 9 MeV) as well as their anisotropies. It consists of two dual double-ended telescopes. EPT1 points in the ecliptic plane along the Parker spiral in both the solar and anti-solar directions; EPT2 points 45° out of the ecliptic plane. The fields of view may be adjusted during the definition phase in the event of accommodation issues. EPT combines the dE/dx -E method with the magnet/foil technique in order to separate electrons from protons and heavier ions, and has extensive heritage from the successful instruments STEREO/SEPT and SOHO/EPHIN.

c) The Low Energy Telescope (LET). LET measures the species H-Ni over the energy range $\sim 1.5 - 60$ MeV/n. LET telescopes each have a 40° full angle FOV for high resolution of the different species, with 6 FOVs both in-ecliptic and out-of-ecliptic to provide particle anisotropies. LET covers the energy range where SEP energy spectral indices steepen ('break'). It can resolve ^3He and multiple heavy ion species in order to identify particle sources as well as the dependence of particle charge to mass ratio on the acceleration and transport processes. LET heritage is from SOHO/ERNE.

d) The High Energy Telescope (HET). HET covers the high-energy particle range for protons (up to 100 MeV) and heavier ions (200 MeV/nuc for O and heavier species), thus providing information on the largest SEP events, which can produce high energy, damaging interplanetary radiation levels. HET has two oppositely directed FOV with 50° full angle and resolves ^3He and multiple heavy ion species. HET's large collecting power allows fast cadence for high-energy heavy ions. During the study phase, the possibility of obtaining limited information on the neutron flux intensity from HET will be investigated.

e) The Suprathermal Ion Spectrograph (SIS). SIS measures the composition of heavy ions (He-Fe) over the energy range ~ 8 keV/n – 10 MeV/n. Ultra-heavy ions in ^3He -rich solar flare events will also be measured over a limited energy range below 1 MeV/n. SIS comprises one telescope with 22° FOV, pointing in the sunward hemispheres and with large (>12 cm 2) detector area required to characterize the previously unexplored ambient suprathermal ion pool in the inner heliosphere. SIS's high mass resolution ($m/\delta m \sim 50$) will allow detection of trace amounts of ^3He , and detailed abundant determination of multiple heavy ion species over the range He-Fe. SIS heritage is from the ACE/ULEIS instrument. The FOV of each of the EPD sensors is shown in Figure 4.3 (upper right). An electrical block diagram showing the 5 separate EPD sensors, common data processing unit and low voltage power supply (CDPU/LVPS) is shown in the bottom panel of Figure 4.3.

4.1.3 Magnetometer (MAG)

The magnetometer (MAG) experiment (Figure 4.4) will provide in-situ measurements of the heliospheric magnetic field with high precision. In addition to studies of the near-Sun heliospheric plasma and fields, MAG will address how the magnetic field links into space and evolves over the solar cycle; how waves and turbulence are generated and dissipated, and how heliospheric structures develop in the inner solar system.

The magnetometer instrument comprises two digital fluxgate sensors operated in the dual-magnetometer mode (both in shadow and mounted on the instrument boom behind the spacecraft body) and an electronics box located inside the spacecraft structure. In-board to out-board sensor separation on the boom will be ~ 2 m. The fluxgate sensor design is highly suited to the Solar Orbiter mission, since it exhibits excellent stability, both with respect to time and changing temperature. A photograph of one of the sensors (cover removed) is shown in Figure 4.4. This sensor design has solid space heritage, having flown successfully on Cassini and Double Star. The dual-magnetometer technique allows background fields induced by the spacecraft to be subtracted from the true heliospheric magnetic field.

In addition to the fluxgate sensors with their own dedicated front-end electronics, the main functional elements of the instrument are an instrument controller unit (ICU) to control the instrument and manage communications with the spacecraft, and a power converter unit (PCU) for provision of secondary voltages to the sensor electronics, ICU and sensor heaters. The instrument block diagram is shown in Figure 4.4 (left). The MAG instrument is largely autonomous in operation, requiring only a minimum of commanding for selecting from a set of science operations modes and corresponding telemetry bit-rates.

Preliminary thermal modelling shows that each sensor will require 0.6 W to maintain the sensors within the operating temperature range. The power of the required heaters will be confirmed once a boom design is selected and more detailed studies of the thermal environment have been completed.

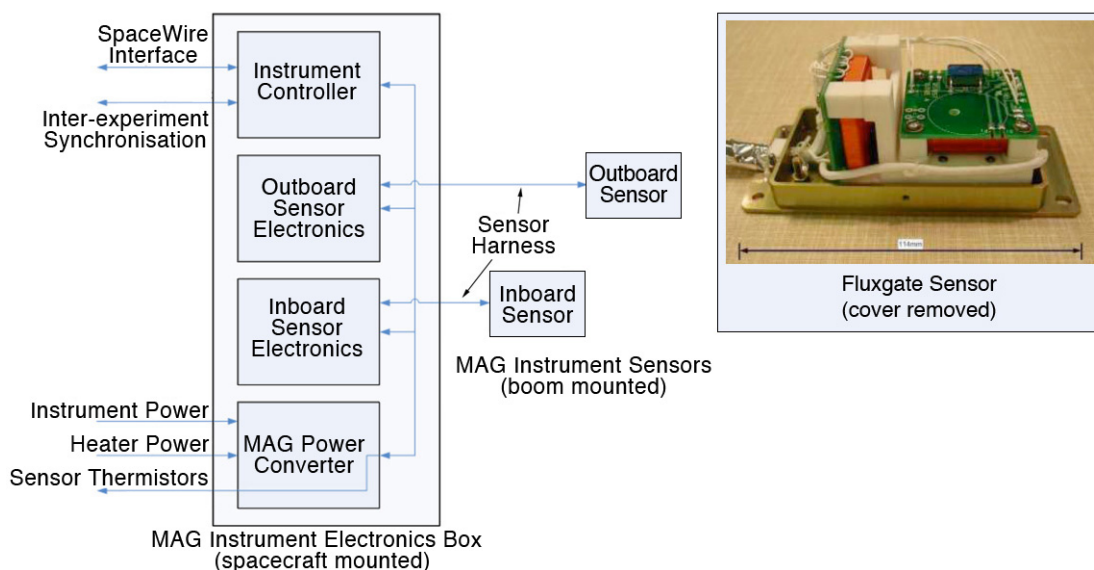


Figure 4.4. Solar Orbiter's magnetometer. One of the sensors (with the cover removed) is shown on the right.

4.1.4 Radio and Plasma Waves (RPW)

The Radio and Plasma Waves (RPW) experiment (Figure 4.5) is unique amongst the Solar Orbiter instruments in that it makes both in-situ and remote-sensing measurements. RPW will measure magnetic and electric fields at high time resolution using a number of sensors/antennas, and it will determine the characteristics of electromagnetic and electrostatic waves in the solar wind from almost DC to 20 MHz.

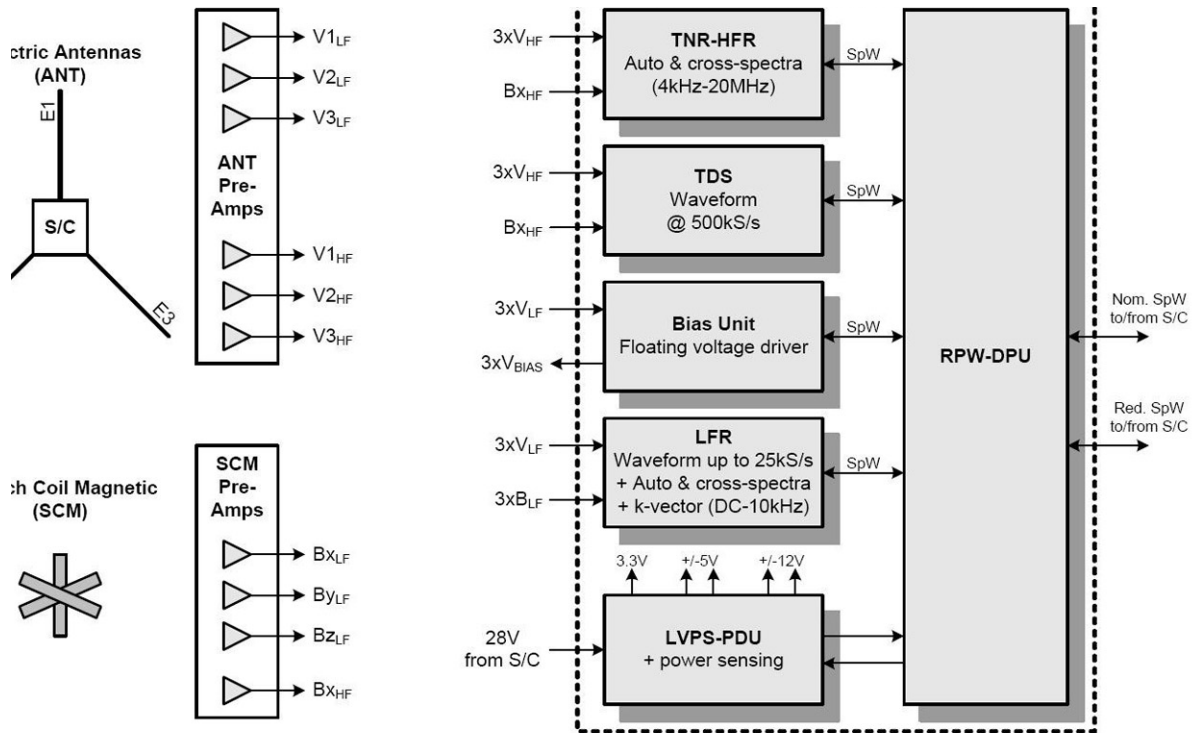


Figure 4.5. Block diagram of Solar Orbiter's Radio and Plasma Waves experiment. The placement of the antennas is illustrated in Figure 4.2 (upper right panel).

RPW has heritage from STEREO and BepiColombo Mercury Magnetospheric Orbiter (MMO) and consists of:

a) The Low Frequency Receiver (LFR). LFR covers both in-situ electric and magnetic measurements from DC to about 10 kHz and will provide both waveform and power spectra in this frequency range. High-level processed data (polarization and propagation properties of the observed waves), with various data rate possibilities (continuous or cyclic transmission, adaptable frequency bandwidth, as well as adaptable frequency and time resolutions) will also be provided by LFR.

b) The Thermal Noise and High Frequency receiver (TNR-HFR). TNR-HFR will determine properties of the ambient electron population from measurements of the local thermal noise around the plasma frequency and remotely detect solar radio emissions. It will provide, at various temporal resolutions, electric power spectra from 4 kHz up to 20 MHz and magnetic power spectral densities from 4 kHz up to 500 kHz.

c) The Time Domain Sampler (TDS). TDS will perform digitization of the electric and magnetic field waveforms in the frequency range from 100 Hz to 250 kHz. These will be pre-processed and a selection of potentially interesting events will be stored in internal memory and later transmitted to the ground.

These three sub-systems (LFR, TNR-HFR, TDS) are connected to two different sensor units: a set of electric antennas (ANT) and a search coil magnetometer (SCM), both of which will be optimized to perform correctly for DC as well as high frequency measurements. The ANT sensor design is optimized to measure both DC/low frequency electric fields and higher frequency radio and thermal noise emissions. A biasing unit (BIAS, as described below) will allow DC electric measurements. ANT consists of a set of three identical antenna monopoles deployed from two corners and one side of the spacecraft (see Figure 4.1, right panel). After deployment, the three monopoles are 125°/ 125°/ 110° apart, in a plane perpendicular to the spacecraft-Sun axis. Each monopole consists of a rigid deployable boom and a deployable antenna sensor. The rigid

deployable boom provides a larger spacing of the antenna sensor from the spacecraft and ensures that the antenna sensor will be fully illuminated and therefore well coupled to the local plasma potential through a photoelectron sheath. This is required for good DC/LF measurements.

The BIAS will drive a constant current to the electric antennas allowing reliable DC/LF electric field and satellite potential measurements by minimizing the impedance in the coupling to the plasma.

The SCM is an inductive magnetic sensor consisting of a core of a high permeability material (ferrite or permalloy) around which a main coil with several thousand turns and a secondary coil with a few turns are wound. The SCM is located on the instrument boom.

These subsystems have a common DPU that handles commands, data and communication with the spacecraft. Together with an LVPS, the four sub-systems will be integrated in a main electronic box (MEB) that will be located inside the spacecraft (Figure 4.5).

4.2 Remote-Sensing Instruments

4.2.1 Polarimetric and Helioseismic Imager (PHI)

PHI will provide high-resolution and full-disk measurements of the photospheric vector magnetic field and line-of-sight (LOS) velocity, as well as the continuum intensity in the visible wavelength range at a cadence of one set of observables per minute. The LOS velocity maps will have the accuracy and stability to allow detailed helioseismic investigations of the solar interior, in particular of the solar convection zone.

The PHI instrument consists of two telescopes (Figure 4.6), a High Resolution Telescope (HRT) that will image a fraction of the solar disk at a resolution reaching ~ 200 km at perihelion, and a Full Disk Telescope (FDT) to image the full solar disk at all phases of the orbit. PHI will carry out measurements with a narrow-band filtergraph at several wavelength positions in a Zeeman-sensitive photospheric spectral line, and in the nearby continuum. At each spectral position, the polarization state of the incoming light will be analyzed. From the observables (the four Stokes parameters that fully describe an electromagnetic wave), a number of solar physical quantities will be retrieved: the LOS flow velocity (v_{LOS}) and the three components of the vector magnetic field (field strength, inclination, and azimuth). From these quantities, the LOS component and the transverse component of the magnetic field vector (B_{LOS} and B_{Trans}) can be derived. Together with the continuum intensity I_c (a proxy for the plasma temperature, which also provides the image context for the other variables), spatial maps of these variables constitute the main data products of the instrument. The off-axis Ritchey-Chrétien HRT will image a fraction of the solar disk at a resolution reaching ~ 200 km at minimum perihelion distance (0.28 AU).

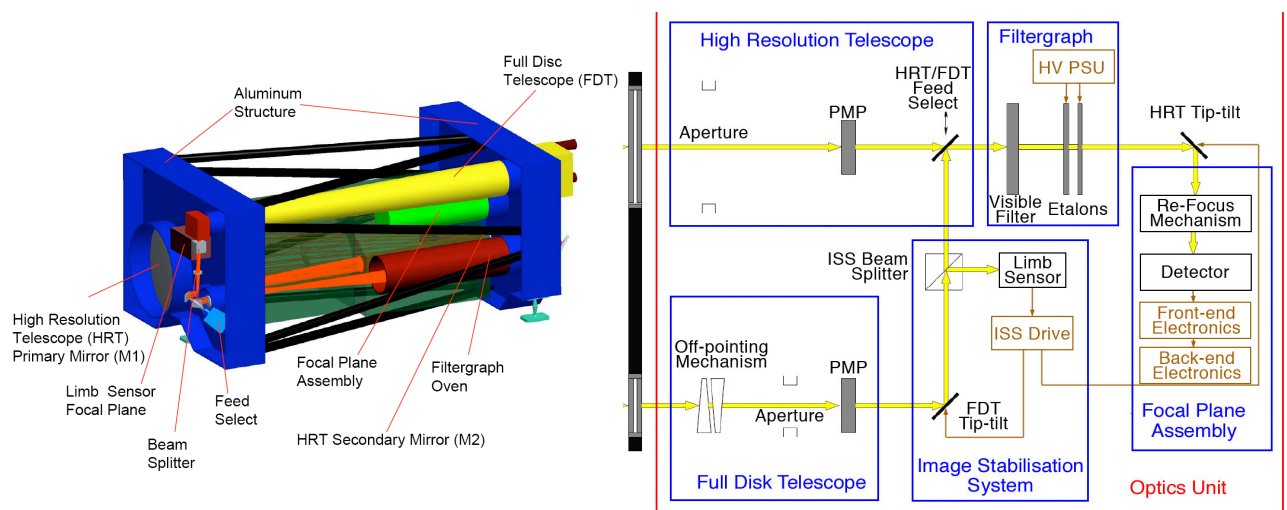


Figure 4.6. Left: 3-D view of Solar Orbiter's Polarimetric and Helioseismic Imager, showing the High Resolution and Full Disk Telescopes. Right: PHI block diagram.

The FDT provides a FOV of 2° with a pixel size of ~ 720 km (at 0.28 AU), giving a complete view of the solar

disk during all orbital phases. The implementation of an off-pointing mechanism (OPM) is being assessed. The OPM would allow the FDT to continue observing the whole solar disk while the spacecraft, including the HRT, is pointing off the solar disk centre. Continuous observations of the full solar disk by the FDT are needed to allow precise sensing of the solar limb and provide stable pointing. PHI will have its own image stabilization system (ISS) that compensates spacecraft jitter and other disturbances. This system is composed of a limb sensor and separate rapid tip-tilt mirrors for the FDT and the HRT.

In order to limit the amount of light entering the instrument, two entrance windows, one for each telescope, are mounted on the spacecraft's heat shield. These windows act as heat rejection filters with a transmission band of about 30 nm width centred on the science wavelength, such that the total transmittance does not exceed 4% of the total incident energy. The feasibility of such a filter has been demonstrated during the ESA Technology Development Activity (TDA) SO-OP-01.

Each telescope has its own polarization modulation package (PMP), located early in the optical path to minimize polarization cross-talk effects. Each PMP consists of two liquid crystal variable retarders (LCVRs) followed by a linear polarizer. Spectral analysis is performed by a Fabry-Pérot filtergraph system (FG) consisting of two lithium niobate (LiNbO_3) etalons which extract a spectral portion of the Fe I 6173 Å absorption line and at a nearby continuum point. The FG provides a tuning range of ± 0.6 Å, which is required for compensating the spacecraft radial velocity of ± 30 km/s plus the range required to scan the spectral line (~ 400 mÅ, depending on the observing mode).

A digital processing unit (DPU) performs image accumulation, pre-processing, and calculation of physical variables (Stokes inversion and data compression), and controls the instrument interfaces with the spacecraft. A functional block diagram of PHI is also shown in Figure 4.6.

4.2.2 Extreme Ultraviolet Imager (EUI)

EUI (Figure 4.7) will provide image sequences of the solar atmospheric layers above the photosphere, thereby providing an indispensable link between the solar surface and outer corona that ultimately shapes the characteristics of the interplanetary medium. Scientific topics to be addressed include monitoring the low atmosphere counterparts of large-scale solar eruptive events such as CMEs and the study of fine-scale processes in the solar atmosphere. EUI will also provide the first-ever images of the Sun from an out-of-ecliptic viewpoint (up to 34° of solar latitude during the extended mission phase). The EUI instrument suite is composed of two High Resolution Imagers (HRI), one at Lyman- α and one in the extreme UV at 174 Å, and one dual band Full-Sun Imager (FSI) working alternatively at the 174 and 304 Å EUV passbands, in addition to a common electronics box containing the data processing unit and power supply as shown in Figures 4.7 and 4.8.

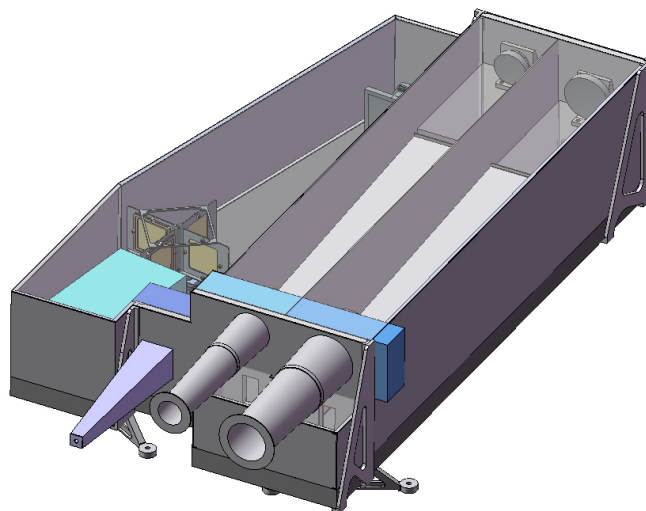


Figure 4.7. 3-D cutaway view of the Extreme Ultraviolet Imager. EUI comprises three imagers, two High-Resolution Imagers (HRI) and a single Full-Sun Imager (FSI).

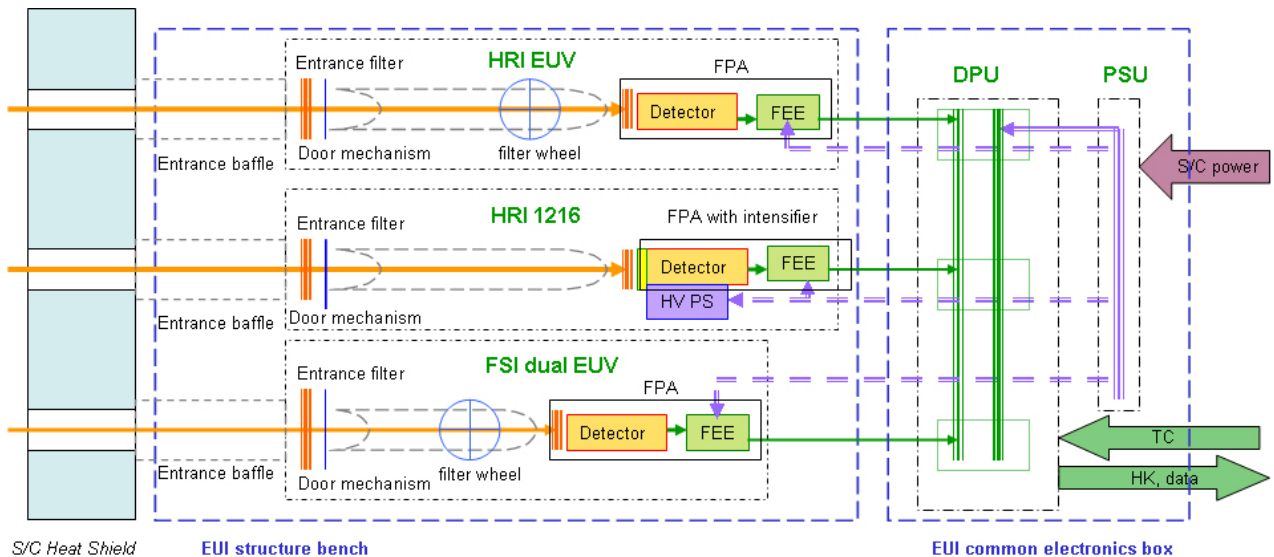


Figure 4.8. EUI functional block diagram.

The technology for building the EUI instrument under the challenging constraints of the Solar Orbiter mission is at a high level of maturity and builds on heritage from past missions (SOHO/EIT, TRACE, STEREO SECCHI/EUVI, PROBA-2 SWAP). In the Solar Orbiter EUI units, the image is produced by a mirror-telescope, working in nearly normal incidence. The EUV reflectivity of the optical surfaces is obtained with specific EUV multilayered coatings, providing the spectral selection of the EUV units (2 HRI and 1 FSI). The spectral selection is complemented with filters rejecting the visible and IR radiation. The UV photons reach detectors (back-thinned active pixel sensor [APS] detectors of 2k x 2k format for the HRI channels and 3k x 3k format for the FSI channel) where they are converted, amplified, and digitized by an A/D converter. For each detector pixel, the resulting signal in DN is proportional to the exposure time and to the solar flux corresponding to the small viewing angle of the pixel in the given band pass.

HRI and FSI have spatial resolutions of 1'' and 9'', respectively. The temporal cadence of HRI depends on the target and can reach sub-second values to observe the fast dynamics of small-scale features. The FSI cadence will typically be of the order of 10 minutes in each passband, but can occasionally reach 10 s. Owing to its high-cadence imaging characteristics, EUI is capable of producing a much higher data volume than can be down-linked within the available telemetry. Two solutions will be implemented. First, state-of-the-art compression algorithms will be developed; a compression factor up to 50 will be carefully selected for each EUI passband so as to ensure that the compression algorithm does not compromise the targeted features. Second, fully autonomous onboard software will be created to perform an intelligent selection of the most interesting data (e.g., observations of an eruptive event) for transmission to the ground.

4.2.3 Spectral Imaging of the Coronal Environment (SPICE)

The SPICE instrument is an EUV imaging spectrograph designed to remotely characterize plasma properties of the solar corona. Specific scientific topics to be addressed by SPICE include studies of solar wind origin by matching in-situ composition signatures in solar wind streams to surface feature composition; studies of the physical processes that inject material from closed structures into solar wind streams; studies of SEP source regions by imaging remotely the suprathermal ions thought to be seed populations of SEPs.

The SPICE instrument consists of a single element off-axis parabolic telescope and a toroidal variable line spaced (TVLS) grating spectrograph with two intensified APS detectors. SPICE also includes a DPU to control each of the mechanisms, perform data compression and provide the SpaceWire interface to the spacecraft. The optical layout and functional block diagram of the SPICE are shown in Figure 4.9.

The off-axis parabola mirror forms an image of the Sun onto the entrance slit assembly containing three interchangeable slits of differing widths. The slit selects a portion of the solar image and passes it to a concave

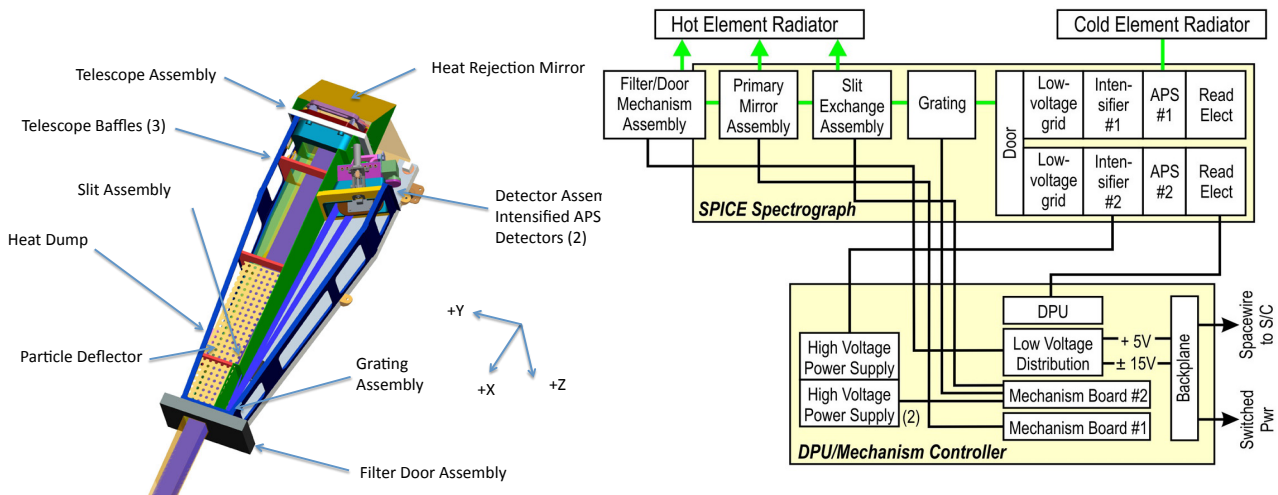


Figure 4.9. The optical layout and functional block diagram of the SPICE instrument.

TVLS grating which re-images the spectrally dispersed radiation onto two array detectors. The two spectral passbands cover the same spatial field of view simultaneously with no scanning of the detectors or grating. The detectors are solar blind, intensified active pixel sensors, and require no visible light rejection filters. The stigmatic spectra produced are magnified, yet maintain high spectral resolution in one dimension and high spatial resolution in the other. The SPICE observing strategy is to produce 2-D spectro-heliograms (spectral images) of selected line profiles and line intensities only. The wavelengths covered by SPICE are 702-792 Å (Band 1), 972-1050 Å (Band 2) and 485-525 Å (2nd order). The selected lines represent the full range of temperatures and heights in the solar atmosphere, from the chromosphere to the flaring corona. SPICE derives heritage from SOHO/CDS, SOHO/SUMER, as well as the RAISE and EUNIS sounding rocket programs.

4.2.4 Spectrometer/Telescope for Imaging X-rays (STIX)

STIX (Figure 4.10) provides imaging spectroscopy of solar thermal and non-thermal X-ray emission from ~4 to 150 keV. STIX will provide quantitative information on the timing, location, intensity, and spectra of accelerated electrons as well as of high temperature thermal plasmas, mostly associated with flares and/or microflares.

STIX is based on a Fourier-transform imaging technique essentially identical to that used successfully by the Hard X-ray Telescope (HXT) on the Japanese Yohkoh mission, and very similar to that used for RHESSI. As shown in the figure, the STIX instrument comprises three mechanically decoupled modules:

a) The Sun shades. The Sun shades required by STIX play two roles. First, they are a prime element of the thermal control system, limiting the incident optical and infrared solar flux seen by the instrument. Second, they preferentially absorb the intense flux of low energy X-rays produced during large flares that would otherwise contribute to pulse pile-up and life time issues for the detectors. The top sunshade has a central 5 mm diameter circular opening for use by the STIX aspect system, and the bottom shade has a corresponding 35 mm diameter opening.

b) The Imager. The STIX imager uses a set of 64 subcollimators, each of which consists of a pair of widely separated grids. X-ray transmission through the grid pairs is a very sensitive function of the direction of incidence, so that the relative count rates of the detectors behind the different subcollimators encode the spatial information. This can be subsequently decoded on the ground to reconstruct images of the source region at different X-ray energies. The grid parameters are chosen to provide imaging information in the form of spatial Fourier components of the source (visibilities) in analogy with the imaging information provided by antenna pairs in a radio interferometer. The tungsten grids are fabricated with the same etch-and-stack process successfully used to make the finer RHESSI grids.

c) The Spectrometer. STIX uses 64 discrete Cadmium-Zinc-Telluride (CZT) planar detectors, one behind each subcollimator, to provide good energy resolution while operating at room temperature. CZT detectors have been flown in space, for example, on NASA's SWIFT mission where 32,768 such detectors are used. A cold finger is required to maintain detectors and electronics at 25°C or less. Moveable attenuators enable STIX to be responsive to the entire expected intensity range of X-ray flux. Such attenuators, based on temperature-sensitive shape memory alloy actuators, have proven to be effective and very reliable on RHESSI.

Telemetered STIX data corresponds to the rates of individual detectors. Data selection, time and energy binning are done on board, so that a telemetry rate of 0.2 kbps can transmit an average of ~2000 images per hour for image reconstruction on the ground. A flare flag with source location can be made available on board in real time.

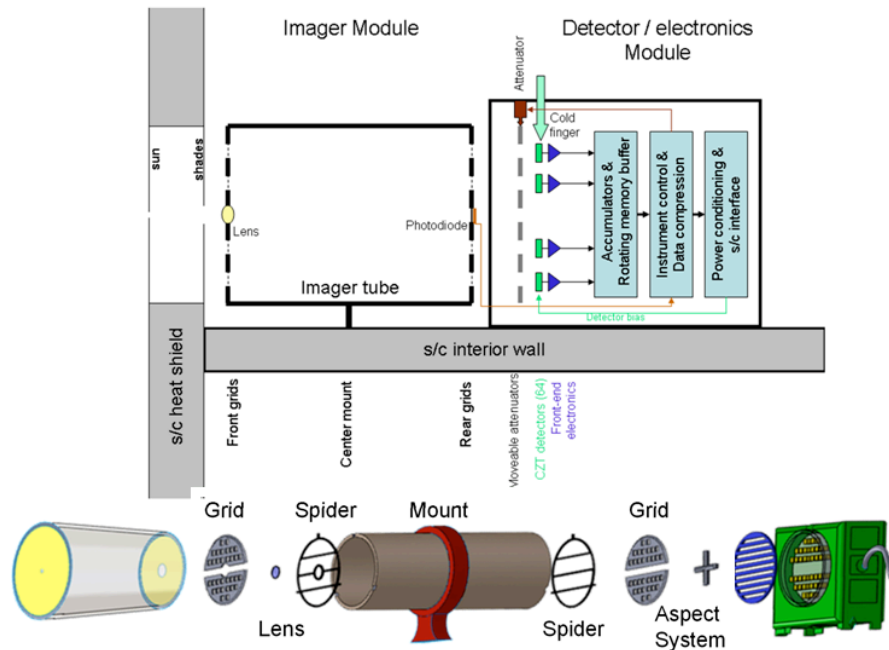


Figure 4.10. The Solar Orbiter Spectrometer Telescope for Imaging X-rays. Top: STIX functional block diagram; Bottom: Exploded view of the instrument.

4.2.5 Multi Element Telescope for Imaging and Spectroscopy (METIS)

The Multi Element Telescope for Imaging and Spectroscopy (METIS, Figure 4.11) will employ broad-band, polarized imaging of the visible K-corona and narrow-band imaging of the UV (H I Ly α , 121.6 nm) and EUV (He II Ly α , 30.4 nm) corona to study the structure and dynamics of the full corona with unprecedented temporal coverage and spatial resolution. METIS will also perform spectroscopy of the H I and He II Ly α lines in a sector of its FOV to study particle velocity distributions along the line-of-sight. METIS is an externally occulted coronagraph with an annular FOV between 1.5 and 3.0 R_{Sun} at a solar distance of 0.28 AU. This region of the corona is crucial in linking the solar atmospheric phenomena to their evolution in the inner heliosphere.

The unique capability of imaging the solar corona in three different wavelength bands by means of a single telescope is achieved by a combination of multilayer coatings of the mirrors, optimized to enhance reflectivity in the He II line, and spectral band-pass filters. Coronal light enters METIS through a hole in the heat shield (the inverted external occulter) and the disk light is reflected back out by a spherical high-rejection mirror. This configuration allows the adoption of an on-axis Gregorian design for the telescope. The suppression of the diffracted light off the edges of the hole and off the rejection mirror is achieved, respectively, with an internal occulter and a Lyot trap. The telescope consists of aspherical primary and secondary mirrors.

A door that is part of the spacecraft heat shield closes the instrument when it is not operating to protect it and to reduce the thermal load on the spacecraft. A filter wheel accommodates two filters: a narrow band

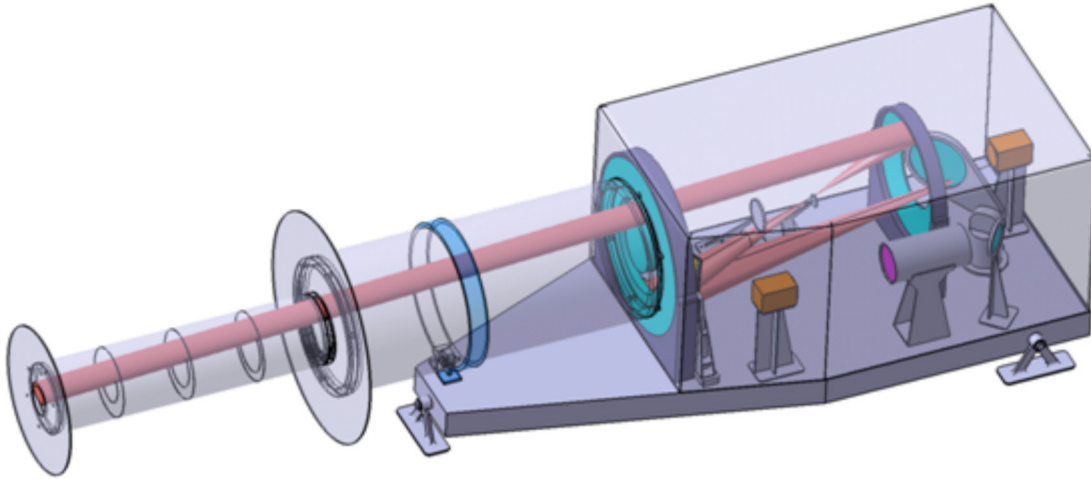


Figure 4.11. 3-D view of the Multi Element Telescope for Imaging and Spectroscopy (METIS).

interference filter (HF) optimized to transmit the H I 121.6 nm line and to reflect visible light, and an aluminium low pass filter (HeF) to block wavelengths above 30.4 nm. With HF, the UV H I 121.6 nm corona and the VL K-corona are imaged simultaneously. With HeF, only the EUV He II 30.4 nm is imaged on the UV detector. The visible light channel includes a polarimeter assembly to observe the linearly polarized component of the K-corona. The polarimeter assembly uses a nematic liquid crystal variable retarder plates (LCVR) and a colour filter to select the spectral operation band. METIS has two detectors: one optimized for observations in visible light (500 – 600 nm), the other dedicated to UV (121.6 nm) and EUV(30.4 nm) detection. Both detectors have 20 μm pixels and an array size of 2048 \times 2048 pixels. An APS is baselined for the visible light detector, while the baseline for the UV detector is an IAPS. An EUV/UV spectroscopy path is included in the METIS design by using a sector of the primary mirror (M1) to feed a multi-slit spectrometer. The grating replaces a sector of the secondary mirror (M2), corresponding to that of M1, and diffracts the spectrum on the portion of the detector which is not used for coronal EUV/UV imaging (Figure 4.12). The grating is a spherical varied line-spaced (SVLS) one with 1800 lines/mm. It diffracts 121.6-nm radiation at 1st order and 30.4-nm radiation at 4th order on the same location on the focal plane. The multi-slit selects 3 angular fields-of-view (FOV) from sun centre (at 1.5°, 1.8° and 2.1°). METIS derives heritage from the UVCS instrument onboard SOHO and the HERSCHEL/SCORE sounding rocket program. A functional diagram of METIS is shown in Figure 4.13.

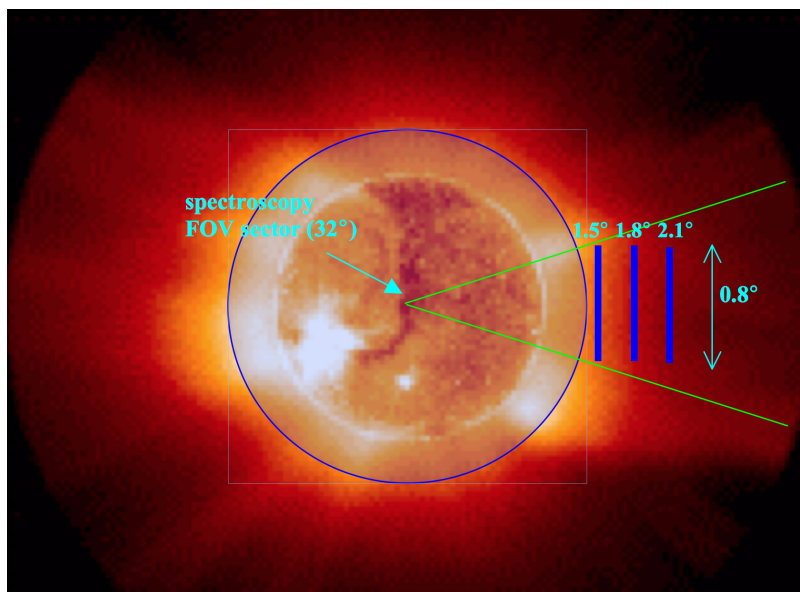


Figure 4.12. METIS field-of-view with spectroscopy sector and slit positions indicated.

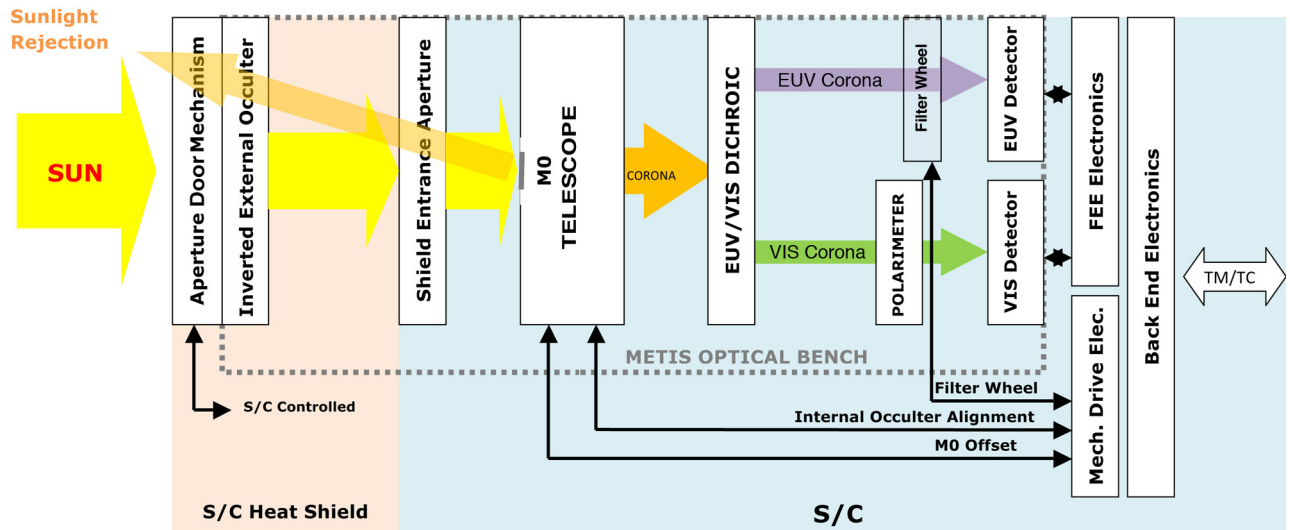


Figure 4.13. METIS functional block diagram.

4.2.6 Solar Orbiter Heliospheric Imager (SoloHI)

The Solar Orbiter Heliospheric Imager (SoloHI) will image both the quasi-steady flow and transient disturbances in the solar wind over a wide field of view by observing visible sunlight scattered by solar wind electrons. The scientific questions to be addressed with SoloHI include the acceleration of SEPs by imaging CMEs and CME-driven shocks; the evolution of CMEs and CIRs in the inner heliosphere; the origin and evolution of solar wind by remotely measuring the structure and turbulence with solar wind streams; providing context for the other in-situ and remote-sensing instruments aboard Solar Orbiter.

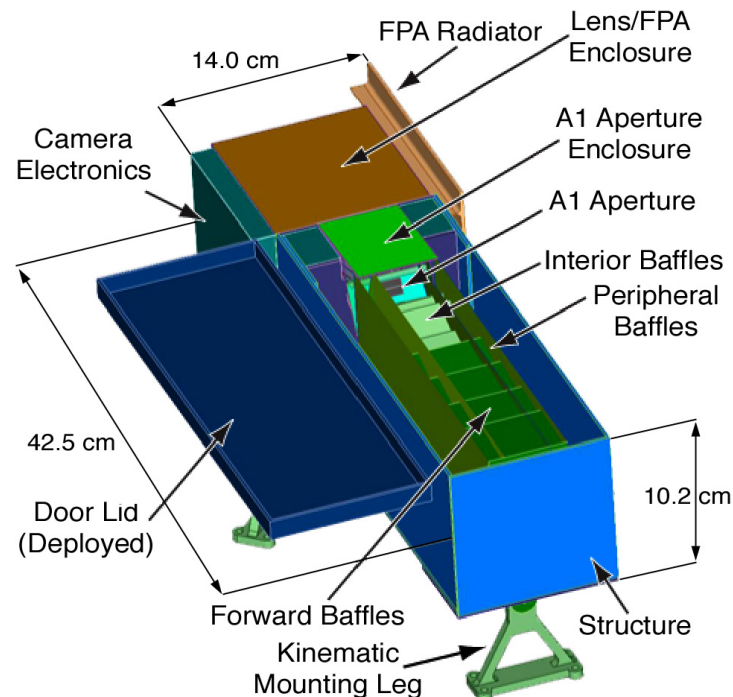


Figure 4.14. 3-D view of Solar Orbiter Heliospheric Imager (SoloHI).

The $40^\circ \times 40^\circ$ SoloHI field of view is centred on the ecliptic plane but is offset by 5° from the Sun centre and covers a range of elongation angles, thereby providing continuous synoptic images of the inner heliosphere with good spatial resolution. SoloHI (Figure 4.14) is an evolution of the design from the SECCHI/HI-1 instrument

on the STEREO mission. It consists of two units: the SoloHI instrument module (SIM) and the SoloHI control electronics (SCE) (Figure 4.15). The SoloHI telescope consists of a wide-angle lens ($f = 59 \text{ mm}$) of aperture 1.53 cm^2 . The SIM is located behind the heat shield, and a system of baffles provides the required rejection of incoming direct and scattered solar radiation. The average predicted stray light level is $< 5 \times 10^{-13} \text{ B/B}_{\text{Sun}}$ at 0.88 AU and $< 6 \times 10^{-14} \text{ B/B}_{\text{Sun}}$ at 0.28 AU . Other than the simple one-shot door, which provides protection against contamination during AIV and launch, there are no moving parts. The 40° field-of-view is imaged onto a customized APS that is cooled to -60°C to mitigate the effects of radiation damage. The SoloHI observing strategy is very flexible. The standard product will be synoptic images of the full field of view every 30 min. During perihelia SoloHI will obtain high cadence ($\sim 15 \text{ s}$) images of a subfield nearest the solar limb for solar wind turbulence studies while still providing synoptic images. Other modes (subfields, binned images) are possible depending on the objectives for the current observational window.

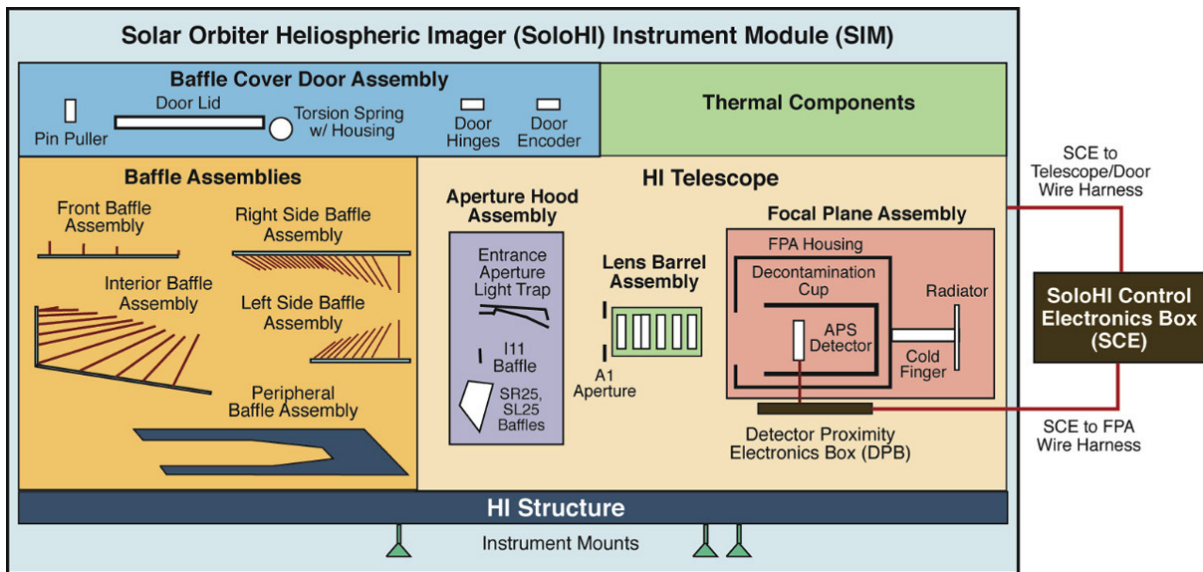


Figure 4.15. SoloHI functional block diagram.

5 Mission Design

The Solar Orbiter mission has undergone extensive study over a period of more than 10 years, both internally in ESA and in industry. This has resulted in a mature, detailed design that satisfies the requirements placed on the mission by the science objectives and addresses the key risk areas. The following section describes the current baseline mission, including the baseline mission profile and spacecraft design.

5.1 Mission and Spacecraft Requirements

The key mission and spacecraft requirements that flow down from the science objectives and drive the mission and spacecraft design are:

5.1.1 Mission Requirements

- During the nominal operational lifetime, the Solar Orbiter operational orbit shall have the following parameters:
 - Minimum perihelion radius larger than 0.28 AU to maximize the reuse of BepiColombo technology.
 - Perihelion radius within 0.30 AU in order to guarantee multiple observations close to the Sun
 - Inclination with respect to solar equator increasing to a minimum of 25° (with a goal of 35° in the extended operational phase).
- At minimum perihelion passage, the spacecraft shall maintain a relative angular motion with respect to the solar surface such that individual solar surface features can be tracked for periods approaching one solar rotation.
- The Solar Orbiter system lifetime shall be compatible with a launch delay of 19 months (launch window locked to the next Venus gravitational assist opportunity).

5.1.2 Spacecraft Requirements

The Solar Orbiter spacecraft shall be a 3-axis stabilized spacecraft using conventional chemical propulsion for orbit manoeuvres and attitude control;

- The Solar Orbiter Spacecraft shall be capable of accommodating the payload complement already selected in response to the ESA AO and NASA SMEX/FOSO;
- The Solar Orbiter spacecraft shall accommodate payload with global resources as defined in Chapter 4.
- For each operational orbit, the Solar Orbiter spacecraft shall allow full operations of the complete payload complement (remote-sensing and in-situ instruments) for three continuous periods of 10 days each, with a maximum of two contiguous periods. Typically, these will be centred on:
 - maximum northern heliolatitude;
 - maximum southern heliolatitude;
 - perihelion passage.

The in-situ instruments will in principle be operational throughout each science orbit.
- The spacecraft shall support a data downlink of 150 kbps at a range of 1 AU with the Malargüe ground station based on standard ESA link budget calculations.

5.1.3 Launch and Launch Vehicle Selection

The Solar Orbiter Spacecraft is planned to be launched by a NASA-provided Evolved Expendable Launch Vehicle (EELV) from Kennedy Space Centre (KSC), USA. The Ariane 5 launcher from Kourou is currently the European back-up launcher.

The current baseline launcher is the Atlas V 401. This lightest version has enough launch capacity for the expected 1800 kg spacecraft separated mass plus the 1194-mm diameter adapter. The launcher is also able to provide a 30-min launch slot that increases the probability of launch.

For each of the three mission profiles a 20-day launch period has been studied in which the trajectory of Solar Orbiter is entirely ballistic so that deterministic Deep Space Manoeuvres are not required. Statistical mid-

course manoeuvres will be necessary for trajectory corrections and navigation of the gravity-assist manoeuvres.

5.2 Baseline Orbit Design

Direct injection into the required operational orbit is beyond the performance of the available launch vehicles (see below) and the capabilities of the spacecraft. Raising the solar inclination angle (with respect to the Sun's equator) to the required value can be achieved, however, by repeated gravity assist manoeuvres (GAM) at Venus, where the relative arrival velocity of the spacecraft with respect to Venus must be ~ 18 km/s. Direct injection into a trajectory from Earth to Venus, arriving at Venus with the required relative velocity, requires an escape velocity from the Earth greater than 10 km/s, which again is beyond the capabilities of the available launch vehicles. By using a sequence of GAMs with Venus and Earth, it is possible to leave the Earth within the capabilities of the foreseen launch vehicle and arrive at Venus with the required high relative velocity. This solution yields a reasonable transfer phase duration of ~ 3.4 years and a reasonable maximum distance to the Sun (although still a driver for the spacecraft design) of just less than 1.5 AU. The initial period of the operational orbit is selected to be resonant with the orbital period of Venus (224.7 days), so that a sequence of Venus GAMs will gradually increase the solar inclination angle of the operational orbit.

5.2.1 Mission Profiles

Three ballistic mission profiles satisfying the above requirements for launches in January 2017 (current baseline), March 2017 and September 2018, respectively, have been studied and are described below. The mission profile for the March 2017 launch provides the overall sizing parameters, exhibiting a maximum Sun distance of 1.47 AU and a minimum Sun distance of 0.28 AU. The longest mission duration corresponds to the January 2017 profile with 10.2 years up to the end of the extended mission phase. All three mission profiles will allow Solar Orbiter to accomplish its science objectives. Table 4.1 summarizes the main characteristics of the mission profiles.

Launch window	Jan 2017	Mar 2017	Sep 2018
Launch Escape Velocity (km/s)	3.65	4.02	3.66
Declination of Asymptote ($^{\circ}$)	-35.5	25.2	-41.5
Max. Sun distance (AU)	1.314	1.468	1.384
Min. Sun distance (AU)	0.284	0.280	0.286
Max. solar inclination ($^{\circ}$)	34.0	36.1	34.0
Min. w_{Surface} ($^{\circ}/\text{day}$)	8.02	8.32	7.53
Duration of cruise phase (y)	3.39	3.15	3.25
Time until perihelion < 0.3 AU (y)	3.50	3.47	4.60
Time until max. inclination (y)	8.31	8.21	7.56
Overall Duration (y)	10.2	9.4	8.8
# Perihelia < 0.3 AU	9	8	7
Shortest period < 0.3 AU (d)	7.5	6.6	5.7
Longest period < 0.3 AU (d)	8.3	9.2	8.3
Accumulated period < 0.3 AU (d)	70.7	62.8	47.5
# Perihelia < 0.4 AU	16	13	12
Shortest period < 0.4 AU (d)	24.0	15.7	16.1
Longest period < 0.4 AU (d)	28.3	27.1	27.0
Time spent < 0.4 AU (d)	419	321	294

Figure 5.1. Summary of trajectory parameters and figures of merit of the three mission profiles. w_{Surface} denotes the minimal relative rotation of Solar Orbiter with respect to the solar surface. Options to extend the mission exist for all three profiles; the accumulated times listed only reflect the current baseline.

(a) January 2017 Mission Profile. The transfer phase of the first mission opportunity begins with a launch in January 2017, leaving the Earth at a velocity of 3.65 km/s and declination of -35.5° . About 4.5 months after launch, a Venus GAM with a pericentre height of more than 9200 km puts the spacecraft in a trajectory towards the Earth. An Earth GAM 10 months later places the spacecraft into an orbit such that another Earth GAM, with a pericentre height of more than 800 km, occurs 2 years later. About 2 months after the last Earth swing-by, a Venus GAM with a pericentre height of 300 km places the spacecraft into a 4:3 resonant orbit with Venus and perihelion radius of 0.284 AU. The first perihelion at this close distance to the Sun is reached 3.5 years after launch.

This orbit is the start of the sequence of resonances 4:3-4:3-3:2-5:3 that is used to raise gradually the solar inclination angle at each Venus GAM. The final maximum value of the solar inclination is 34° . The perihelion radius rises slightly above 0.3 AU in the second and third resonant orbit, but is pushed down to 0.29 AU in the last 5:3 resonant orbit. The characteristics of the trajectory are shown in Figures 5.1 and 5.2 and summarized in Table 4.2. The key mission events listed in Table 5.2 are launch and early orbit phase (LEOP), checkout and verification phase (CVP), cruise, science nominal mission phase, and science extended mission phase.

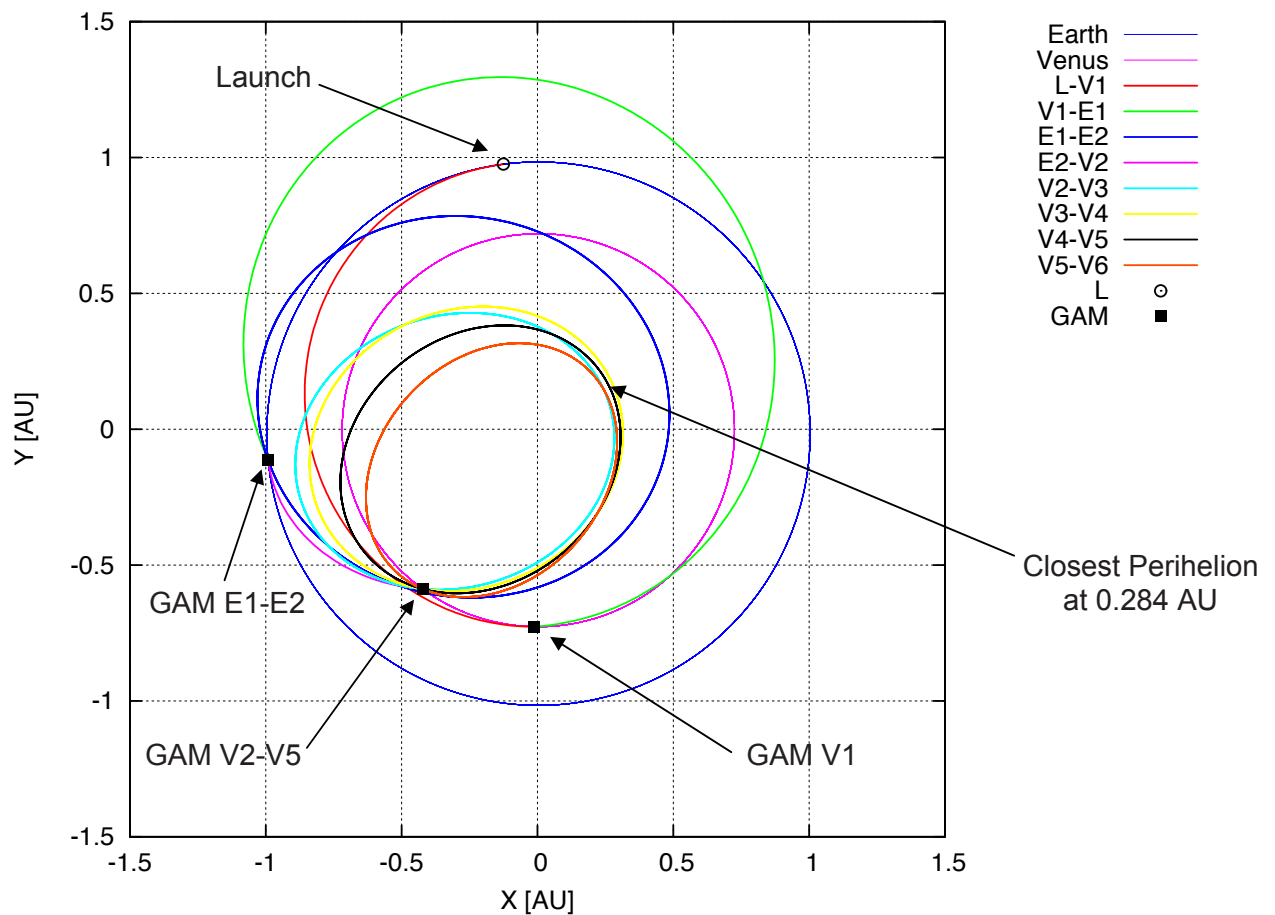


Figure 5.2. Solar Orbiter's trajectory viewed from above the ecliptic (January 2017 launch).

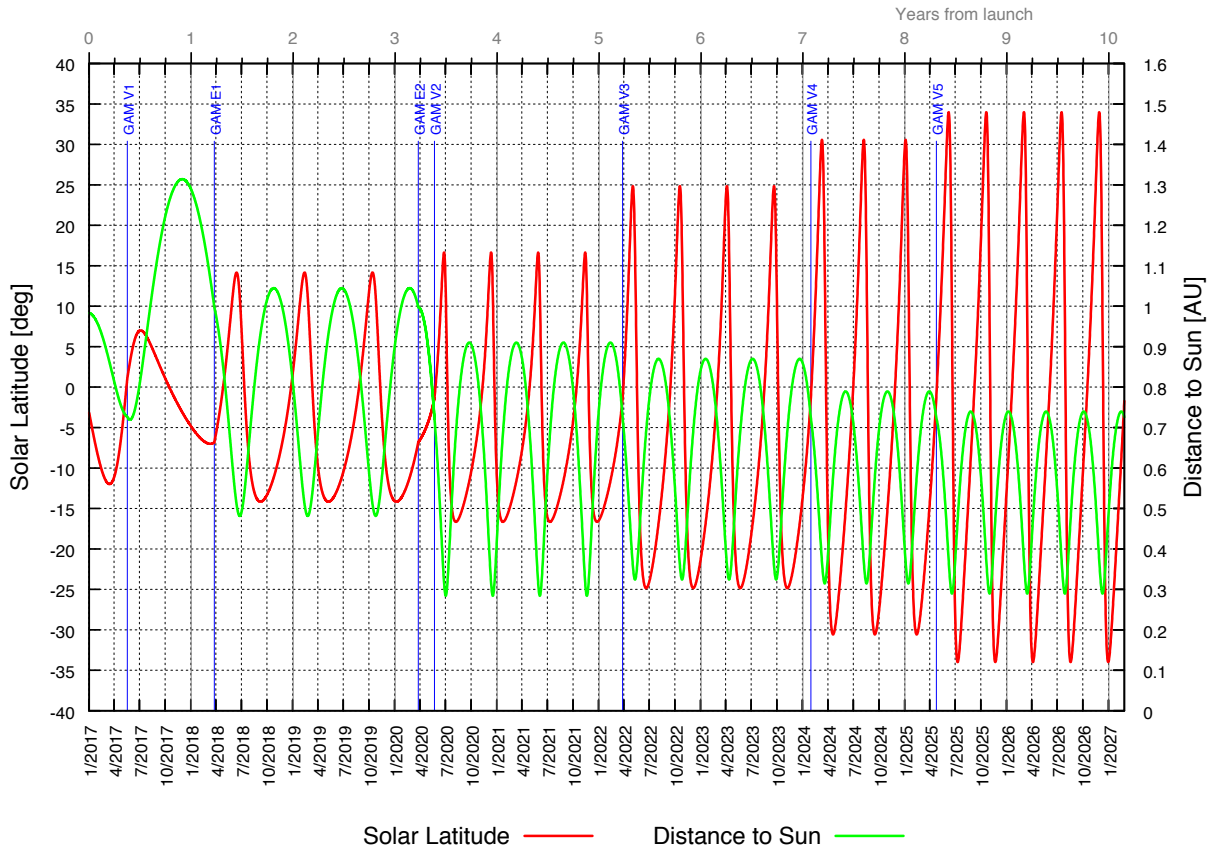


Figure 5.3. January 2017 mission profile, showing solar latitude (red) and heliocentric distance (green) of Solar Orbiter as a function of time. Also indicated are the times at which gravity-assist manoeuvres at Venus and Earth occur (blue).

Mission Phase Duration (days)	Event	Date	Flight Time (days)	Aphelion (AU)	Perihelion (AU)	Ecliptic Inclination (°)	Solar Inclination (°)
LEOP (7)	LAUNCH	2017-01-01	0	0.984	0.726	5.03	11.98
	LEOP end	2017-01-08	7	0.984	0.726	5.03	11.98
CVP (90)	CVP end	2017-04-15	97	0.984	0.726	5.03	11.98
Cruise (1100)	GAM V1	2017-05-18	137	1.314	0.720	0.87	7.01
	GAM E1	2018-03-26	449	1.045	0.482	9.98	14.16
	GAM E2	2020-03-25	1179	0.998	0.311	1.72	7.99
	GAM V2 – Cruise end	2020-05-22	1237	0.910	0.284	9.93	16.65
Science Nominal Mission (1348)	GAM V3	2022-03-27	1911	0.870	0.324	18.11	24.84
	GAM V4 – ENM	2024-01-30	2585	0.789	0.315	23.83	30.57
Science Extended Mission (1124)	GAM V5	2025-04-24	3035	0.740	0.290	27.25	33.99
	Arrival V6 – EEM	2027-02-27	3709				

Table 5.1. January 2017 mission summary (ENM: End of Nominal Mission, EEM: End of Extended Mission).

Mission Launch	Absolute Minimum Sun Distance (AU)	Absolute Maximum Sun Distance (AU)	Absolute Maximum Earth Distance (AU)	Maximum Solar Latitude (°)	Maximum Angular Rate (°/day)
January 2017	0.284 First achieved after GAM V2 2020-07-02	1.314 2017-12-01	1.899 2020-09-25	33.99 First achieved after GAM V5 2025-06-07	8.067 First achieved after GAM V2 2020-07-01

Table 5.2. January 2017 mission summary (continued).

(b) March 2017 Mission Profile. The transfer phase for this mission profile begins with a launch in March 2017, with an escape velocity from the Earth of 4.02 km/s and declination of the escape velocity of about 25.2°. About 6 months after launch, a Venus GAM with a pericentre height of more than 7000 km places the spacecraft in a trajectory towards the Earth. An Earth GAM 11 months later puts the spacecraft into an orbit such that another Earth GAM occurs 22 months later. For both Earth swing-bys the pericentre altitude is at least 3000 km.

The second Earth GAM inserts the spacecraft into a heliocentric orbit in which Venus is encountered 9 months later, after 1.4 revolutions around the Sun. The perihelion of this orbit is at the minimum radius of 0.28 AU about 3.5 years after launch, which allows starting the science phase before the second Venus GAM.

The spacecraft arrives at Venus with a hyperbolic velocity of 20.38 km/s, the highest in all the mission profiles. A sequence of resonances 1:1-1:1-4:3-3:2-3:2 is performed then at Venus in order to increase gradually the solar inclination. This sequence has been designed in order to provide multiple perihelion passes below 0.3 AU during the 4:3 and the first 3:2 resonant orbits. The maximum value of the solar inclination of 36.1° is reached in the final 3:2 resonant orbit 8.2 years after launch. The characteristics of the March 2017 mission profile are summarized in Table 4.3.

Mission Phase Duration (days)	Event	Date	Flight Time (days)	Aphelion (AU)	Perihelion (AU)	Ecliptic Inclination (°)	Solar Inclination (°)
LEOP (7)	LAUNCH	2017-03-08	0	0.993	0.603	0.41	7.28
	LEOP end	2017-03-15	7	0.993	0.603	0.41	7.28
CVP (90)	CVP end	2017-06-20	97	0.993	0.603	0.41	7.28
Cruise (1055)	GAM V1	2017-08-26	171	1.468	0.680	0.65	6.71
	GAM E1	2018-07-10	489	1.147	0.426	0.00	7.25
	GAM E2 – Cruise end	2020-05-03	1152	1.035	0.280	1.67	5.91
Science Nominal Mission (1397)	GAM V2	2021-02-01	1426	1.112	0.335	7.16	13.67
	GAM V3	2021-09-13	1650	1.077	0.370	14.81	21.35
	GAM V4	2022-04-26	1875	0.904	0.290	18.87	25.41
	GAM V5 – ENM	2024-02-29	2549	0.822	0.282	24.92	31.47
Science Extended Mission (899)	GAM V6	2025-05-23	2998	0.776	0.328	29.58	36.13
	Arrival V7 – EEM	2026-08-16	3448				

Table 5.3. March 2017 mission summary.

Mission Launch	Absolute Minimum Sun Distance (AU)	Absolute Maximum Sun Distance (AU)	Absolute Maximum Earth Distance (AU)	Maximum Solar Latitude (°)	Maximum Angular Rate (°/day)
March 2017	0.280 Achieved after GAM E2 2020-08-27	1.468 2018-02-26	2.005 2020-11-26	36.13 First achieved after GAM V6 2025-07-03	8.325 Achieved after GAM E2 2020-08-27

Table 5.4. March 2017 mission summary (continued).

(c) September 2018 Mission Profile. The transfer phase for this mission profile begins with a launch in September 2018, with an escape velocity from the Earth of 3.66 km/s and declination of the escape velocity of -41.5° . About 5 months after launch, a Venus GAM with a pericentre height of more than 11000 km places the spacecraft in a trajectory towards the Earth. An Earth GAM 10 months later puts the spacecraft into an orbit such that another Earth GAM occurs 22 months later. 2 months after the last Earth swing-by the spacecraft arrives at Venus with a hyperbolic velocity of 19.3 km/s. A sequence of resonances 1:1-1:1-4:3-3:2-3:2 is then performed at Venus during the science phase such that the solar inclination is gradually raised up to the final maximum value of 34° . The design of this sequence of resonances has been driven by the minimization of the maximum length of communications interruption due to safe mode during solar conjunctions. A first 4:3 resonance like in the January 2017 mission profile, while more attractive in terms of science, would exceed the limit of the current spacecraft design. The perihelion distance therefore rises slightly during the two 1:1 resonant orbits and drops below 0.3 AU for the 4:3 and the first 3:2 resonant orbits. The first perihelion within this distance occurs 4.6 years after launch. The maximum solar latitude is reached 7.6 years after launch. The characteristics of the September 2018 mission profile are summarized in Table 4.4.

Mission Phase Duration (days)	Event	Date	Flight Time (days)	Aphelion (AU)	Perihelion (AU)	Ecliptic Inclination (°)	Solar Inclination (°)
LEOP (7)	LAUNCH	2018-09-17	0	1.014	0.661	2.88	8.20
	LEOP end	2018-09-26	7	1.014	0.661	2.88	8.20
CVP (90)	CVP end	2018-12-23	97	1.014	0.661	2.88	8.20
Cruise (1091)	GAM V1	2019-02-19	154	1.384	0.699	2.67	4.71
	GAM E1	2019-12-22	460	1.099	0.466	0.00	7.25
	GAM E2	2021-10-17	1125	1.000	0.288	0.18	7.37
	GAM V2 – Cruise end	2021-12-18	1188	1.105	0.342	1.76	9.00
Science Nominal Mission (1124)	GAM V3	2022-07-31	1413	1.079	0.367	10.14	17.39
	GAM V4	2023-03-13	1638	0.901	0.293	15.01	22.26
	GAM V5 – ENM	2025-01-15	2312	0.818	0.286	21.63	28.88
Science Extended Mission (808)	GAM V6	2026-04-09	2761	0.770	0.334	26.73	33.97
	Arrival V7 – EEM	2027-07-03	3210				

Table 5.4. September 2018 mission summary.

Mission Launch	Absolute Minimum Sun Distance (AU)	Absolute Maximum Sun Distance (AU)	Absolute Maximum Earth Distance (AU)	Maximum Solar Latitude (°)	Maximum Angular Rate (°/day)
September 2018	0.286 Achieved after GAM V5 2025-03-01	1.384 2019-08-16	2.003 2022-05-02	33.97 First achieved after GAM V6 2026-06-30	7.527 Achieved after GAM V4 2023-04-22

Table 5.5. September 2018 mission summary (continued).

5.3 Spacecraft Design Overview

5.3.1 Mission Architecture Overview

The spacecraft design offers a stable platform to accommodate the combination of remote-sensing and in-situ instrumentation in an electromagnetically clean environment with 37 unobstructed fields-of-view for 21 separate sensors. The 2' co-alignment of the remote-sensing instruments on a very stable platform, combined with 1''-over-10s Relative Pointing Error performance and long science windows, will allow simultaneous and high-resolution observation of solar transients and of their link to the solar wind.

5.3.2 Mission Elements

The elements of the Solar Orbiter mission are described below.

5.3.3 Launch Segment

The baseline launch vehicle for the Solar Orbiter mission is the Atlas V 400 series (version 401) with 4m-diameter fairing and Centaur upper stage, launching from Cape Canaveral. In the nominal scenario, this launch vehicle will insert the Solar Orbiter spacecraft directly into an Earth escape trajectory in January 2017 with a declination of -35.5° and a V-infinity of 3.65 km/s. The backup launch vehicle options are the Delta IV M from Cape Canaveral and Ariane 5 from Kourou, which will target the same injection conditions on the same launch date. The backup launch date for the mission is September 2018, with a declination of -48.4° and a V-infinity of 3.69 km/s.

5.3.4 Space Segment

The Space Segment consists of the Solar Orbiter platform and payload.

5.3.5 Ground Segment

The Ground Segment consists of the Operations Ground Segment and the Science Ground Segment. The Operations Ground Segment comprises the Mission Operations Centre (MOC) at ESOC, responsible for performing all mission operations and raw data archiving and distribution to the instrument teams. The MOC architecture will be nearly identical to the one presently used for other recent planetary missions. A backup MOC may be available at Cebreros. The MOC consists of the following functional elements:

- Mission Control System (MCS) and Mission Planning System (MPS, part of MCS)
- Flight Dynamics System (FDS)
- Operations Archive
- Offline Evaluation System
- On-Board Software Maintenance System (OBSMS)
- Overall Simulator (OS)
- Security Distribution System.

The Ground Segment comprises the following ground stations:

- Malargüe (nominal for all operations throughout the mission)
- New Norcia (back-up for all operations in critical phases where additional tracking support is required)
- Cebreros (back-up when Malargüe is down for maintenance, and back-up for all operations in critical phases where additional tracking support is required).

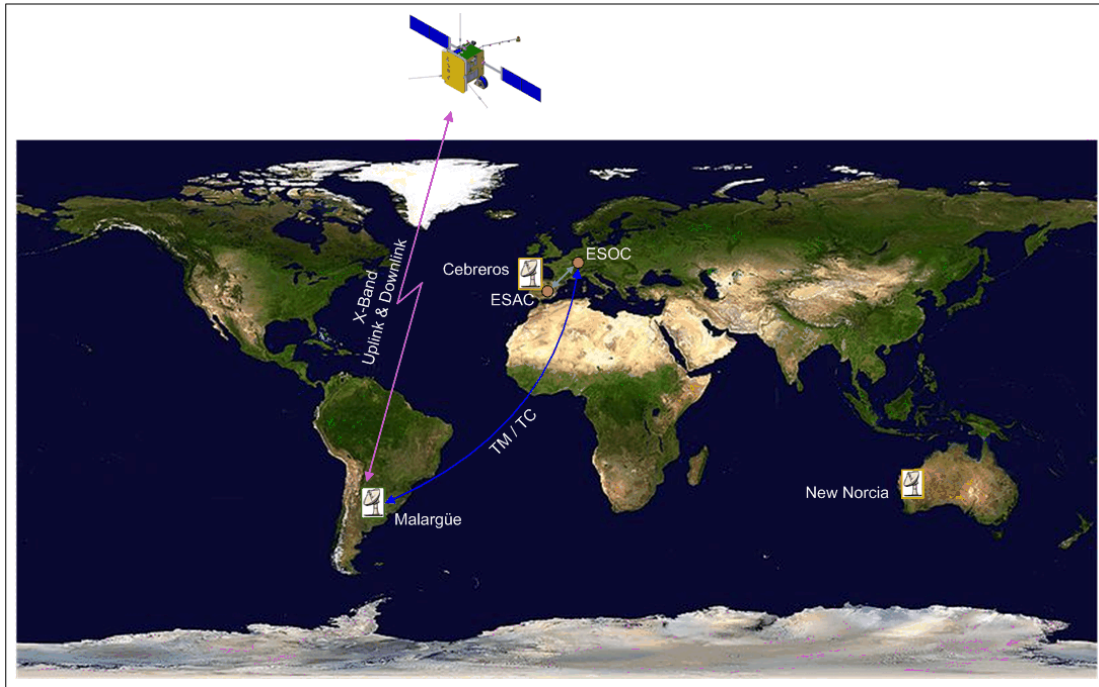


Figure 5.4. Solar Orbiter Ground Segment with the Mission Operations Centre, the ground stations and the Science Operations Centre.

The Science Ground Segment, comprises the Science Operations Centre (SOC) at ESAC, which will be responsible for mission planning and generation of payload operations request to the MOC as well as science data archiving. The SOC will be operational for the active science phase of the mission, i.e. from the beginning of the Cruise Phase onwards. The hand-over of payload operations from the MOC to the SOC is performed at the end of the Near Earth Commissioning Phase (NECP), during which in addition to payload commissioning, the SOC operation is validated. Accordingly, the SOC is active during the NECP, but not yet operational. Instrument teams are provided with data products via the DDS (Data Distribution System). The ground segment will be described in more detail in Chapter 7.

5.3.6 Functional Architecture

The design drivers for the Solar Orbiter spacecraft stem from the mission's technical and performance requirements and from the need to minimize the total cost of the mission. Technology developments are avoided as far as possible, in order to keep the mission cost within its M-class status, through the use of technologies and engineering design lessons learnt from previous missions, in particular BepiColombo (which has a similar environment to Solar Orbiter).

Thermo-Mechanical. The thermo-mechanical architecture is designed to facilitate spacecraft survivability and provide the instruments with a suitable thermal and dynamic environment, in particular in support of pointing requirements. The spacecraft structure is sized to interface with a standard 1194-mm-diameter launcher adaptor and to withstand the launch environment of the Atlas V, Delta IV and Ariane 5 launchers, whilst fitting within the 4m-diameter fairing of the Atlas/Delta launchers. The structure is complemented by the heat shield assembly which protects the entire spacecraft body and the majority of externally-mounted equipment at all

times including during the worst-case anticipated pointing failures. Feed-throughs are included in the heat shield to provide the required unobstructed fields-of-view to those instruments which require a view of the Sun. Door mechanisms are included for protection.

Data Handling. All spacecraft command and control tasks, including attitude control and FDIR (Failure Detection, Isolation and Recovery) for the platform and instruments, are performed by the On-board Computer (OBC) featuring internally redundant ERC-32SC processor modules. The data handling is based on packet telemetry and telecommand. The OBC interfaces with spacecraft units via a MIL-STD 1553B data bus and via a SpaceWire network with the payload units. Payload science data are routed to the Solid State Mass Memory which can store up to 549 Gbit. The storage capacity can be increased further to 823 Gbit by activating a nominally redundant memory bank. All platform and instrument data can be routed to ground following the store-and-forward concept of Solar Orbiter. Time synchronization is achieved by distribution of time information and synchronization signals by the OBC.

Attitude Control and Propulsion. After separation from the launcher and in case of safe mode, Fine Sun sensors and gyros are used to measure the attitude and support rate reduction spacecraft orientation. A gyro-stellar (star tracker & gyroscope) attitude control system takes the control once attitude has converged. The Fine Sun sensors are then used as independent monitoring devices, along with a 2nd inertial measurement unit (IMU), in support of the top-level FDIR which enforces the Sun-pointing attitude of the spacecraft to within a transient off-pointing of 6.5° from the spacecraft-Sun-line during all credible attitude failures. A redundant suite of 10 N dual-seat-valve thrusters is used for safe mode attitude control, wheel off-loading and ΔV manoeuvres. The thrusters are complemented by a set of four reaction wheels used during nominal modes, and also during science windows to provide low-noise control in support of the Relative Pointing Error (RPE) requirement of 1" over 10 s.

Electrical Power. In view of the demanding thermal environment at perihelion, the solar array is based on the design chosen for the BepiColombo MPO. It is designed to supply 974 W to the platform at the worst-case aphelion of 1.47 AU (in excess of the sizing power demand from the platform of 919 W), corresponding to the January 2017 mission scenario. The Power Conditioning and Distribution Unit uses an efficient Maximum Power Point Tracker and provides a regulated main bus voltage of 28 V. The lithium-ion battery size is determined by the LEOP phase and the battery pack serves to provide supplementary power at other points in the mission such as eclipse periods encountered during flybys.

Telemetry, Tracking and Command. The Telemetry, Tracking and Command Subsystem provides the communication link capability with the Earth in X-band. The subsystem supports simultaneous telemetry, telecommand and ranging. Low-Gain Antennas (LGAs) are used for LEOP. Steerable Medium- and High-Gain Antennas are used for the mission phases beyond LEOP (LGAs can also be used as back-up, except when close to the maximum Earth distance of 2 AU). During nominal science operations, 4-hour communication periods (net duration of science data download) with the ground station are foreseen, and will be increased to 8 hours whenever this is useful to the total science data return, geometry of the pass permitting.

5.4 Solar Orbiter Configuration

5.4.1 Introduction & Configuration Drivers

The configuration of the Solar Orbiter spacecraft mediates between the many conflicting drivers and constraints of each of the individual units on-board the spacecraft. All units on the spacecraft have been iteratively accommodated to arrive at an optimal configuration given the overall system-level drivers and constraints of the mission. The process of unit accommodation is dominated by the following key considerations:

- (a) The importance of thermal and thermo-mechanical considerations in the allocation of units to the various bays of the spacecraft and external surfaces; in particular:
- The interaction between remote-sensing instrument locations, aperture locations in the heat shield, and

the resulting performance of the heat shield at a local level, leading to analysis to demonstrate that the feed-through locations on one side of the heat shield (i.e. in relative proximity to each other) are thermally allowable.

- Minimization of the thermal interaction between the appendages exposed to the Sun (RPW-ANT, solar arrays and particularly the HGA), the heat shield and the rest of the spacecraft body, leading to the location of the HGA above the $-Z$ panel of the spacecraft, which is radiator-free and covered in MLI, and the use of shaped-reflector radiators for the remote-sensing instruments underneath the solar array yokes
- The thermal interaction between the solar arrays and the RPW-ANT, which constrains the allowable combinations of RPW-ANT position and solar array tilt direction, and which must be considered in tandem with the solar radiation pressure-induced torque profile of the spacecraft which determines the frequency of wheel off-loading which is a key parameter to be minimized.
- The combined dissipative and received thermal loads (when observing the Sun) of the remote-sensing instruments, and their positions relative to other high dissipation units, to ensure that sufficient radiator area exists to provide their Hot Element (HE)/Cold Element (CE) interface temperatures (particularly CE interface to the detectors which require the radiators to provide detector temperatures of typically -30°C).
- The identification and maintenance of adequate panel radiator area on the various faces of the spacecraft, heavily constrained by the presence of sun-exposed appendages such as the HGA and RPW antennas.
- The relative positions between thermally critical instruments and their targeted radiator areas.
- The geometrical constraints associated with solar-illumination of the sensitive HE/CE instrument radiators and the provision of spacecraft power.
- The necessity to maintain sun-pointing during some manoeuvres, combined with the presence of the heat shield and high number of payload elements, which heavily constrains the available locations and orientations for thrusters; this requires achieving a thruster configuration which provides pure force/torque capability with reasonable efficiency for all force/torque directions.
- Consideration of the critically-important freedom to roll around the spacecraft-Sun-line when manoeuvring in order to define the optimal thruster configuration.
- Thermo-elastic deformation considerations for APE/PDE and co-alignment which lead to common payload module mounting locations for co-alignment and pointing-critical remote-sensing instruments (all except SoloHI).

(b) The operating and environmental requirements of the various payloads which obviously have priority when defining the configuration, particularly:

- The FOV requirements of all payload elements, which must be met without interference from instruments to the maximum extent possible.
- Electromagnetic, particulate and molecular cleanliness requirements of certain key instruments.
- The combination of the previous two factors in necessitating the use of an instrument boom for instruments that require it.
- Provision, for as long as possible, of high-stability pointing performance ($1''/10$ s RPE) which leads to consideration of the solar radiation pressure-induced torque contributions from the spacecraft appendages, and constrains the tilt direction of the solar arrays given the dominating action of the HGA as a torque-arm.
- The necessity to protect all the instruments from the Solar flux during close approach periods, leading to an over-sized heat shield operating in tandem with an attitude watchdog function.
- The need from most instruments for nitrogen purging up until launch; this requirement favours the collocation of remote-sensing instruments on a common module which simplifies and shortens purging-line routing.
- The conflicting need for a FOV to the Sun for all remote-sensing instruments (except SoloHI) as well as the SWA-PAS/HIS instruments, leading to a requirement for several feed-through apertures in the heat shield of the spacecraft.
- The additional conflicting requirement of certain instruments (in particular SoloHI) for a near-sun FOV which is in conflict with protection of the instrument at all times.

(c) The operational reality of the mission, which often conflict with (a) and (b), in particular with their effect on the required movements of key spacecraft appendages, including:

- The wide range of HGA positions that must be accessed in order to achieve an RF-link with the Ground Station, which in turn must be considered when locating the HGA and has led to the HGA position above the $-Z$ panel away from a direct view with any radiators.
 - The possible necessity to stow the HGA during close perihelion passages due to the severity of the thermal environment, provision for which is made by leaving sufficient volume in the shadow of the heat shield to stow the HGA without clashing with the instrument boom.
 - The need to avoid blinding of the star trackers by the instrument boom tip or moon during LEOP, given the constraints on spacecraft orientation, leading to tilting of the star tracker boresights away from the $-X$ axis.
- (d) Mechanical considerations encountered during the mission:
- Placement of the various deployable appendages to ensure existence of suitable hold-down locations (i.e. near or on shear wall points).
 - De-coupling of the heat shield from the rest of the spacecraft in order to maintain the stability of the structure, particularly the payload module which houses the alignment-sensitive remote-sensing instruments.
 - The large number of deployable appendages on the spacecraft (seven in total) which imposes challenges to avoid any instances of interference between deployable items.
- (e) The industrialization requirement for maximum modularity to facilitate streamlined AIT and substantial subcontractor involvement at subsystem level.

5.4.2 Spacecraft Configuration

The Solar Orbiter spacecraft configuration (Figure 5.4) is dominated by the presence of the heat shield located at the top of the spacecraft in order to protect the spacecraft from the intense direct solar flux when approaching perihelion. The heat shield is over-sized to provide the required protection to the spacecraft box and externally-mounted units, in combination with the attitude-enforcement function of the FDIR. The mechanical platform revolves around a robust, reliable and conventional concept with a central cylinder, four shear walls and six external panels. This concept is inspired by Astrium's Eurostar 3000 spacecraft platform. The design meets Solar Orbiter's mission requirements according to a low-risk and low-cost philosophy. The selected platform provides very efficient accommodation, which is critical in meeting the volumetric constraints of the Atlas/Delta 4-m fairings, and critically allows a modular build-up of the spacecraft, with opportunities to group related units and subsystems together (see Figure 5.5 for an illustration of the spacecraft accommodated in the Atlas, Delta IV and Ariane 5 launchers). The implementation of large and numerous side access panelling offers easy access to the equipment up to a late stage of the integration process, thus ensuring concise and flexible AIT. The conventional technology involved allows wide and open competition for the mechanical subsystem along with good guarantees that the procurement schedule will be met.

The instrument locations are the result of repeated accommodation iterations and optimizations as knowledge of requirements has accumulated. The remote-sensing instruments which need to observe the Sun through heat shield feed-throughs (EUI, METIS, PHI, SPICE and STIX) are accommodated immediately behind the heat shield onto a single panel providing good co-alignment, maximum modularity and, crucially, simplified heat rejection. Each remote-sensing instrument's optical bench has its respective electronic box located immediately behind it for harness mass reduction. The highly dissipating remote-sensing instruments benefit from a simple and reliable heat-dissipation system consisting of thermal straps connected to radiators located immediately below them on the payload module. The in-situ instruments are accommodated in accordance with their field-of-view requirements, with the vast majority located on the same panel as the remote-sensing instruments to increase the overall level of modularity.

The HGA is mounted on a steerable boom and located away from the orbital plane of the spacecraft – this maximizes opportunity for communication with the ground irrespective of the spacecraft orientation (i.e. unhindered by the spacecraft body or appendages). The spacecraft provides a highly stable platform for the remote-sensing instruments ($1''/10$ s RPE) which is particularly important for those having a very high duty cycle of over 95% during a typical 10-day long science windows. This stability is achieved through the symmetric design of the spacecraft and its appendages and efficient solar radiation pressure management making use of high-performance large wheels for storing momentum and an efficient wheel offloading strategy.

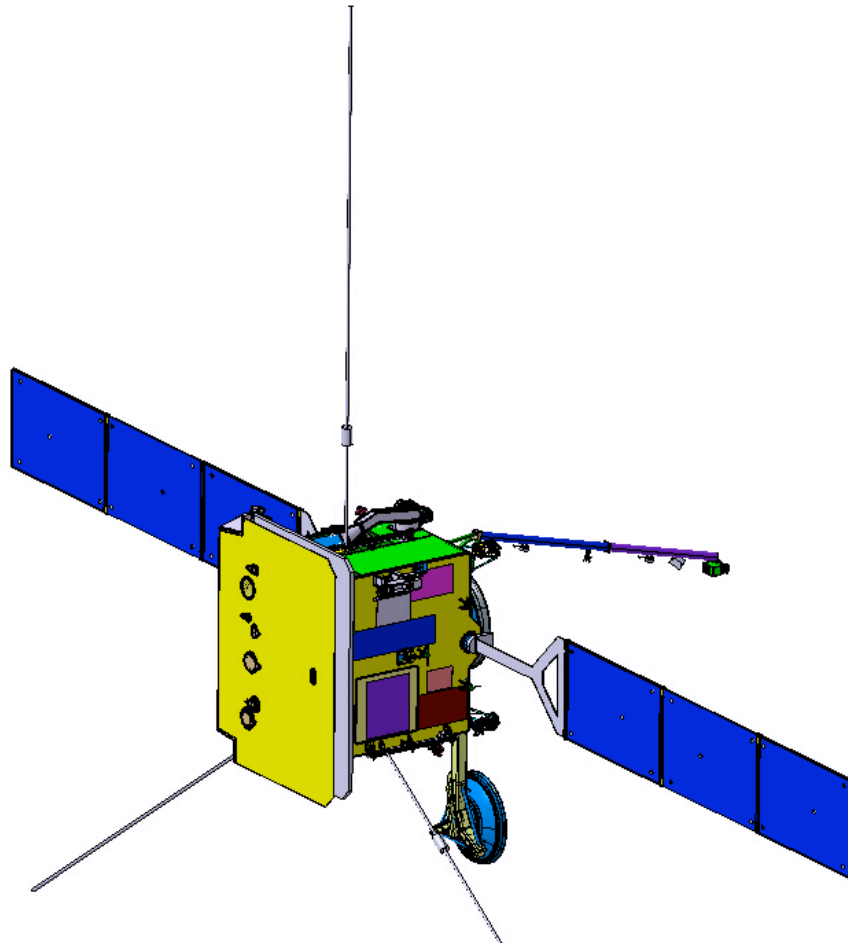


Figure 5.5. Front isometric view of the nominal spacecraft configuration with the three RPW antennas, high-gain antenna, instrument boom and solar arrays deployed.

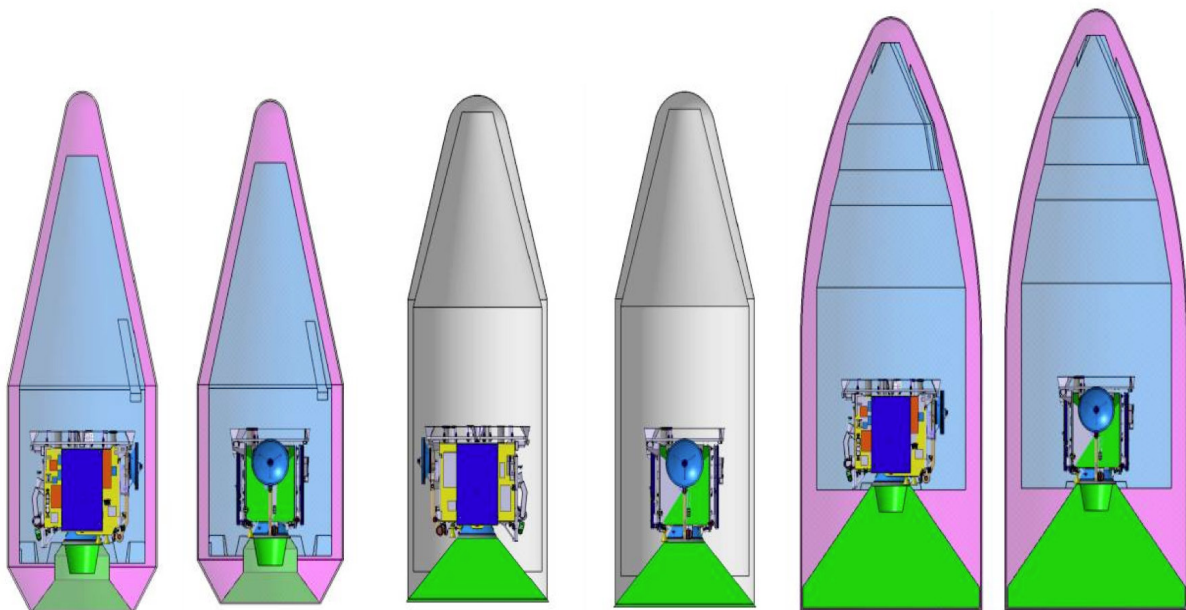


Figure 5.6. Views of the spacecraft accommodated in the Atlas, Delta IV and Ariane 5 launchers.

The Electrical Power Subsystem (EPS) and Data Handling Subsystem (DHS) accommodation is also characterized by its high degree of modularity and efficiency, the guideline being to bring functionally related units together as close as possible.

Critically, adequate clearance between units has been implemented to provide an efficient routing of the electrical and data harness between the units. This clearance has taken into account classical allocations at connector faces for connector dimensions and harness bend radii, which along with the accessibility during AIT, provides confidence that the configuration is sensible and can be constructed in a streamlined and rapid manner.

The solar arrays (two wings, single-axis controlled, each featuring three panels to provide adequate power during all phases of the mission) are connected to the primary structure in stowed configuration via five hold down and release mechanisms, aligned with the spacecraft internal panels to achieve a rigid interface and efficient mechanical design. The solar array driving mechanism is located at the intersection of the shear walls and the lower floor, providing a rigid attachment point also in deployed configuration.

5.4.3 Configuration Features to Support Industrialization

The functional and logical decomposition into subsystems has led to a modularization of the spacecraft that facilitates external procurement. In the case of Solar Orbiter, design and development of the identified subsystems is performed fully by the respective subcontractor, and integration and verification tasks are interlaced with prime level tasks during AIT and partially completed by the subcontractor on satellite level. The spacecraft configuration has been optimized to support this high-level of subcontractor involvement during industrialization, exhibiting a high degree of modularity at subsystem-level, in support of geo-return, fast-track implementation and substantial subcontractor involvement at subsystem-level.

Accordingly, the spacecraft configuration has clear interfaces, which mirror interfaces in the industrialization approach favoured by ESA. The modularity also serves to support testing and integration by de-coupling areas of the design in a way which maximizes scope for parallelization of activities, and minimizes the critical path during AIT. The main features of the spacecraft configuration which support industrialization are:

Propulsion Assembly. The propulsion subsystem is mounted on the core structure of the spacecraft (the central cylinder/cone plus shear walls); furthermore the entire pipework assembly (valves, pressure transducers, test ports etc) is located on a single common panel within the core assembly (the $-Z$ shear panel). This approach favours the early integration of the core mechanical and propulsion assemblies in tandem, reduces integration time, allows later delivery and integration of the outer panels without affecting the CPS, and generally simplifies and accelerates the AIT schedule.

TT&C Subassembly. The core TT&C subsystem (transponders, traveling-wave tube amplifier, radio frequency distribution unit) is located on a common subpanel of the $+Y$ shear wall of the spacecraft, from which waveguides disperse to the four antennas located around the spacecraft. This approach allows the TT&C subsystem to be largely assembled and tested separately prior to simple integration with the spacecraft, favouring an industrialization approach where the TT&C subsystem and bulk of testing is performed by a subcontractor. The antenna assemblies, HGA, MGA and LGA, are designed to allow their integration and dismantling from the spacecraft without the need to remove any spacecraft panel. The validation of compatibility with the ground segment is managed on the basis of EM units installed into the RF Suitcase.

Heat Shield Subassembly. The heat shield subassembly (including the feed-throughs, doors and associated mechanisms) is required to be a separable subsystem, which can be assembled and tested separately, until simple integration with the spacecraft late in the AIT schedule. The adopted approach of heat shield alignment by design supports this approach.

Feed-throughs, Doors and Mechanisms. The assembly of heat shield and feed-throughs, doors and mechanisms constitutes a single module that can be mounted and dismantled from the spacecraft without need of opening any other structure panel. This module can be tested independently from the rest of the spacecraft, in particular under high solar constant conditions.

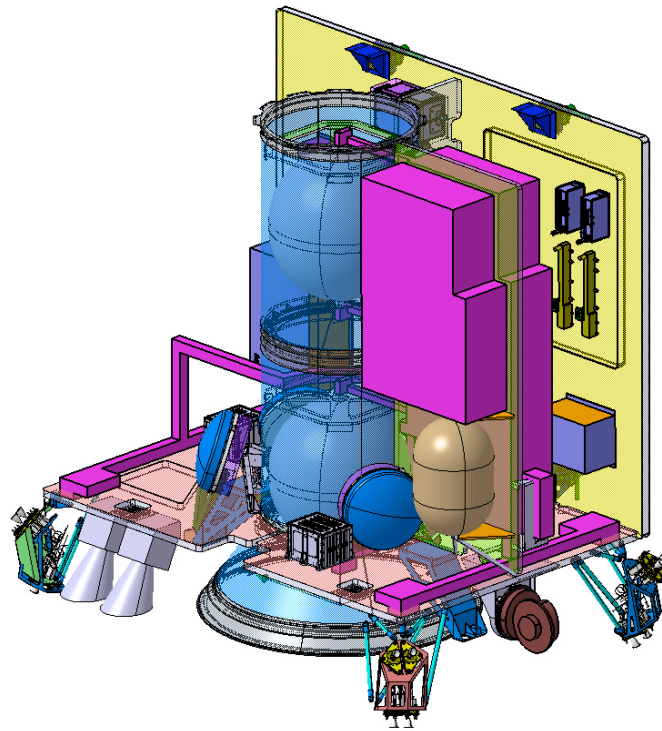


Figure 5.7. Core structure with service module view, showing the accommodation of most of the bus units on the spacecraft.

Service module. The majority of bus units are located on a common panel (the +Y panel of the spacecraft, Figure 5.6). This supports assembly away from the core structure and provides ease of access during integration.

Payload module. Similarly the majority of the payload elements are mounted on a common subassembly (the -Y panel of the spacecraft, Figure 5.7). This high level of modularity significantly decouples instrument development and their integration into the satellite from the platform development and test programme. This supports separate integration and simplified alignment of the majority of instruments (and star trackers) away from the rest of the spacecraft structure, particularly the Sun-viewing remote-sensing instruments. It also supports simplified purging line routing, and mitigates schedule impacts of integration after staggered delivery of payload elements.

Instrument Boom. The instrument boom will be treated as a distinct subsystem, tested separately and integrated on to the spacecraft at a late stage. The mechanical and electrical interfaces of the instrument boom are therefore designed to allow its integration and dismounting from the spacecraft body without the need to remove any spacecraft panel, again providing maximum flexibility in the AIT process.

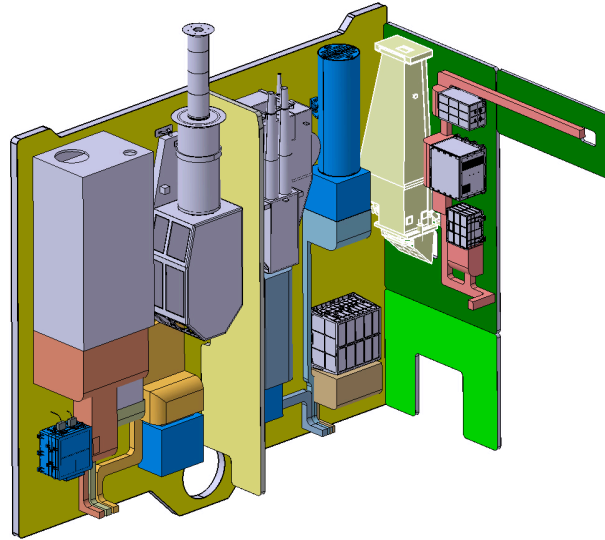


Figure 5.8. Isometric view of the payload module showing the common-panel mounting of the remote-sensing instruments which are subject to the co-alignment requirement.

5.4.4 Spacecraft Configuration versus Mission Timeline

The Solar Orbiter spacecraft has five nominal configurations throughout the course of the mission, with an additional contingency configuration; these are summarised in Figure 5.8, along with the periods over which they are used.

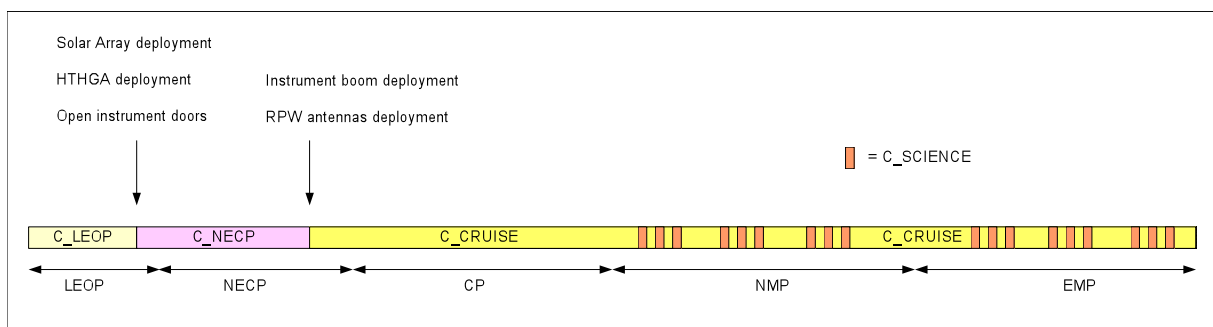


Figure 5.9. Representation of the relationship between mission phases and spacecraft configurations.

The spacecraft begins the mission in C_LEOP, with all spacecraft appendages stowed; during LEOP the spacecraft configuration changes to C_NECP, through deployment of the solar array and HGA; during the Near Earth Commissioning Phase of the mission the configuration changes to C_CRUISE through deployment of the remaining payload-related appendages (the RPW antennas and the instrument boom). C_CRUISE is essentially maintained throughout the remainder of the mission, except for the remote-sensing observation science windows during which C_SCIENCE is entered (which differs only insofar as the feed-through doors may close and open). Note that in C_CRUISE and C_SCIENCE the HGA may be stowed behind the shadow of the heat shield if needed.

5.4.5 Payload Accommodation

The spacecraft configuration has to accommodate multiple heads and electronic boxes for the remote-sensing and in-situ instruments, with various requirements on fields-of-view, temperature (stability), pointing, alignment and environment. The payload complement for the Solar Orbiter mission consists of the following

instruments, as shown in Figure 4.1. Five of the remote-sensing instruments have tight co-alignment and pointing requirements. They need to be protected from the solar flux, but at the same time they need fields-of-view that allows them to observe the solar disk and/or the corona. These instruments, EUVI, METIS, PHI, SPICE and STIX, are accommodated internally to the spacecraft and looking through apertures in the spacecraft heat shield. The instruments reside in a benign thermal environment, except for the flux that enters directly through their front apertures. In order to deal with this direct flux, the instruments need a large number of thermal interfaces to keep their detectors and electronics at acceptable temperature levels. They are therefore located on an external spacecraft panel, allowing easy connections to thermal radiators. The co-alignment and pointing performance are achieved by the five instruments on the $-Y$ wall, together with the star tracker (this module includes a local extension into the $+Z$ panel for SPICE, which cannot be mounted on the $-Y$ panel due to its specific orientation requirements). The spacecraft and instruments are protected by a heat shield. Eight feed-throughs in the heat shield provide the required fields-of-view for the five internally mounted instruments.

Boom-mounted instruments. Five instrument units need to be mounted on a 4m-boom (Figure 5.9), away from the spacecraft but still protected from direct solar flux: MAGIBS, RPW-SCM, MAGOBS, EPD-STEIN and SWA-EAS. The relative positions of the instrument units on the boom have been optimized by the instrument teams. Of key importance for the overall observations from Solar Orbiter is to correctly determine the DC and AC magnetic fields. Since the spacecraft and its instruments will be generating magnetic disturbances, the magnetic sensors need to be located on a boom, separated as much as possible from the spacecraft. Two detectors (MAGIBS and MAGOBS) will be deployed on the boom to detect DC magnetic fields. Having two detectors allows removal of the magnetic disturbance of the spacecraft to be calibrated out of the data. The AC magnetic fields are sensed by the search coil magnetometer, RPW-SCM, located between MAGIBS and MAGOBS. The AC magnetic fields are sensed by the search coil magnetometer, RPW-SCM, located between MAGIBS and MAGOBS.

SWA-EAS is mounted at the tip of the boom. EAS consists of two identical sensor heads that together provide an all-sky (4π steradian) field-of-view that is required to fully measure the electron velocity distributions from the solar wind. The accommodation at the tip of the boom is required to maximize the unobstructed field-of-view and to minimize interference from the spacecraft in the measurement of the solar wind electrons. Just below EAS, also at the end of the boom is EPD-STEIN. STEIN is a double-ended telescope with back-to-back $44^\circ \times 65^\circ$ fields-of-view covering both directions as close as possible along the Parker spiral, while avoiding any obstructions of its field-of-view by the solar arrays or the RPW antennas.

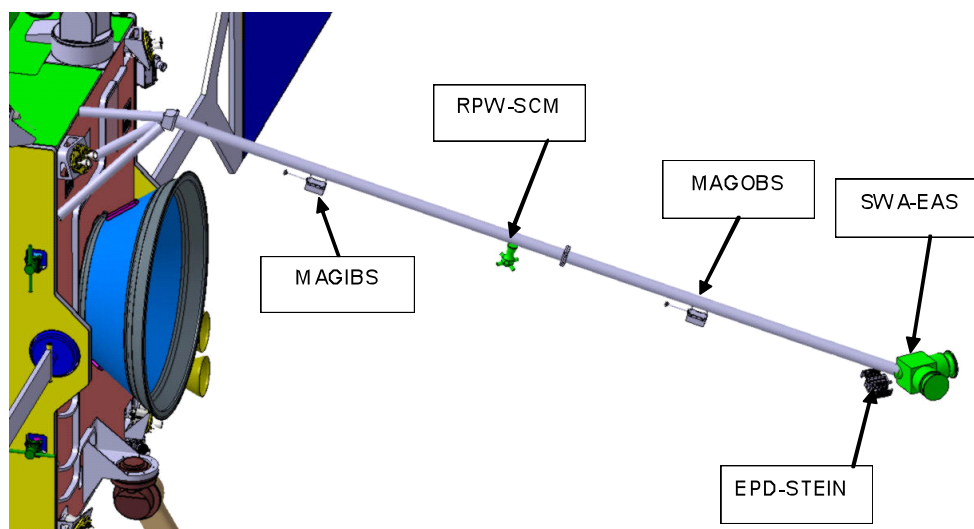


Figure 5.10. The RPW-SCM, MAGOBS, MAGIBS and SWA-EAS sensors are mounted on a boom to minimize the spacecraft-generated magnetic field interferences and to provide unobstructed fields-of-view.

SoloHI. The Solar Orbiter Heliospheric Imager (SoloHI) will be observing visible sunlight scattered in the heliosphere. It has a wide field-of-view that will encompass much of the orbit of the Solar Probe Plus spacecraft, which is crucial to provide a contextual link between observations from Solar Orbiter and from Solar Probe Plus. The SoloHI field-of-view is centred on the ecliptic plane but is offset from the Sun, and

covers a range of elongation angles from 5° to 45° . Because SoloHI will be observing visible light that is many orders of magnitude weaker than the direct sunlight from the photosphere, its stray light requirements are extremely tight. The wide field-of-view and tight stray light requirements prohibit mounting the SoloHI instrument internally, since the instrument would have to look through a heat shield feed-through. Therefore SoloHI is mounted externally, offset from the spacecraft wall so that it can look over the edge of the heat shield.

The instrument integrates its own specialised baffling required to achieve the high levels of stray light rejection required. The baffle design poses a requirement on the position of the heat shield edge with respect to the instrument baffles, and the tolerance thereof.

SoloHI is mounted on the +Y wall of the spacecraft, where it has a clear view of a straight heat shield edge and no sources of stray light other than from the unavoidable solar arrays and RPW antennas. The instrument is designing its optical baffles to deal with the latter stray light sources.

RPW-ANT. The RPW electric antenna system (RPW-ANT) is a set of high-sensitivity electric sensors included in the RPW suite of experiments. They are multi-purpose sensors, able to act both as radio wave antennas as well as voltage sensors to detect plasma waves.

At DC/low frequency electric fields, the antennas are coupled to the local plasma potential through a photoelectron sheath. By measuring the differential potential between the antennas, the electrical field strength and direction can be measured. The potential of the antennas is set by equilibrium between photoelectron current, plasma current and a bias current applied to the antennas to reduce sensitivity to plasma properties. In order to obtain the same reference for the three voltage sensors it is important to have them equally illuminated by the Sun.

RPW-ANT consists of three identical antennas deployed from the opposite corners of the spacecraft. They are oriented perpendicular to the spacecraft-Sun axis, at an angle of 125° between the top antenna and the two lower antennas and 110° between the two lower antennas. Each antenna design is based on a combination of a rigid deployable arm and deployable electric sensors. The deployable and rigid arm provides a larger spacing of the antenna sensor from the spacecraft and ensures that the antenna sensor will be fully illuminated.

EPD. EPD is a suite of instruments that will measure protons, electrons and ions over a wide range of frequencies in-situ on the Solar Orbiter spacecraft. The sensors are all externally mounted, with a common data processing unit/low-voltage power supply (CDPU/LVPS) mounted inside the spacecraft. EPD-STEIN was already discussed as part of the boom-mounted sensors. The accommodation of the remaining sensors on Solar Orbiter is discussed hereafter.

The Suprathermal Ion Spectrograph (SIS) consists of one telescope located near a single electronics box with the power and data interface to the CDPU/LVPS. The sunward-looking telescope is looking over the heat shield in a similar way as SoloHI. Its field-of-view has a boresight direction that is pointed approximately 20° west of the spacecraft-Sun line and has a 22° full cone angle. The field-of-view requirements dictate an instrument location on the -Y wall of the spacecraft. Just as for SoloHI it is necessary to raise the sunward-looking telescope away from the spacecraft wall, which means that under worst case failure conditions the instrument can receive direct Sun illumination for short durations on some parts.

The High Energy Telescope-Electron and Proton Telescope (HET-EPT) is a sensor unit that combines two double-ended sensor heads and an electronics box in a single unit, of which there are two mounted on the spacecraft. The first unit is pointing in the orbital plane along the nominal Parker spiral magnetic field direction towards and away from the Sun. The second unit is pointing at 45° out of this plane towards North and South. There is some flexibility on this pointing that can be used to avoid obstructions of the fields-of-view.

The Low Energy Telescope (LET) is the most complex to physically accommodate on the spacecraft since it has been designed to gather 3-D anisotropy information both in and out of the ecliptic plane. It therefore has six telescopes, combined in two units of three telescopes each. The fields-of-view of have a cone angle of 40° , and are separated from each other by 60° .

For all of the EPD sensors, the orientations of the lines of sight have been optimized by several iterations with the PI. Due to the complexity of finding the right balance between minimising any obstructions to the fields-of-view, finding suitable locations for the sensors on the spacecraft exterior, and maximising science return from the sensors, further iterations may be required to optimize the accommodation of EPD units.

SWA-PAS and SWA-HIS. The role of the Solar Wind Analyser (SWA) suite of instruments is to provide comprehensive in-situ measurements of the solar wind plasma including high time-resolution velocity distributions and composition of solar wind ions and electrons up to suprathermal energies. The electron sensor, EAS, is mounted on the boom and was already discussed above. The other two sensors, PAS (Proton Alpha Sensor) and HIS (Heavy Ion Sensor) are looking through corners cut out from the heat shield. Both sensors include an electrostatic analyser to deflect charged particles and hence build up a 3-D or 2-D velocity distribution. Hence the sensors have a wide field-of-view, which poses a limit on the thermal protection that can be offered by the spacecraft heat shield. The PAS and HIS sensors therefore include a local heat shield, which will need to be compatible with the spacecraft heat shield.

The sensors deflect particles coming through their front aperture. Incident sunlight goes through and exits at the back of the sensors. The light cones exiting at the back have been taken into account in overall spacecraft configuration so that they do not impact on other payload units or spacecraft appendages.

The required fields-of-view of the sensors are such that they both need to be located on the $-Y$ side of the spacecraft. Hence one occupies the $-Y/+Z$ corner and the other one occupies the $-Y/-Z$ corner. PAS, the smaller of the two units, was placed in the $-Y/-Z$ corner, so that thermal interaction with the RPW antenna is minimized.

5.5 System Budgets

This section describes the current best estimate system-level budgets.

5.5.1 Mass Budget

The overall mass budget is summarised in Table 5.6. It is driven by the need to accommodate both the 2017 nominal and 2018 back-up launch opportunities, which correspond to different ΔV requirements and hence propellant loading needs, and the different capabilities of the launch vehicles. The following approach has been used to calculate the mass budget:

- At equipment level, the ‘basic mass’ figures are given a margin which depends on the unit maturity level (7% for an off-the-shelf unit; 10% for a modified unit; 25% for a new unit). This approach results in a reliable unit ‘nominal mass’.
- For units which re-use BepiColombo technology development in an adapted design, (Solar Generator, High and Medium Gain Antennas), the mass estimates for Solar Orbiter use the same margins as used on the BepiColombo project. For the Heat Shield, which does require an original development, the mass estimates are based on robust pre-development activities already performed, including breadboarding and several thermal tests.
- The separated mass is based on the dry mass plus inclusion of the required propellant mass as calculated in the propellant budget. The total separated mass is 1800 kg, as specified by NASA who provide the launch vehicle, with includes an ESA-controlled system margin of 120 kg (controlled by ESA) and a Prime Contractor-controlled system margin of 18.2% (calculated from current budget against the 1800 kg specified limit), resulting in a total system margin of 28%.

5.5.2 Power Budget

The sizing power consumption for the solar generator is the hibernation mode during the largest transfer aphelion distance of 1.468 AU corresponding to the March 2017 mission scenario. This mode has a modest power requirement of 919 W but occurs under specific flux conditions of only 630 W/m².

For the rest of the mission, the solar array is considerably over-sized and produces more power than is required. The spacecraft is required to provide 180 W of power at a regulated 28 V to the payload during the science phase.

		Total Dry (w/o adapter)	1099.4	13.5%	148.9	1248.3	1191.1
		System Margin		18.2%		227.5	4.6%
		ESA Fixed Margin				120.0	
		Total Dry with Margin (w/o adapter)				1597.4	
Consumables							
	1	Propellant load - Transfer	173.47	0.0%	0.0	173.47	
	1	Propellant load - RCS	15.0	100.0%	15.0	30.0	
	1	Pressurant load	0.8	0.0%	0.0	0.8	
		Consumables subtotal	189.3	7.9%	15.0	204.25	0.0
		Total Separated Mass (w/o adapter)				1800.0	

Table 5.5. Solar Orbiter Mass Budget (in kg).

5.5.3 Link Budget

The link budgets are compliant with the telecommand and housekeeping telemetry needs in all mission phases, even in case of High-gain Antenna failure or non-availability (in the latter case via the Medium Gain Antenna) to the Malargüe baseline ground station.

The operational mode telemetry downlink provides the required 150 kbps at 1 AU (reference case) via the High-gain Antenna to Malargüe.

5.5.4 Data Storage Budget

The storage capacity simulations of Solar Orbiter's solid state mass memory (SSMM) cover the range of possible launch dates in 2017 and 2018. The maximum data volume to be stored in the January 2017 case is 539 Gbit. This value is based on a communications performance of 150 kbps at 1 AU and spacecraft design allocation and on instrument-aggregated data production according to a reference/nominal mission profile (in-situ instruments generating science data continuously, remote-sensing instruments only generating science data during three 10-day windows per orbit). The time profiles of available telemetry data rate and on-board data storage are shown in Figure 5.12.

The SSMM is identical to the BepiColombo unit, except for the size of the memory modules. Solar Orbiter uses 256 Gibit modules (which corresponds to 274.5 Gbit as 1 Gibit = 2^{30} bits), which enables the SSMM to meet the maximum data storage requirement throughout the spacecraft life, i.e. assuming the loss of one of the three modules.

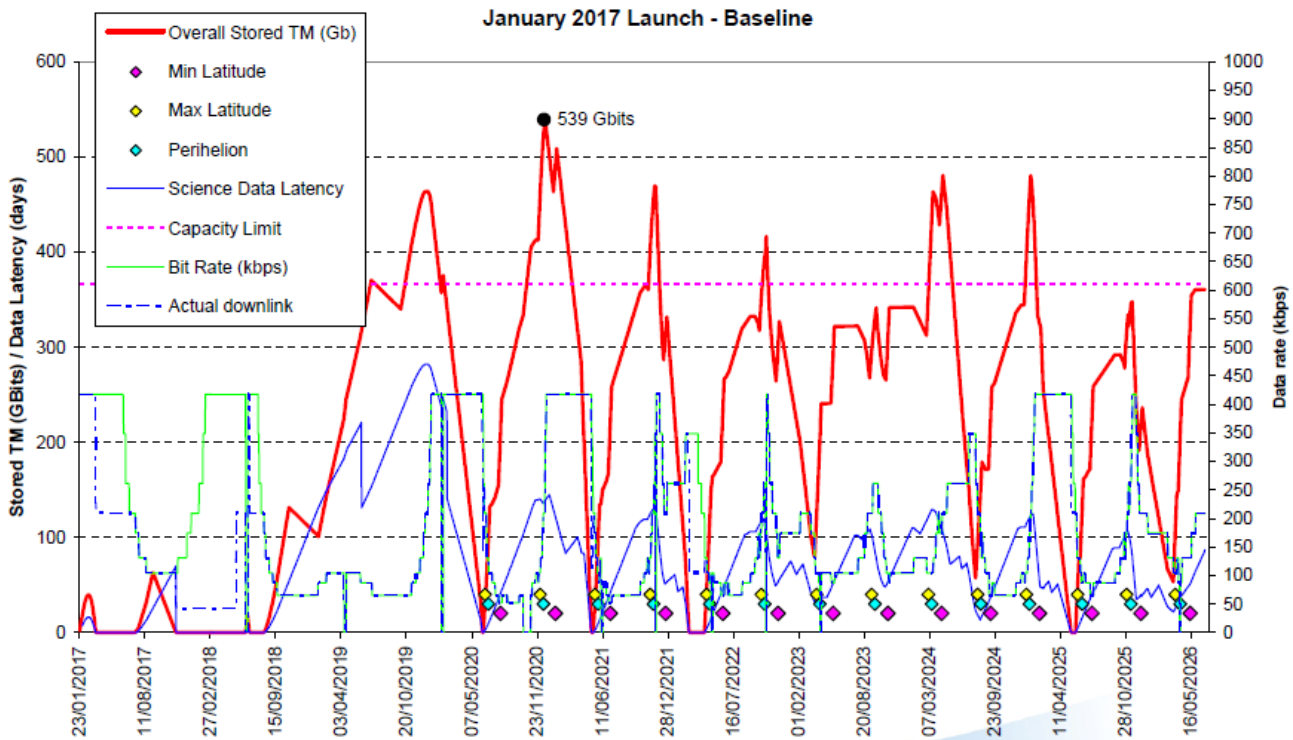


Figure 5.11. Time-dependent telemetry rate and on-board data storage.

5.5.5 Pointing Budget

The absolute pointing error (APE) of all instruments line of sight during science windows shall be less than $3.5'$. The APE error around all instruments line of sight shall be less than $20'$. The pointing requirements are both specified in terms of half-cone angle at 95% confidence level. The APE performance is driven by the thermo-elastic deformations experienced as the spacecraft distance to the Sun varies from 0.28 to 0.8 AU. The current budget for the APE errors of instrument line of sight gives an error of about $2.0'$ in the extreme hot case and $1.5'$ in the extreme cold case. The APE is within specification for all instruments.

The RPE of all instruments line of sight during science windows is marginally within the specification of $1''$ over 10 s, half-cone angle at 95% confidence level. It is essentially affected by control stability, i.e. mechanisms and reaction wheel actuation. The RPE requirement of $2''$ over 10 s about line-of-sight (X-axis) is also met.

5.6 Technical Challenges

The very nature of the Solar Orbiter mission implies that a number of spacecraft components are technologically critical. This is due to the very large solar flux (up to 12.7 Earth solar constants) experienced at perihelion, and also to the large variations in spacecraft-to-Sun distance, with the attendant variations in the solar radiation environment. The spacecraft critical items are generally those exposed to the Sun: solar arrays, High-gain Antenna, heat shield, attitude control sensors, and thermal control materials. The TCS design and the ground test facilities will also require critical emphasis.

Solar Arrays. Because of the very high solar flux to which Solar Orbiter's arrays will be exposed, a design specific to Solar Orbiter but closely based on BepiColombo's Mercury Planetary Orbiter (MPO) technology and equipment (solar cells, blocking diodes, shunt diodes, coatings) will be used. The solar array surface will comprise Optical Solar Reflectors (OSRs) and solar cells. The solar array will be tilted around its longitudinal axis to maintain the cell temperature within manageable limits, as inherited from BepiColombo, with a slightly higher solar flux and longer lifetime but with the benefit that, contrary to BepiColombo, Solar Orbiter does not have to cope with any thermal flux from Mercury and is always sun-pointing.

High-temperature high-gain Antenna. As noted earlier, the HTHGA reflector will be inherited from the BepiColombo mission but must be adapted (pointing mechanism, coating, mounting frame) to Solar Orbiter, possibly resulting in a higher mass. For thermal reasons, the HTHGA may have to be folded several times during the mission to place it in the shade of the spacecraft.

Heat Shield. The radiative heat shield is a development specific to Solar Orbiter. The choice, development, and verification of the materials and design are critical to the survival of the spacecraft. While the heat shield keeps most of the spacecraft in the shade, some of the baffles, doors, and mechanisms are exposed to the solar flux and have critical interfaces with the scientific instruments. It should be noted that representative heat shield prototypes have already undergone testing.

Fine Sun Sensors and Failure Protection. In view of the high solar fluxes experienced at 0.28 AU, the Fine Sun sensors will have to be adapted and to incorporate a filter in order to minimize heat absorption. In addition to nominal operations, the Fine Sun Sensors and Solar Orbiter FDIR will have to maintain a Sun pointing attitude of the Spacecraft to within 6.5° from Sun line following any contingencies or credible attitude failures, e.g. an open thruster valve.

Thermal Control Materials and Subsystem. High-temperature materials and coatings may be partly inherited from BepiColombo and adapted to Solar Orbiter requirements, but extra materials selection and qualification is likely to be necessary in order to meet simultaneously thermal performance, contamination control, conductivity and lifetime requirements. The critical Thermal Control Subsystem will require extensive use of heat pipes and other high-performance items.

High Solar Flux Test Facilities. A combination of specially adapted, large-size, moderate-to-high solar flux test facilities (e.g. the ESTEC Large Space Simulator as adapted for BepiColombo) and smaller, very high flux vacuum test facilities (e.g. the ESTEC VTC1.5 as adapted for both BepiColombo and Solar Orbiter) is necessary to verify the spacecraft and unit designs as well as materials properties, interfaces, and local thermal effects.

Radiation Environment. While many units will be re-used or adapted from BepiColombo, the differences between the radiation environments to which the two missions will be exposed must be taken into account for their qualification (see the following section).

5.7 Mission Environment

Very little is known about the space environment in the innermost regions of the solar system. In many cases, no observations have been made at the range of heliospheric distances covered by Solar Orbiter, and an appropriate scaling has to be applied to a model valid for 1 AU. Table 5.6 shows the scaling factors for the baseline trajectory of Solar Orbiter (January 2017 launch). The environmental factors of particular relevance to the Solar Orbiter mission are the solar irradiance, the properties of the solar wind, and energetic particle radiation.

Solar Irradiance. The solar flux varies with solar activity, which is highly variable over a solar cycle. For the baseline trajectory, the average solar flux is 3961 W/m^2 , the maximum flux (at 0.28 AU) is 17424 W/m^2 , and the minimum (at 1.32 AU) is 784 W/m^2 .

Energetic Particle Radiation. Figures 5.11 and 5.12 show the predicted solar proton fluences and total radiation dose for the Solar Orbiter mission.

	Mean Sun-spacecraft Distance r_{RMS} (AU)	Mean distance scaling factor $(1/r^2)_{\text{RMS}}$
Closest Perihelion	0.28	12.76
Farthest Aphelion	1.32	0.57
Average over total mission	0.76	3.87
Closest Perihelion during nominal science mission	0.28	12.8
Farthest Aphelion during nominal science mission	0.91	1.21
Average over nominal science mission	0.70	4.26

Table 5.6. Mission scaling factors.

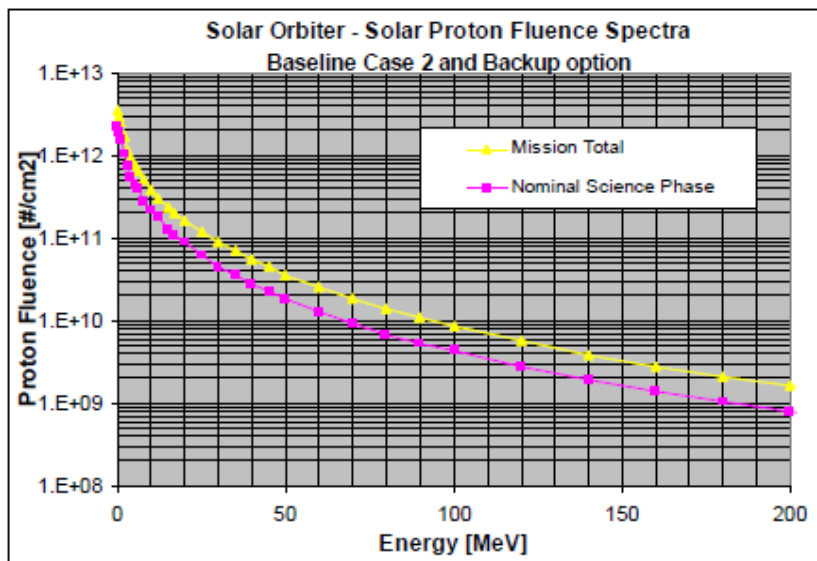


Figure 5.12. Integrated proton flux spectrum.

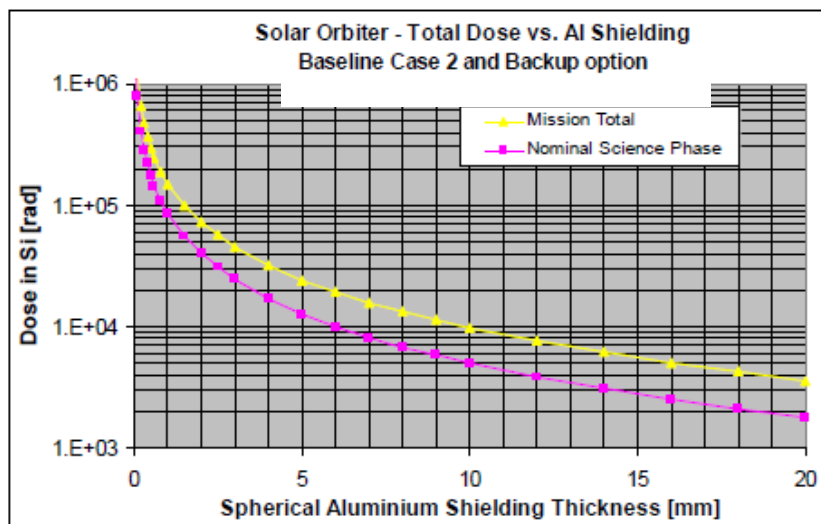


Figure 5.13. Equivalent shielded total dose.

6 Supporting Observations and Models

6.1 Space-Based Observations Supporting Solar Orbiter Science

6.1.1 Solar Probe Plus

The NASA Solar Probe Plus (SPP) mission, currently at the end of its phase A study, is a mission devoted to the in-situ exploration of the outer solar corona, and is therefore highly complementary to Solar Orbiter. Solar Probe Plus is a ~ 7 year mission, planned to be launched in 2018 and whose final elliptical orbit has an 88-day period and a perihelion at $9.5 R_{\text{Sun}}$ from Sun center. Since its scientific payload consists primarily of in-situ instruments complemented by a Wide Field Imager, SPP and Solar Orbiter can together address many questions in powerful new ways. Significant examples are different types of alignment, illustrated in Figure 6.1, which occur about 15-20 times during nominal missions: the left panel shows the case of SPP and Solar Orbiter radially aligned. In this configuration the radial evolution of solar wind properties, including shock and turbulence properties, can be studied directly. The middle panel shows cases of alignment along a nominal IMF spiral, where energetic particles travelling past one of the two spacecraft will later move past the other, permitting direct tests of energetic particle transport and scattering since the source function is determined at one of the spacecraft and result is seen at the other. The right panel shows cases of quadrature alignment, where Solar Orbiter remotely observes plasma low in the corona that later passes by SPP, allowing tests of radial evolution of solar wind plasma, shocks, and other structures. When Solar Orbiter enters the high latitude phase of its mission, alignments with SPP will allow latitude gradient studies. Since both spacecraft's orbital motions are in the same direction, these alignment periods can range from a few days to over a month, depending on the radial distances at the time. Finally, there are many periods when Solar Orbiter, SPP, and Earth lie within a 30° or 60° wedge, which is ideal for studies of larger structures such as high speed streams, or large CME-driven interplanetary shocks.

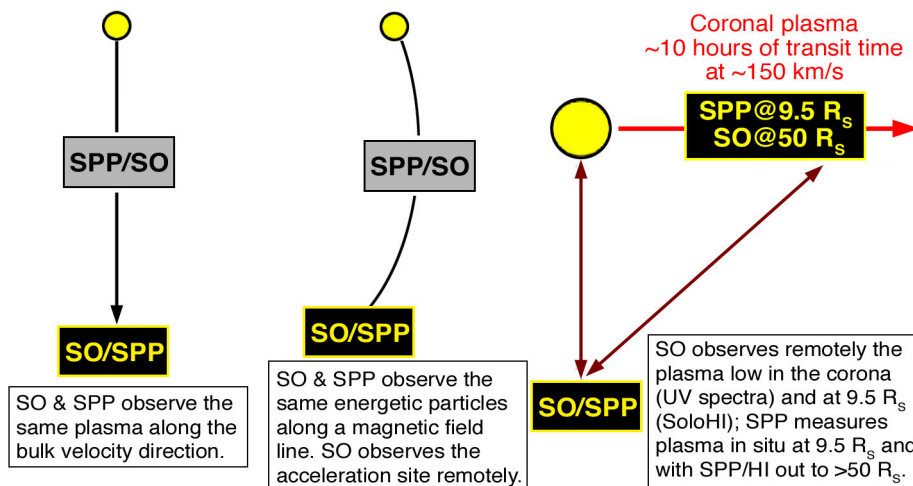


Figure 6.1. Solar Orbiter and Solar Probe Plus will provide multiple opportunities for coordinated observations from complementary vantage points.

6.1.2 Solar-C

JAXA's Solar-C is Japan's next-generation solar physics mission that is presently under study. Following the great success of Hinode (Solar-B), the ISAS/JAXA Solar-C working group have been studying two options, an out-of-ecliptic mission (option A), and a high-resolution spectroscopic mission (option B). In March 2011, this working group released an interim report which concludes that option B will be presented as the first-priority Solar-C mission to ISAS/JAXA. The model payload consists of a Solar UV/visible/IR telescope, an EUV/FUV high-throughput spectroscopic telescope, and an X-ray imaging (spectroscopic) telescope. This payload will offer excellent synergies with Solar Orbiter by combining Solar-C's focus on remote sensing from a geosynchronous orbit, which permits larger telescope apertures and higher telemetry, with Solar Orbiter's unique

out-of-ecliptic perspective and combined remote-sensing and in-situ instrumentation.

Other missions in the planning stage may contribute to heliophysical science and will be coordinated under the ILWS initiative.

6.2 Ground-Based Observations Supporting Solar Orbiter Science

Ground-based instruments in the visible and radio range will support Solar Orbiter observations. Spectropolarimetric on-disk observations in the visible and infrared will provide the photospheric magnetic field vector from a different viewing angle (with the Advanced Technology Solar Telescope (ATST) and the European Solar Telescope (EST)). Coronagraphic observations of the density and the magnetic field vector in the corona (with the Coronal Solar Magnetism Observatory (COSMO)) will be most valuable, especially during perihelia in quadrature and give plasma properties in the coronal region observed by Solar Orbiter from straight above. Radio observations with the large arrays of LOFAR (Low Frequency Array) and ALMA (Atacama Large Millimeter Array) will allow high-resolution observations of the thermal and magnetic structure of the chromosphere and the corona. Availability of the Global Oscillation Network Group (GONG) or a similar successor will make it possible to carry out stereoscopic helioseismology for the first time, probing the deep interior of the Sun.

6.3 Theory, Modelling, and Scientific Closure

Underlying the science objectives of Solar Orbiter are some of the most important outstanding questions in solar and heliospheric physics, and more generally in plasma astrophysics, today. They are also some of the most challenging, namely the complex coupling of physical processes across multiple spatial and temporal scales. Microscopic physical processes lead to the formation of macroscopic solar wind streams; kinetic, small-scale processes combine with large-scale ones (e.g., to accelerate particles in shocks or compression regions); CME evolution is determined by its micro- and macroscopic interaction with the ambient corona and solar wind. The powerful high-resolution and high-cadence measurements during near-corotation will allow Solar Orbiter to discriminate between spatial and temporal variations and to correlate small-scale solar phenomena with larger ones both remotely and in-situ. Solar Orbiter's instrumentation and observational strategy are innovatively designed to tackle these problems, to understand the coupling from the global MHD scales of the Sun's corona to the local kinetic scales of wave and particle distributions in the heliosphere.

However, observations alone will not be sufficient. Theory and modelling will be key to provide the interpretive framework and also be required to elucidate the multi-scale connections among the coronal and heliospheric phenomena observed. Theory and modelling efforts are integral parts of the Solar Orbiter mission and each instrument team has equally talented scientists responsible for the theory and modelling aspects of their investigations.

Moreover, our understanding of both global and local processes has advanced considerably in recent years. Several large-scale programs are under way in Europe, the U.S., and world-wide to develop global MHD models that encompass the whole corona-heliosphere system. At the same time, there have been broad advances in theories for basic mechanisms such as particle acceleration and reconnection in collisionless plasmas. We expect that the theories and models will greatly increase in sophistication during the next five to ten years, and that Solar Orbiter will play a key role in testing and refining these powerful new models. For example, data-driven 3-D MHD models of the initiation and development of solar wind streams and CMEs are now being developed and should be in a production state by the time Solar Orbiter delivers data. One of the crucial missing items for such models have been measurements of the photospheric field on the *entire* $4\text{-}\pi$ steradian surface of the Sun, not just the one half which happens to face the Earth at any given time. Thus Solar Orbiter will not only provide fundamentally new and important missing data, but also provide a powerful tool to verify model predictions and provide quantitative information about the state of the heliosphere in a wide range of latitudes and heliocentric distances.

The first attempts of data assimilation in flux-transport models herald a new phase in the development of solar dynamo theory, from probing the fundamental principles to detailed models that embrace the potential for predictions. Observed data are fed as input into such models in order to tie them closely to the actual development of the solar conditions. Helioseismic measurements of sub-surface differential rotation and

meridional flow, particularly at high latitudes, together with the detailed maps of the polar magnetic fields that will be obtained by Solar Orbiter, will supply the essential information required to perform critical tests of the central concepts for the flux-transport model and other approaches to understand the solar dynamo. On this basis, Solar Orbiter data will set the stage for quantitative and potentially predictive modeling of the solar cycle.

7 Ground Segment and Operations

7.1 Ground Segment Facilities and Services

The Solar Orbiter ground segment will make maximum reuse of the ESA/ESOC/ESAC infrastructure for Deep Space missions, and in particular those parts developed and used for the BepiColombo and Rosetta missions. The overall ground segment architecture reflects the standard architecture of a typical interplanetary scientific mission. Its main components are:

- The ground stations, which belong to the ESA network.
- The Mission Operations Centre (MOC), located at ESOC, Darmstadt, in charge of all mission operations planning, execution, monitoring and control. The Mission Operations Centre includes infrastructure and computer hardware as well as the flight control system comprising data processing and flight dynamics software.
- The Science Operations Centre (SOC), located at ESAC, Villafranca, in charge of scientific operations planning, data archiving and scientific analysis support.
- The communications network, linking the various remotely located centres and stations to support the operational data traffic.

7.1.1 Ground Stations and Communications Network

The Solar Orbiter mission will nominally be supported by a single ESA ground station, except in critical mission phases, where support by multiple ground stations will be required. There will not be a dedicated ground station, but any of the three ESA deep space terminals can be used (New Norcia in Australia, Cebreros in Spain and Malargüe in Argentina), shared with other missions depending on the visibility pattern and availability profile. For the sake of simplicity, and considering the parallel operations with BepiColombo, it is expected that the Malargüe station will be mainly used for Solar Orbiter.

Where additional tracking support is required (e.g. for Δ -DOR tracking in critical phases), one of the other ESTRACK deep space antennas will be used in addition.

No NASA-Deep Space Network (DSN) support is planned for nominal and contingency operations. Nevertheless, the spacecraft shall be compatible with the DSN, since possible use of DSN in support of tracking campaigns around planetary fly-bys will be considered when defining the details of the ESA-NASA memorandum of understanding.

The ground station network assumed during LEOP (7 days after launch) will consist of the maximum visibility windows from at least two deep space stations (e.g. New Norcia and Malargüe) plus one 15m station. The location of the latter will be selected depending on the ascent trajectory, to optimize visibility around separation of the spacecraft from the launcher.

Malargüe will be used over the full visibility (ca. 10 hours/pass, daily passes) through the Near Earth Commissioning Phase (3 months duration). During the cruise phase, 9 hours passes from Malargüe will be taken 3 times per week. On average, this will allow 8 hours per pass of science telemetry downlink.

For the nominal (full science) mission phase after Venus GAM-2, it is assumed that Malargüe will take daily passes of 9 hours duration (8 hours dedicated to science telemetry downlink).

All ESA stations will interface with the control centre at ESOC via the OPSNET communications network. OPSNET is a closed Wide Area Network for data (telecommand, telemetry, tracking data, station monitoring and control data) and voice.

7.1.2 Mission Operations Centre

The Solar Orbiter mission will be operated by ESOC, and it will be controlled from the Mission Operations Centre (MOC). During near-earth commissioning phase, cruise, and the science operations phase, mission control will be conducted from a dedicated control area, which will be an adaptation of, or may be shared with, the existing ones of other interplanetary missions like Rosetta, Mars Express, ExoMars or BepiColombo.

The MOC is equipped with workstations for access to the operational data processing systems. It will be staffed by dedicated Solar Orbiter spacecraft operations staff and experts in spacecraft control, flight dynamics

and network control, who will be shared with other ESA missions. The computer (hardware and software) configuration used in the Mission Operations Centre for the Solar Orbiter mission will be derived from the existing infrastructure, which consists of:

- A mission dedicated control system used for real time telemetry processing and for command preparation and execution, telemetry and command log, archiving, and also for non real-time mission evaluation;
- A mission planning system supporting command request handling and planning and scheduling of spacecraft and payload operations.
- Workstations hosting the flight dynamics system (ORATOS), which supports all activities related to attitude and orbit determination and prediction, preparation of slew and orbit manoeuvres, spacecraft dynamics evaluation and navigation in general;
- Workstations hosting the science telemetry data distribution and instrument command reception system (data disposition system). The data disposition system supports the acquisition and storage of raw scientific, housekeeping and auxiliary data to be accessible from remote locations.
- A system simulator, providing a realistic software simulation of the ground station and spacecraft for pre-launch ground segment verification, staff training and procedure validation throughout the mission.

All computer systems in the MOC will be redundant with common access to data storage facilities and peripherals. All computing systems will be connected by a Local Area Network (LAN) to allow for rapid data transfer of and joint access. The external connections to the SOC and PI's institutes will use commercial/public networks.

7.2 Science Operations

7.2.1 Science Operations Centre

The SOC is responsible for science operations planning within the framework of the Science Operations Working Group. The requests for payload science operations generated by the individual PI teams will be collected at the SOC and merged into a single payload operations request to be submitted to the MOC on a periodic basis. The MOC will be in charge of including the requests in the overall mission operations timeline to be uplinked periodically to the spacecraft.

In support of the science operations planning process, the SOC receives payload raw data and auxiliary data from the MOC, including orbit and attitude profiles, event predictions, time correlation details and other mission specific information. The SOC will also construct a mission data archive, including all spacecraft raw data and auxiliary data received from the MOC, plus additional information resulting from basic pre-processing of the science telemetry.

The Principal Investigators (PIs) are responsible for operating and monitoring their own instruments, and for processing both their housekeeping and science telemetry into useful uncalibrated and calibrated data products that will be made available to the scientific community through the infrastructure of the SOC. In particular, PIs are in charge of:

- The generation of requests for instrument science operations, which will be forwarded to the SOC.
- The monitoring of the health and safety of their instrument, through the SOC or the MOC as required.
- Reformatting their instrument housekeeping and science telemetry into uncalibrated data products (level-1 data) and provide these to the SOC.
- Calibrating their science level-1 data products into level-2 data products useful for scientific analysis and provide them to the SOC for archiving.
- Providing reformatting and calibration software to the SOC for long-term archiving.
- Providing software to the SOC so instrument quicklook data products can be generated and distributed to all parties.

7.2.2 Science Operations Planning

The science return of the Solar Orbiter mission will be maximized by coordinating operations and data taking among instruments. Every science objective described in Chapter 2 requires coordinated observations among

several in-situ and remote-sensing instruments, and the strength of the Solar Orbiter mission stems from the synergy and comparative analysis of in-situ and remote-sensing observations.

The orbit characteristics of Solar Orbiter evolve significantly from one orbit to the next (as discussed in detail in Chapter 5), as do the designated encounter periods in which Solar Orbiter will be out of contact with Earth. Thus detailed planning by the science working team (SWT) and science operations centre (SOC) will be required for every science orbit. This endeavour will be very similar to what has been used highly successfully in the Joint Observation Programmes (JOPs) of ESA's SOHO mission. Below, we discuss two operating modes to illustrate how Solar Orbiter's science objectives can be met within the designed mission profile.

7.2.3 Sample Science Orbits

As discussed in more detail in Chapter 5, certain subsections of every 150/168-day orbit are designated as part of the 'encounter period.' An encounter typically consists of a 10-day window centred around perihelion for high-resolution imaging studies and two 10-day windows centred around the highest latitudinal extents reached during that specific orbit or maximum corotation (minimal angular velocity of the spacecraft with respect to the Sun). In-situ instruments operate during the entire orbit whereas the remote-sensing instruments operate primarily during the 30 days within the encounter windows.

The first case to consider is a nominal orbit in which we have the lowest telemetry rate and which therefore places the most severe constraint on choosing what kind of data to acquire. Solar Orbiter has been designed around this 'worst' or nominal case in which in-situ instruments are assumed to be operating along the entire orbit and the remote-sensing instruments are operating for three 10-day periods during the encounter period at the data rates given in Table 3.7. Spacecraft memory has been sized to ensure that all data can be transmitted to Earth for this case. All science objectives of Solar Orbiter can be met in this nominal telemetry mode.

There will also be more favourable cases, based on celestial mechanics, where Solar Orbiter will have a higher than nominal telemetry rate (see Figure 5.10). This will be used to increase the measurement opportunities in several ways, which will be determined by the SWT/SOC. For example, some remote-sensing instruments will acquire additional synoptic context images to support the key science goal of Solar Orbiter – how does the Sun create the heliosphere? In-situ instruments will increase the amount of data acquired at enhance cadence to study turbulence, capture fine structure of shocks and current sheets or event onset times. Helioseismic studies will benefit from an increased temporal baseline, and high-resolution studies of solar source regions will be able to extend outside the 10- or 30-day windows. In these orbits, as a baseline, the telemetry allocation of each instrument will be increased proportionally to the overall increase.

7.2.4 Inter-Instrument Communication and Burst Mode

Using the functionality of the on-board SpaceWire bus, instruments can communicate with each other, making it possible for teams to coordinate operations without incurring additional workload for the spacecraft operations team. Since the telemetry rates from Solar Orbiter, like those of many missions, are limited, the spacecraft will be equipped with a large (823 Gbit) mass memory that will store up to about two months of data at average rates, to allow for variable downlink speeds. However, the instruments are not limited to taking data at one rate and a number of coordinated and targeted data rate selection mechanisms will be implemented.

Burst Mode. Coordinated burst-mode data acquisition will enable detailed studies of the microphysics of the solar wind. Approximately 10% of the data return is expected to be in burst mode, with ~10 times the data rate of normal mode, corresponding to ~1% of the time. For instance, this mode could be used to study solar flares, which explosively release magnetic energy, driving shocks and accelerating particles. STIX would detect the flare's onset and location and trigger high time resolution measurements by remote-sensing instruments to determine the properties of the flare site and its evolution, as well as measurements by RPW to measure radio emission from accelerated particles and by EPD to measure accelerated particles passing the spacecraft. The burst mode could also be used to study shocks crossing the spacecraft. They would be detected in the magnetic field and plasma and would trigger short burst mode measurements by Solar Orbiter's in-situ suites (MAG, RPW, SWA, and EPD) to quantify shock substructure and the motion and acceleration of particles nearby. Rolling buffers within the instruments will make it possible to store high-cadence data from upstream of the shock trigger time.

Small-scale kinetic processes could be measured using coordinated burst mode measurements of the magnetic and electric fields and particle distributions by Solar Orbiter's MAG, RPW and SWA. By sharing data on local plasma and field conditions, the instruments would trigger short burst mode intervals to ensure a wide coverage of different plasma regimes. In addition, some remote-sensing instruments will take high-cadence measurements of sub-fields of view. These can be planned based on known positions of active regions, but also in response to triggers based on emission levels of rapid changes in observed conditions.

Sharing of Magnetic Field Direction. Magnetic field directions can be shared among the in-situ instruments to produce reduced velocity distribution functions on board Solar Orbiter, thus greatly reducing the telemetry requirements. The local magnetic field direction is important to particle instruments in order to compute reduced data products such as temperature anisotropies or pitch-angle distributions. The Solar Orbiter magnetometer will transmit the measured magnetic field direction in real time to other instruments via the SpaceWire bus. The generation of high time resolution data and accurately reduced distribution functions requires precise timing knowledge between the contributing instruments, which will be achieved by synchronizing instrument clocks with the spacecraft via the SpaceWire bus. An accuracy of ~100 ms can be achieved and will be used to ensure synchronization of sampling between instruments.

7.3 Mission Operations Concept

7.3.1 Principles

The main principles which are driving the Solar Orbiter operations concept can be summarised as follows:

General. Maximum possible exploitation of commonality with BepiColombo, both in the area of ground segment tools and facilities and in the sharing of manpower and expertise in the development and operations teams.

Pre-launch. (a) Joint approach to pre-launch spacecraft system level testing between the spacecraft manufacturer and the spacecraft operations team; (b) Synergy between spacecraft manufacturer and operators in the preparation of operational documentation, spacecraft user manual, operations database, etc.;

In-Flight. (a) Minimization of real-time contact during low activity phases. This means low frequency of contacts but also as short as possible duration of each contact (dictated by science data return requirements); (b) Maximization of off-line operations (planning, on-board schedule execution, minimization of the need for real-time interaction);

Spacecraft Operability. (a) Spacecraft autonomy and its relation to level of ground control in the various phases of the mission: the starting level for autonomous functions is the one of BepiColombo, with improvements and modifications based on actual operational experience; (b) Full, consistent and intelligent use of the packet telemetry and telecommand concepts in the spacecraft avionics architecture.

7.3.2 Spacecraft Operations Approach

Due to the long signal propagation delay the spacecraft will be required to support off-line operations. After the initial spacecraft commissioning, all telecommands required to carry out the mission will be loaded in advance on the mission timeline for later execution. All telemetry generated on-board will be stored for later retrieval by ground. In order to support the off-line operations approach required for a deep space mission, the following autonomy capabilities have been specified for the spacecraft:

- To support On-board Control Procedures, as a way to autonomously execute complex procedures including decision loops which ground cannot support due to the propagation delay. On-board Control Procedures also provide the required flexibility to adjust procedures defined pre-launch to the environment while in the routine orbit around the Sun and the aging spacecraft, as is the case with ground procedures.
- To detect and autonomously recover any single failure, and to reconfigure itself to a safe back-up mode in

case the detected failure is not recoverable.

To provide the necessary flexibility in allocation of on-board storage areas to different payload users and for the retrieval of engineering and science data according to the priority of the on-going operations, the storage on board will be organised in so-called “packet stores”. Dedicated packet stores will be created and assigned to each instrument for science telemetry packets. This will allow allocation of storage resources according to the individual instrument requirements without risk of interference across instruments in case of telemetry generation exceeding the assigned and planned resources.

An automated process will be established to allow re-dump of missed parts in the downlink. This process is, with the existing on-board and ground software architectures, very manual and cumbersome and could not be used on a regular basis. For this reason, the spacecraft will be required to support a closed-loop protocol on the downlink. As this feature will be implemented on BepiColombo, reuse of the identical protocol and associated functionality is assumed. This protocol will allow automated gap-filling in a reliable manner without heavy operator intervention. The average time for re-dump will be included in the planning process as a variable that can be adapted on a regular basis according to the experience. In order to optimize the downlink bandwidth usage, it shall be possible to run multiple closed loop downlink transactions in parallel.

The nominal RF link to/from the spacecraft will be degraded when the Sun-Earth-Spacecraft angle becomes lower than 5° (based on X-band experience). Degradation of the signal also affects tracking measurements. For this reason the mission shall be designed such that critical navigation activities (e.g. manoeuvres, planet swing-bys) do not take place within 5° (TBC) angular separation from the Sun as seen from Earth.

The spacecraft will be able to operate autonomously during the solar conjunctions, but is not required to continue mission product generation continuously, as this would have driven the size of major onboard resources such as the mission timeline and the mass memory. Therefore, science operations in this period will have to be adjusted to the available on-board resources.

7.3.3 Payload Operations Approach

Operations of the payload instruments will undergo the same offline approach and rules adopted for the spacecraft. In addition all scientific operations will be conducted via an offline planning process and under the coordination of the Science Operations Centre.

During the cruise phase until Venus GAM-2 the in-situ instruments will be operated, according to the PI requests and following the regular planning process, and the data generated will be downloaded typically 3 to 6 days later. In this phase of the mission the remote-sensing instruments will be inactive, and only operated for a short, non-interactive functional checkout of a few hours twice per year.

After Venus GAM-2 the full payload complement will be operated. The daily ground station contacts available in this phase will allow the downlink of the data within a shorter period from the generation time, which can be as short as 1-2 days, depending on the exact payload operations profile. Exceptions will be the periods around conjunction and science windows, where larger data latency will have to be taken into account.

Payload instruments contingencies, as well as maintenance and troubleshooting activities (e.g. on-board software updates, anomaly investigations) will be handled outside the normal planning process and with a direct interface between the PI team and the MOC. Presence of the PI team experts at the MOC will also be possible, where required to support near-real time decision processes.

7.3.4 Data Delivery

All telemetry data are received at ESA/ESOC and filed in a central archive in form of raw telemetry packets. Access to this archive by the users community (restricted to the Science Operations Centre, Principal Investigators institutes and authorised science institutes), is provided via the ESOC DDS. Auxiliary mission information (e.g. orbit and attitude profiles, event files, telecommand history, mission planning information, etc.) will be produced at ESOC and made available to the authorised external users community via the DDS.

7.3.5 Mission Planning

The mission planning approach for all routine science operations phases will be built on the experience of

the precursor planetary missions Mars Express and Venus Express. In addition, it is planned to make use of the system currently being developed in support of BepiColombo and Rosetta. In a typical mission planning scenario the PI teams provide, at fixed deadlines and with a fixed periodicity, inputs to the SOC through the Science Operations Working Group for the requested science operations. The SOC passes a consolidated request to the MOC which checks the requests against mission, environmental and resource constraints. A baseline science plan, which already takes into account the major constraints, will have to be established long before submitting the final science operations requests to the mission planning process. The mission planning scenario for the routine science operations phase will therefore be divided into different levels:

- Long-term planning will fix the trajectory and the ground station schedule. This process typically will take place once for each mission phase before the 2nd Venus fly-by, and once for every orbit around the Sun after the 2nd Venus fly-by.
- Medium-term planning will fix the usage of spacecraft resources. This process typically will take place once for each mission phase before the 2nd Venus fly-by, and around every month during the full science phase (after the 2nd Venus fly-by).
- Short-term planning will generate detailed schedules of commands for the spacecraft and for the ground stations. This process will take place typically every week. The SOC will provide detailed operations requests which are imported by the MOC into a single plan, and will undergo final detailed resource and constraints checks.

7.3.6 Science Management Plan

Following endorsement by the Solar System Working Group (SSWG) and the Space Science Advisory Committee (SSAC), the draft Science Management Plan (SMP) for Solar Orbiter was presented to Science Programme Committee (SPC) at its 120th meeting on 12-13 November 2007. Comments were provided in writing subsequent to the meeting and incorporated in the revised document (ESA/SPC(2007)49, rev. 1 Annex dated 4 December 2007), which was then approved via a written procedure. The draft SMP was a reference document for the Solar Orbiter AO issued on 18 October 2007. A revised version of the SMP will be submitted to ESA's Advisory Structure and subsequently to SPC for approval in Q4 2011. Key elements of the SMP are summarized below.

The SMP describes the implementation of those aspects of the project, up to and including the post-operational phase, that are required to ensure fulfilment of the mission's scientific objectives, and to optimize its scientific return, with special emphasis on payload procurement, science operations, and data management. Specifically, the SMP summarizes the main aspects of the mission and provides a description of how the scientific community will be involved with the mission, and the selection of the instruments that constitute the Solar Orbiter scientific payload. The plan outlines the role of the Solar Orbiter science advisory structure, and the ESA science management tasks from instrument selection to data distribution and archiving. The SMP also addresses the roles of the Solar Orbiter investigators, as well as their interaction with the SWT.

Scientific Participation. As outlined in the SMP, the possible modes of participation in the Solar Orbiter programme are:

- Principal Investigator (PI), heading an instrument consortium
- Co-Principal Investigator (Co-PI), appointed if a major development is carried out in a country/institution different from the one of the PI; a Co-PI will have similar rights to those of a PI, but the PI will remain the formal interface to the Project Office
- Co-Investigator (Co-I), a member of an instrument consortium providing an instrument

Payload Selection. In accordance with the SMP, and to ensure that the scientific return of Solar Orbiter is of the highest quality, an independent international Payload Review Committee (PRC) reviewed (in close cooperation with ESA technical, programmatic and financial analysis teams, and supported by industry) all instrument proposals submitted to ESA in response to the AO.

Financial. The financial status of the PI teams will have to be guaranteed by the Lead Funding Agency. The Lead Funding Agency will be considered responsible vis-à-vis ESA for all financial matters related to the

selected investigations. Co-I teams are required via their national funding agencies to seek agreement with the Lead Funding Agency on financial matters related to the selected investigations.

Post-Operations Phase and Data Archiving. Data archiving for Solar Orbiter will follow the same model as that used by previous ESA PI missions in the solar and heliophysics domain (e.g., SOHO). Reduction of science data is under the responsibility of PI teams. Following in-orbit commissioning, the PI teams retain exclusive data rights for the purpose of calibration and verification for a period of 3 months after the receipt of the original science telemetry and auxiliary orbit, attitude and spacecraft status information. Upon delivery to the ESA SOC, the data will be made available to the scientific community at large through the ESA science data archive. The PI teams will provide records of processed data with all relevant information on calibration and instrument properties to the ESA science data archive. The format for the spacecraft data shall be compatible with those defined for the ESA science data archive. The ESA science archive will be the repository of all mission products. A copy of this archive will reside with NASA.

8 Management

8.1 Project Background Within the Cosmic Vision Programme

The first Call for Missions for the "Cosmic Vision 2015-2025" plan was issued in March 2007, advertising a launch opportunity for a "medium" (M) mission in 2017 and one for a "large" mission in 2020. In November 2008, Solar Orbiter became a candidate M mission for Cosmic Vision slice 1, for a target launch in 2017 (back-up in 2018), assuming NASA provision of the launch vehicle and several payload elements. The down-selection process from the mission Announcement of Opportunity to the mission implementation is described in details in document ESA/SPC(2009)37. Following the completion of the Assessment Phase activities that were carried out for the concepts selected in response to the first Call for Missions, a scientific ranking of the proposed mission concepts was performed by the Space Science Advisory Committee (SSAC) and approved by the Science Programme Committee (SPC) at its 128th meeting on 17-18 February 2010 (ESA/SPC(2010)3, rev.1).

Three M-class missions are at present competing in the first Cosmic Vision slice – Euclid, Plato and Solar Orbiter – with the objective to implement two of them for a target launch date in 2017/2018. The final down-selection will be taken by SPC on 4 October 2011, based on programmatic consolidation of the missions and on their effective science return. The Solar Orbiter spacecraft configuration is in a well-advanced state as it has already been the subject of a preliminary definition phase, and is envisaged for a nominal launch in 2017.

In keeping with the recommendations of the SPRT Report adopted by Council Resolution (ESA/C(2007)107) and the lessons learnt from recent experience in the Science Programme, and in keeping with the recommendations resulting from independent technical reviews conducted to limit development risks, the orbit of Solar Orbiter was revisited in order to remain approximately within the solar illumination levels that are expected for BepiColombo. The new orbit configuration was endorsed by the science community and effectively removes the major development risk element previously identified for Solar Orbiter by now allowing to rely on the solar cell technology of BepiColombo. The heat shield protecting the spacecraft and its payload from the high solar flux is the other high risk element that is specific to Solar Orbiter. A substantial technology development effort has already been engaged into, to reach a hardware demonstration of the heat shield concept. Furthermore, the platform equipment relies on state-of-the-art technologies or otherwise take large benefit of BepiColombo development. In March 2011, NASA informed ESA that, as a consequence of budgetary pressures, it had become necessary to reduce its contribution to the payload to 1 full instrument and 1 sensor. Specifically, the Spectral Imaging of the Coronal Environment and Suprathermal Ion Spectrograph investigations would not be funded. Given the scientific importance of these investigations, their measurement capabilities will be recovered through the inclusion of European-lead instruments with contributions from member states and ESA.

Altogether, Solar Orbiter is now evaluated as being mature enough to plan for a nominal launch in 2017 with satisfactory schedule margins, assuming nominal progress for the science payload development. Based on the above considerations, the SPC endorsed the proposal of the Executive to bring forward the Solar Orbiter mission with a "fast track" implementation approach (i.e. initiation of the Consolidation and Implementation Phase in 2011 rather than 2012) enabling launch in 2017, with the request to submit the mission at the October 2011 SPC meeting for final adoption. By that time, a Multi Lateral Agreement (MLA) for the payload should also be ready to be recommended for signature by the SPC. This revised approach allows a one-year gain on the schedule originally foreseen by the baseline Cosmic Vision implementation plan.

8.2 Procurement Approach, Industrial Organization and Project Phasing

The Executive took into consideration the lessons learnt from the missions that are currently under development in the Science Programme, and more widely in the Agency, when defining the procurement approach for Cosmic Vision missions, in particular with regards to the industrial consortium building up and to geo-return needs. The analysis and relevant recommendations from the Themes 1 to 4 included in document ESA/C(2010)20, "Cost and Calendar of ESA Projects", have been taken into account. The procurement approach is designed to

allow a maximum flexibility of geo-return through the implementation of a dedicated subsystem layer and will be generally applicable to the other M missions.

Following several study phases, the Phase B1 Preliminary Definition Phase industrial study was initiated in March 2008 with a pre-defined industrial organization, building on BepiColombo developments. This study was performed by a core team led by Astrium Ltd, Stevenage (UK), and comprising Astrium GmbH, Friedrichshafen (Germany), and Thalès Alenia Space Italy, Torino.

In order to make maximum use of the available time, the Solar Orbiter Preliminary Definition Phase (Phase B1) with Astrium Ltd was extended with a "Bridging Phase" (Phase B1X) to secure further progress on the design activities while completing the necessary documentation for the start of the Consolidation Phase in early 2011. This "Bridging Phase" concentrated on the completion of the running configuration optimizations, solidification of payload interface definitions, some pre-development activities in the field of thermal control and Heat Shield, communications, and the preparation of the procurement actions for the early part of the Implementation Phase and core team build-up.

A Consolidation Phase is carried out as a first part of the implementation and started with the kick-off of phase B2/1 in early 2011. It will conclude with the selection of the first layer of subsystem industrial contractors, thus consolidating the industrial consortium, and the consolidation of the programmatic scenario (cost and schedule) by October 2011, based on actual committing proposals for sub-systems and selected critical equipment. During Phase B2/1, all elements of the Solar Orbiter spacecraft shall be defined to a level of detail and understanding such that the detailed design, manufacturing and verification phases (Phases C/D) can commence. Phase B2/1 includes a Systems Requirements Review (SRR) in June/July 2011. The final industrial organization will be completed mostly through a process of competitive selection and according to the ESA Best Practices for subcontractor selection, also taking into account geographical distribution requirements. The selection process will, however, be constrained as well by the necessity to re-use existing hardware designs and units to the maximum extent possible, in particular from the BepiColombo project, in order to contain the project cost, schedule and technological risk within acceptable bounds.

Following the Consolidation Phase, the Implementation Phase will proceed with the kick-off of phase B2/2 at the end of 2011 which will include a Preliminary Design Review (PDR). The Implementation Phase will lead to the flight model delivery of Solar Orbiter consistent with a launch in January 2017. It is to be noted that the Solar Orbiter requirements are also fully compatible with the next launch opportunities in March 2017 or September 2018.

The principal objective of Phase C/D is to realize the Solar Orbiter Spacecraft in full conformance with the specifications and plans defined, and agreed by ESA, during Phase B2. This will result in the delivery of the fully validated Solar Orbiter Spacecraft to ESA. The detailed design phase (Phase C) will be concluded with the Critical Design Review (CDR). The subsequent Phase D will comprise the Qualification Review (QR) when all subsystems and equipment/unit level Qualification Reviews have successfully taken place. Phase D will end with the Acceptance Review (AR).

In Phase E1, the Contractor will provide ESA with support for the launch campaign, support to the operation of the spacecraft during the Launch and Early Orbit Phase (LEOP), and support to operation of the spacecraft during the commissioning phase and the payload validation phase, up to the In-Orbit Commissioning Review (IOCR).

8.3 ESA-NASA Collaboration

NASA and ESA have a mutual interest in exploring the near-Sun environment to improve the understanding of how the Sun determines the environment of the inner solar system and, more broadly, generates the heliosphere itself, and how fundamental plasma physical processes operate near the Sun.

ESA is providing the spacecraft bus, integration of the instruments onto the bus, mission operations, and overall science operations. NASA is providing an Evolved Expendable Launch Vehicle (EELV) that will place the Solar Orbiter spacecraft into an inner heliospheric orbit with perihelia ranging from 0.28 to 0.38 AU and aphelia from 0.73 to 0.92 AU. The Solar Orbiter nominal science mission will begin with a series of perihelion passes where the spacecraft is nearly corotating with the Sun. It will then use multiple Venus gravity assist manoeuvres to move its orbital inclination to progressively higher heliolatitudes, reaching 25° by the end of the nominal prime mission phase and around 34° by the end of the extended mission.

The ESA portion of the Solar Orbiter mission is part of the ESA Science and Robotic Exploration Program. The NASA portion of the mission is funded by NASA Headquarters' Science Missions Directorate (SMD) Heliophysics Division, and is being implemented by the Solar Orbiter Collaboration Project Office within the Living With a Star Program Office at NASA/GSFC.

The collaboration between ESA and NASA will be documented in a Solar Orbiter Memorandum Of Understanding (MOU). The details of implementation and day-to-day working organization at Project Office level will be documented in a Solar Orbiter Joint Project Implementation Plan (JPIP). The MOU and the JPIP are to be agreed and ready for signature by the time of the down-selection by ESA's SPC on 4 October 2011.

8.4 Summary Master Schedule

Particular attention must be paid to the environmental test program duration, which is exceptionally complex for this spacecraft due to the necessity of multiple spacecraft-level and lower-level thermal tests, including Sun simulation at various solar intensities.

The baseline schedule (Table 8.1) contains an ESA-mandated and -controlled 6-month margin, placed between spacecraft Flight Acceptance Review and the start of the 4-month launch campaign to be conducted at the Kennedy Space Center, Florida.

In addition to the baseline January 2017 launch opportunity, an opportunity exists to launch in March 2017, with an adapted sequence of Gravity Assist Manoeuvres and correspondingly slightly different flight operations schedule. The spacecraft requirements ensure its compatibility with both the January and March 2017 opportunities, as well as with the back-up launch opportunity in September 2018, all with sufficient launch windows of at least 20 days and even in most cases 30 days, with daily slots of at least 30 minutes (the latter to be confirmed by detailed analyses). The exact durations of the cruise, nominal science and extended science phases depend on the actual launch date but are always on the order of 3 years each, adding up to a total nominal mission duration of 6 to 7 years and a total extended mission duration of 9 to 10 years.

8.5 Management Requirements

ESA defines the management requirements applicable to the Solar Orbiter industrial team during the Implementation Phase, regarding in particular:

- Basic project management and control
- Project breakdown structures
- Schedule management
- Financial and cost management
- Contract change management
- Configuration management
- Document management
- Logistics and inventory management
- Progress and performance reporting and evaluation
- Project reviews
- Applicability of management requirements and tasks, tailored to the specific Solar Orbiter implementation phase, as derived from ECSS Standards
- Formal and informal means of communication
- Risk Management

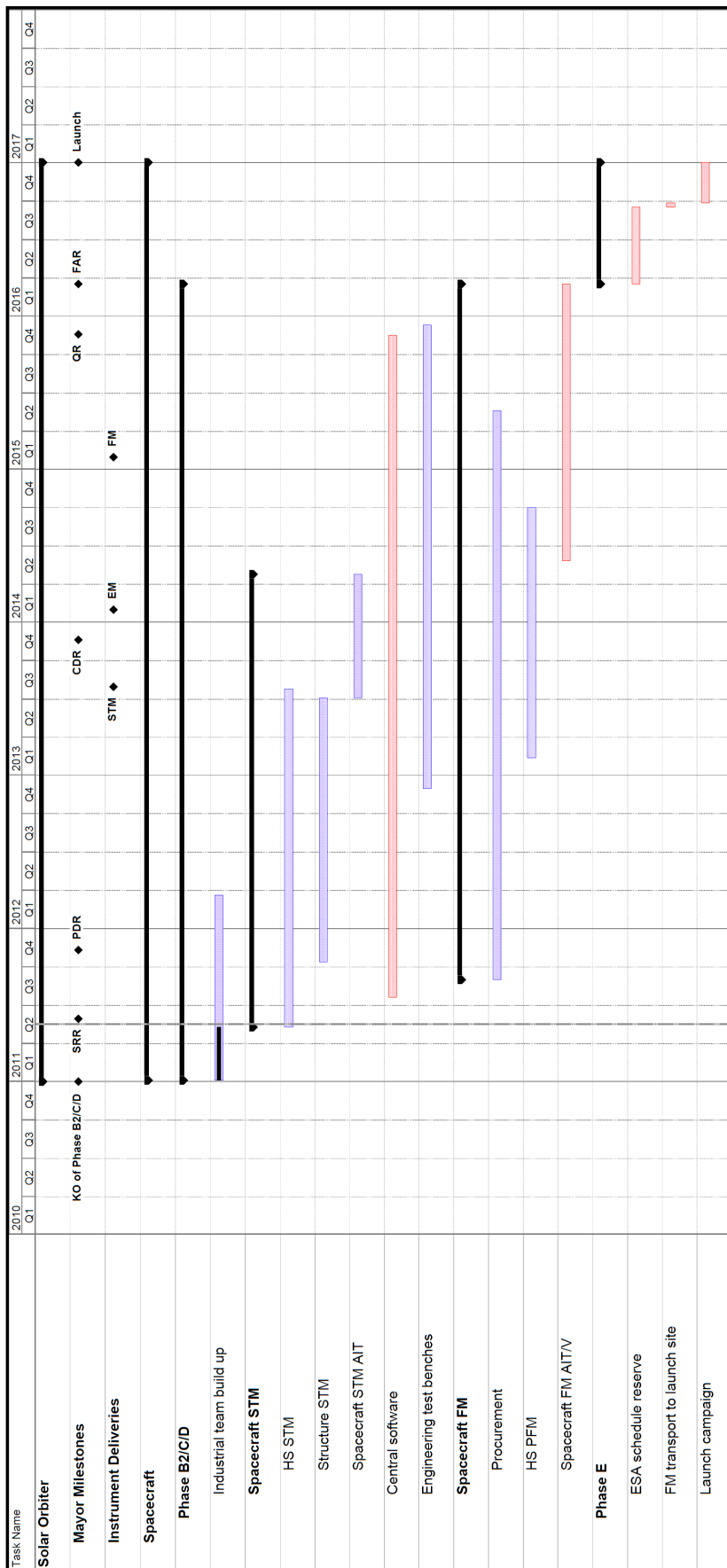


Table 8.1. Solar Orbiter Master Schedule.

A Appendix

A.1 References

- Antonucci E, Abbo L, Dodero, MA. 2005. *Astron. Astrophys.*, 435/2:699
- Aschwanden MJ. 2006. *Space Sci. Rev.* 124:361
- Axford WI, McKenzie J. 1992. In *Solar Wind Seven*, eds. E Marsch, R Schwenn. Pergamon
- Bale SD, Mozer FS. 2007. *Phys. Rev. Lett.* 98:205001
- Beck JG. 2000. *Solar Phys.* 191:47
- Borovsky JE. 2008. *J. Geophys. Res.* 113:A08110
- Breech B, et al. 2008. *J. Geophys. Res.* 113: A08105
- Brun AS, Miesch MS, Toomre J. 2004. *Astrophys. J.* 614:1073
- Bruno R, et al. 2001. *Planet Space Sci.* 49:1201
- Cargill PJ, et al. 2006. *Space Sci. Rev.* 124:249
- Cirtain J, et al. 2007. *Science* 318:1580
- Corbard T. 1998. PhD thesis, Université de Nice
- Cohen CMS, et al. 2007. *Space Sci. Rev.* 130:183
- Cranmer SR, van Ballegooijen AA, Edgar RJ. 2007. *Astrophys. J. Suppl.* 171:520
- De Pontieu B, et al. 2009. *Astrophys. J* 701:L1
- De Pontieu B, et al. 2011 *Science* 331:55
- Desai MI, et al. 2006. *Space Sci. Rev.* 124:261
- Dikpati M, Charbonneau PA. 1999. *Astrophys. J.* 518:508
- Dikpati M, Gilman PA. 2008. *J. Astrophys. Astron.* 29:29
- Dodero, MA, Antonucci E, Giordano S, Martin R. *Solar Phys.* 183/1:77-90
- Drake JF, et al. 2009. *Astrophys. J.* 700:L16
- Fisk LA, Schwadron NA, Zurbuchen TH. 1999. *J. Geophys. Res.* 104:19765
- Fisk LA, Zurbuchen TH. 2006. *J. Geophys. Res.* 111:A09115
- Fisk LA, Gloeckler G. 2007. *Space Sci. Rev.* 130:153
- Geiss J, Bochsler P. 1985. In *CNES Isotopic Ratios in the Solar System*, p. 213
- Geiss J, et al. 1995. *Science* 268:1005
- Getman KV, et al. 2008. *Astrophys. J.* 688:418
- Giacalone J, Kota J. 2006. *Space Sci. Rev.* 124:277
- Gizon L, Birch AC. 2005. *Living Rev. Solar Phys.* 2 (cited 30 August 2009)
- Gopalswamy N. 2006. *Space Sci. Rev.* 124:145
- Gopalswamy N, et al. 2001. *Astrophys. J.* 548:L91
- Gopalswamy N, et al. 2002. *Geophys. Res. Lett.* 29:106
- Gopalswamy N, et al. 2008. *Astrophys. J.* 674:560
- Hansteen V, Leer E. 1995. *J. Geophys. Res.* 100:21577
- Harvey JW, et al. 2007. *Astrophys. J.* 659:177
- Horbury TS, Forman MA, Oughton S. 2008. *Phys. Rev. Lett.* 101:175005
- Howe R, et al. 2006 *Solar Phys.* 235:1
- Jackiewicz J, Gizon L, Birch AC. 2008. *Solar Phys.* 251:381
- Kleckner BE, Möbius E, Popecki MA. 2006. *Space Sci. Rev.* 124:289
- Kohl JL, et al. 1997 *Solar Phys.* 175/2:613
- Kohl JL, et al. 1998. *Astrophys. J.* 501:L27
- Kohl JL, et al. 2006. *Astron Astrophys. Rev.* 13:31
- Lamb DA, et al. 2008. *Astrophys. J.* 674:520
- Lamb DA, et al. 2009. *Astrophys. J.* in press
- Lee MA. 2007. *Space Sci. Rev.* 130:221
- Li X et al. 1998. *Astrophys. J.* 501:L33
- Lin J, Forbes TG. 2000. *J. Geophys. Res.* 105:2375
- Lin RP. 2006. *Space Sci. Rev.* 124:233

- Lites B, et al. 2007. *Publ. Astron. Soc. Japan* 59:S571
- Lockwood M, Stamper R, Wild MN. 1999. *Nature* 399:437
- Lugaz N, Manchester WB, Gombosi TI. 2005. *Astrophys. J.* 634:651
- Lynch BJ, et al. 2004. *Astrophys. J.* 617:589
- Makarov VI, Tlatov AG, Sivaraman KR. 2000. *Solar Phys.* 214:41
- Mann G, et al. 2003. *A&A* 400:329
- Marsch E. 2006. *Living Rev. Solar Phys.* 3
- Marsch E. 2006. *Astron. Astrophys.* 457-699
- Marino R, et al. 2008. *Astrophys. J.* 677 L71
- Martinez Pillet V. 2006. In *Proceedings of the Second Solar Orbiter Workshop*, eds. R Marsden, L Conroy. Noordwijk, Netherlands
- Mason GM. 2007. *Space Sci. Rev.* 130:231
- Matteini L, et al. 2007. *Geophys. Res. Lett.* 34:L20105
- McComas D, et al. 2008. *Geophys. Res. Lett.* 35:L18103
- McIntosh S, Davey AR, Hassler DM. 2006. *Astrophys. J.* 644:L87
- Mewaldt RA. 2006. *Space Sci. Rev.* 124:303
- Mewaldt RA, et al. 2007. *Space Sci. Rev.* 130:207
- Ontiveros V, Vourlidas A. 2009. *Astrophys. J.* 693:267
- Owens MJ, Crooker NU. 2006. *J. Geophys. Res.* 111:A10104
- Owens MJ, et al. 2008. *Geophys. Res. Lett.* 35:L20108
- Neugebauer M, et al. 1995. *J. Geophys. Res.* 100:23389
- Palmer ID. 1982. *Rev. Geophys. Space Phys.* 20:335
- Parnell CE, et al. 2009. *Astrophys. J.* 698:75
- Patsourakos S, Vourlidas A. 2009. *Astrophys. J.* 700:L182
- Pietarila Graham J, Danilovic S, Schüssler M. 2009. *Astrophys. J.* 693:1728
- Richardson IG, Cane HV. 2004. *Geophys. Res. Lett.* 31:L18804
- Roth M. 2007. In *Modern Solar Facilities – Advanced Solar Science*, eds. F. Kneer et al. Göttingen, Germany
- Rouillard AP, Lockwood M, Finch I. 2007. *J. Geophys. Res.* 112:A05103
- Schrijver CJ, et al. 1997. *Astrophys. J.* 487:424
- Schrijver CJ, Title AM. 2001. *Astrophys. J.* 551:1099
- Schwadron NA, McComas DJ. 2003. *Astrophys. J.* 599:1395
- Schwadron NA, McComas DJ. 2008. *Astrophys. J.* 686:L33
- Sheeley NR. 1991. *Astrophys. J.* 374:386
- Smith CW, et al. 2001. *J. Geophys. Res.* 106:18625
- Smith EJ, et al. 2000. *Astrophys. J.* 533:1084
- Thieme KM, Marsch E, Schwenn R. 1990. *Ann Geophys.* 8:713
- Telloni D, Antonucci E, Doderio MA. 2007. *Astron. Astrophys.* 476:1341
- Thompson MJ, et al. 2003. *Ann Rev. Astron Astrophys.* 41:599
- Tsuneta S, et al. 2008. *Astrophys. J.* 688:1374
- Tu CY, Marsch E. 1990. *J. Geophys. Res.* 98:1257
- Tu CY, et al. 2005. *Science* 308:519
- Tylka AJ, et al. 2005. *Astrophys. J.* 625:474
- von Steiger R, et al. 1997. *Adv Space Res.* 15:3
- Vourlidas A, et al. 2003. *Astrophys. J.* 598:1392
- Vršnak B, Cliver EW. 2008. *Solar Phys.* 253:215
- Wang YM, Sheeley NR. 2006. *Astrophys. J.* 653:708
- Wang YM, Nash AG, Sheeley NR. 1989. *Astrophys. J.* 347:529
- Wang YM, et al. 2007. *Astrophys. J.* 660:882
- Zhang J., Dere KP. 2006. *Astrophys. J.* 649:1100
- Zirin H. 1987. *Solar Phys.* 110:101

A.2 Acronyms

A/D	Analog-to-Digital
AIV	Assembly, Integration, & Verification
ALMA	Atacama Large Millimeter Array
ANT	Antenna (RPW)
AO	Announcement of Opportunity
AOCS	Attitude and Orbit Control System
APE	Absolute Pointing Error
APM	Antenna Pointing Mechanism
APS	Active Pixel Sensor
ASR	Assessment Study Report
ATST	Advanced Technology Solar Telescope
AU	Astronomical Unit
BCR	Baseline Critical Review
BIAS	Biassing Unit (RPW)
CDPU	Common Data Processing Unit
CDS	Coronal Diagnostic Spectrometer
CIR	Corotating Interaction Region
CME	Coronal Mass Ejection
COMMS	Communication System
COSMO	Coronal Solar Magnetic Observatory
CPS	Chemical Propulsion System
CSL	Centre Spatiale de Liège
CVP	Checkout and Verification Phase
CZT	Cadmium-Zinc-Telluride
DC	Direct Current
DDS	Data Distribution System
DMS	Data Management System
DPU	Data Processing Unit
DPU	Digital Processing Unit
DSM	Deep Space Manoeuvres
DSN	Deep Space Network
EA	Electrostatic Analyser
EAS	Electron Analyser System
EELV	Evolved Expendable Launch Vehicle
EEM	End of Extended Mission
EID-B	Experiment Interface Document, Part B
ENM	End of Nominal Mission
EPD	Energetic Particle Detector
EPHIN	Electron Proton Helium Instrument
EPS	Electrical Power Subsystem
EPT	Electron Proton Telescope
ERNE	Energetic and Relativistic Nuclei and Electron (experiment)
ESA	European Space Agency

ESAC	European Space Astronomy Centre
ESOC	European Space Operations Centre
EST	European Solar Telescope
ESTEC	European Space Research and Technology Centre
ESTRACK	ESA Tracking Station Network
EUI	Extreme Ultraviolet Imager
FDIR	Failure Detection, Isolation and Recovery
FDT	Full Disk Telescope
FEE	Front End Electronics
FG	Filtergraph
FIP	First Ionization Potential
FOSO	Focused Opportunity for Solar Orbiter
FOV	Field of View
FSI	Full Sun Imager
GAM	Gravity Assist Manoeuvre
GI	Guest Investigator
GONG	Global Oscillation Network Group
HCS	Heliospheric Current Sheet
HELEX	Heliophysical Explorers
HET	High Energy Telescope
HGA	High-gain Antenna
HIS	Heavy Ion Sensor
HMF	Heliospheric Magnetic Field
HMI	Heliioseismic and Magnetic Imager
HRI	High Resolution Imager
HRT	Hard X-ray Telescope
HRT	High Resolution Telescope
HTHGA	High-Temperature High-Gain Antenna
HTMLI	High-Temperature Multi-Layer Insulation
IAC	Instituto de Astrofísica de Canarias
IAPS	Intensified Active Pixel Sensor
ICME	Interplanetary Coronal Mass Ejection
ICSTM	The Imperial College of Science, Technology, and Medicine
ICU	Instrument Controller Unit
IDS	Interdisciplinary Scientist
ILWS	International Living with a Star
IMF	Interplanetary Magnetic Field
IMU	Inertial Measurement Unit
ISS	Image Stabilization System
JHU/APL	Johns Hopkins University Applied Physics Laboratory
JPL	Jet Propulsion Laboratory
JOP	Joint Observation Programme
JSTDT	Joint Science and Technology Definition Team
KSC	Kennedy Space Center

LASCO	Large-Angle and Spectrometric Coronagraph
LCVR	Liquid Crystal Variable Retarder
LEOP	Launch and Early Orbit Phase
LET	Low Energy Telescope
LF	Low Frequency
LFR	Low Frequency Receiver
LGA	Low Gain Antenna
LOFAR	Low Frequency Array
LOS	Line of Sight
LVPS	Low Voltage Power Supply
LWS	Living with a Star
MAG	Magnetometer
MDI	Michelson Doppler Imager
MEB	Main Electronics Box
METIS	Multi Element Telescope for Imaging and Spectroscopy
MEX	Mars Express
MGA	Medium Gain Antenna
MLI	Multi-Layer Insulation
MMO	Mercury Magnetospheric Orbiter
MOC	Mission Operations Centre
MPS	Max-Planck-Institut für Sonnensystemforschung
NASA	National Aeronautics and Space Administration
NRL	Naval Research Laboratory
OBC	On-Board Computer
OBDH	On-Board Data Handling
ORATOS	Orbit and Attitude Operations System
OSR	Optical Solar Reflector
PAS	Proton Alpha Sensor
PHI	Polarimetric and Helioseismic Imager
PCDU	Power Conditioning and Distribution Unit
PCU	Power Converter Unit
PMP	Polarization Modulation Package
PRC	Payload Review Committee
RAL	Rutherford Appleton Laboratory
RCS	Reaction Control (Sub)system
RFDU/WGI	Radio-Frequency Distribution Unit / Wave Guide Interface
RHESSI	Reuven Ramaty High Energy Solar Spectroscopic Imager
RIU	Remote Interface Unit
RMS	Root-Mean-Square
RPE	Relative Pointing Error
RPW	Radio Plasma Waves (experiment)
S/C	Spacecraft
SA	Solar Array
SAA	Solar Aspect Angle

SADE	Solar Array Drive Electronics
SCE	SoloHI Control Electronics
SCM	Search Coil Magnetometer
SCOS	Spacecraft Control and Operation System
SEP	Solar Energetic Particle
SEPT	Solar Electron Proton Telescope
SIM	SoloHI Instrument Module
SIS	Suprathermal Ion Spectrograph
SMEX	Small Explorer
SMP	Science Management Plan
SNR	Signal-to-noise
SOAD	Science Operations Assumptions Document
SOC	Science Operations Centre
SOHO	Solar and Heliospheric Observatory
SoloHI	Solar Orbiter Heliospheric Imager
SOT	Science Operations Team
SOT	Solar Optical Telescope
SPC	Science Programme Committee
SPICE	Spectral Imaging of the Coronal Environment
SPP	Solar Probe Plus
SRR	System Requirements Review
SSAC	Space Science Advisory Committee
SSMM	Solid State Mass Memory
SSWG	Solar System Working Group
STEIN	SupraThermal Electrons Ions and Neutrals
STEREO	Solar Terrestrial Relations Observatory
STIX	Spectrometer/Telescope for Imaging X-rays
SUMER	Solar Ultraviolet Measurements of Emitted Radiation
SWA	Solar Wind Analyzer
SwRI	Southwest Research Institute
SWT	Science Working Team
TCS	Thermal Control Subsystem
TDA	Technology Development Activities
TDS	Time Domain Sampler
TNR-HFR	Thermal Noise and High Frequency Receiver
TOF	Time of Flight
TRACE	Transition Region and Coronal Explorer
TVLS	Toroidal Variable Line Spaced
TWTA	Traveling Wave Tube Amplifier
UCL/MSSL	University College London/Mullard Space Science Laboratory
ULEIS	Ultra Low Energy Isotope Spectrometer
UV	Ultraviolet
VEX	Venus Express